Characterization of high-frequency time-domain effects arising from the transmission line substitutions of reactive components in a buck converter

John Maree

2024

Declaration

I declare that this dissertation is my own, unaided work. It is being submitted for the degree of Master of Science in Engineering to the University of the Witwatersrand, Johannesburg. It has not been submitted before for any degree or examination to any other University.

2024-07-30

Signed: John Maree

Date: 2024-07-30

Signature

Contents

List of Figures

List of Tables

Abstract

The work presented in this dissertation is a continuation of a line of research that suggests that the energy storage components within a DC-DC converter may be a source of high frequency effects in power converter circuits. It is shown that for physically large energy storage components, conventional models are insufficient for modelling the effects of these components and that a transmission line approach is required. Very little work has been done within switching circuits using transmission line theory for the primary components themselves, specifically regarding the time-domian effects of these components. A significant finding of this work is that it is shown that both in simulation and experimental results these components do indeed have a measurable effect on the output of the converter. Furthermore, this dissertation explores time-domain quantification methods for these distributed effects, and shows that the delay ratio between the transmission lines is a key parameter in determining the magnitude of the effects. This work provides strong experimental evidence for the existence of distributed effects occurring from energy storage components within a DC-DC converter, and indicates that this area of research is worth further investigation.

Advancements into our understanding of the high-frequency operation of DC-DC converters have become increasingly rare, necessitating a new perspective. This work focusses on using transmission line theory to model energy storage components within a DC-DC converter, and investigating the effects of doing so. The research firstly introduces the design, simulation and experimental evidence for inductors and capacitors using transmission line theory. In fact, it is shown that in order to accurately model a physically large reactive component, transmission line modelling is required. Thereafter, these components in a physically large form are then applied to a DC-DC buck converter circuit where it is shown that the converter manifests high frequency effects that are not predicted by conventional models, but is adequately shown using transmission line models. The effects of these components are then investigated, and it is shown that the delay ratio between the transmission lines is a key parameter in determining the magnitude of the effects. This work provides strong experimental evidence for the existence of distributed effects occurring from energy storage components within a DC-DC converter, and indicates that this area of research is worth further investigation.

Chapter 1

Introduction

The DC-DC converter is arguably the most ubiquitous power-electronic circuit in existence, and its usage is only increasing as the world moves towards more efficient electronics and renewable energy sources. Synchronous buck converters are especially popular due to their simplicity, efficiency and ability to step-down voltages suitable for modern IC's.

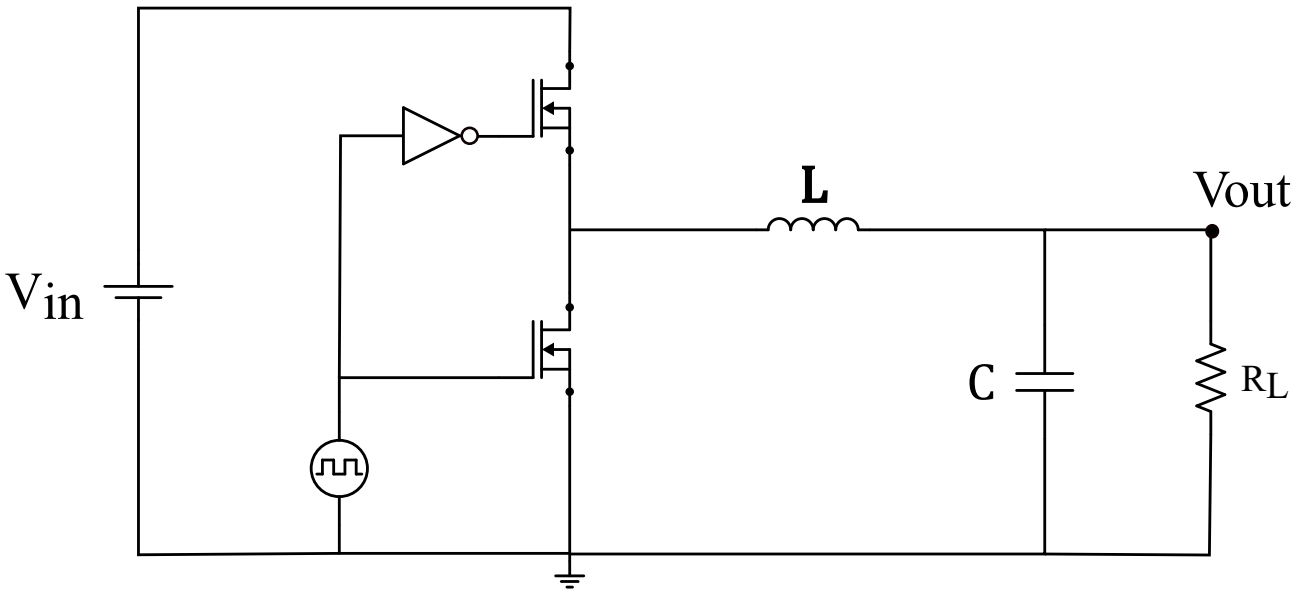

Figure 1.1: Synchronous DC-DC buck converter

With the demand for ever more efficient and smaller power converters, considerable effort has been put towards decreasing the size of the energy storage components within the converter; apart from heat sinks these components occupy the most volume in modern converters. Size reduction is typically achieved through the use of higher switching frequencies [1]. However, as switching frequencies increase, the switching-losses and electromagnetic interference (EMI) of circuits also tend to become more prevalent. Usually, EMI design methods follow a set of generally accepted design guidelines which among many factors are primarily centred around careful component placement (topology, relative component positioning, return path minimization),

switching schemes, increasing rise- and fall times and filtering networks [1], [2]. While this does keep end-products within the desired Electromagnetic Compatibility standards, designing for EMI has yet to consider how the internal construction of reactive components themselves may potentially contribute towards the high-frequencies of a circuit and eventually towards EMI.

As switching speeds get increasingly fast, rise- and fall times get increasingly smaller. This poses an interesting question: what happens to the time-domain output of switching circuits when the rise- and fall times of the switching devices become smaller than the time it takes voltage and current waveforms to travel within the energy storage components. This concept is related to the apparent 'electrical size' of the components; here we define an electrically small component as a component where the time taken for voltages and currents to travel through the component is less than the rise- and fall times of the switching devices (or input signal i.e., square wave edge). The opposite is true for electrically large components. When a component is electrically small, the internal construction of the components become visible on the time-domain voltages and currents within the circuit, and a different perspective towards modelling these reactive components is required for accurately quantifying these effects. Furthering understanding into how these components interact with one another is important for the design of future power converters, and is the main focus of this study.

As mentioned, there is a need to account for the transit time of voltages and currents within reactive components. Traditional models or 'lumped-element' models for reactive components lack this information, however distributed models (also referred to as transmission line models) account for just this, and often more accurately than lumped-element models for high-frequency analysis [3]–[6]. They achieve this by offering a more spatial and temporal perspective of the energy storage components, utilising transmission line theory to ultimately account for some of the effects that are not modelled by conventional lumped-element models.

Figure 1.2 shows an example of a distributed model for an MLC capacitor [3], [5]. When the internal construction of the capacitor is modelled, a distributed model is obtained which can subsequently take into account the effects of the physical construction of the capacitor on the signals passing through it. The model should also look familiar, and is indeed a transmission line equivalent LC network; Which opens up a considerable amount of knowledge that could be applied towards these distributed components. A similar process can be followed for inductors, both of which will be covered in Chapter 3.

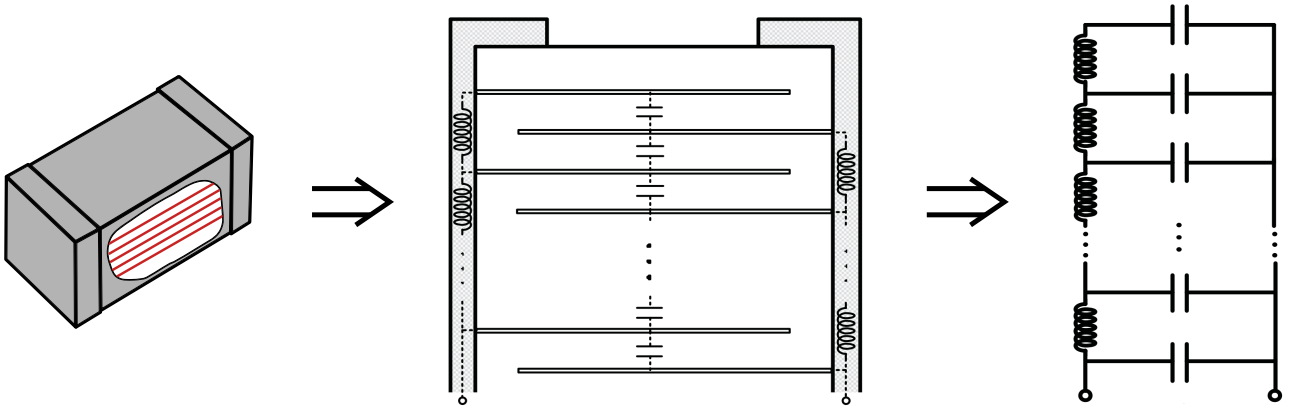

Figure 1.2: Distributed MLC Capacitor Model, extracted from [3], [5]

This work is going to focus on the usage of distributed components within a DC-DC buck converter. The capacitor and inductor components are replaced with physically massive transmission line (or distributed) equivalent components in simulation as well as experimentally. Physically massive meaning that from a transmission line perspective, the round-trip delay of the distributed components is much larger than the rise- and fall times of the switch. This is done to force distributed effects into an observable scale on the output voltage of the buck converter for further analysis. Figure 1.3 shows the buck converter circuit diagram with distributed components, where the components are modelled as ideal lossless delay transmission lines.

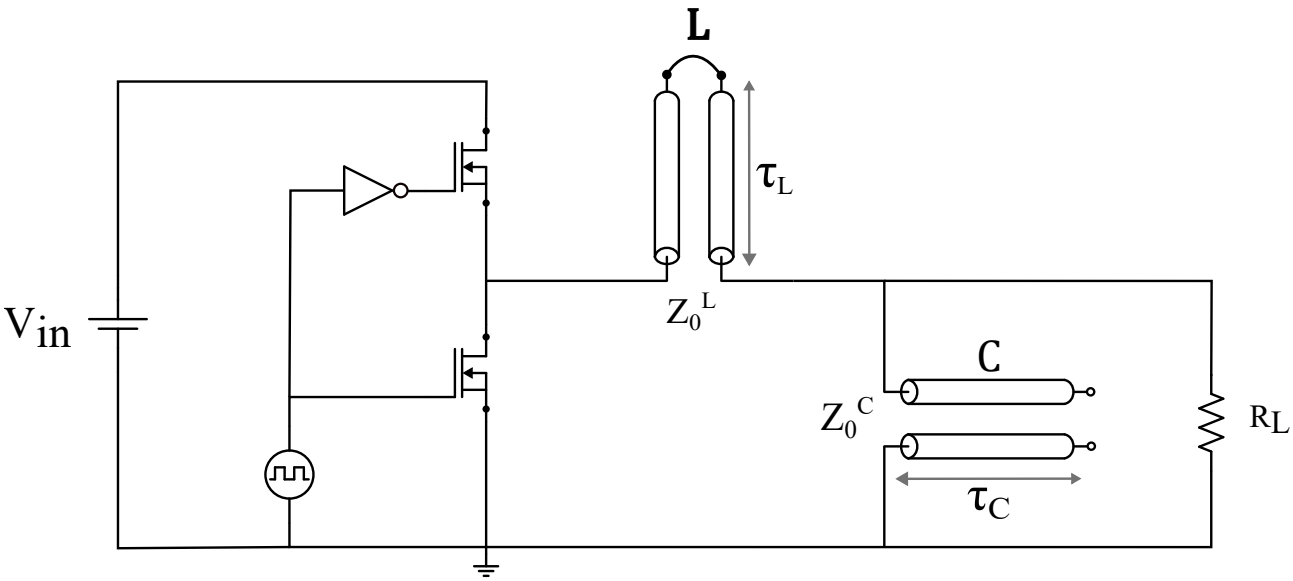

Figure 1.3: Buck converter where the capacitor and inductor are replaced with (or modelled as) distributed components

When we force these distributed effects into the open, it is shown that the output voltage of the buck converter is significantly affected by the distributed components. Specifically, high-frequency time-domain effects are observed on the output voltage waveform of the buck converter (see Figure 1.4, where typical parameter values were used in the simulation for illustration purposes. Detailed modelling of this Figure will be done in Chapters 3 and 5). These effects are not observed when using equivalent lumped-element models for the capacitor and inductor, both in simulation and experimentally.

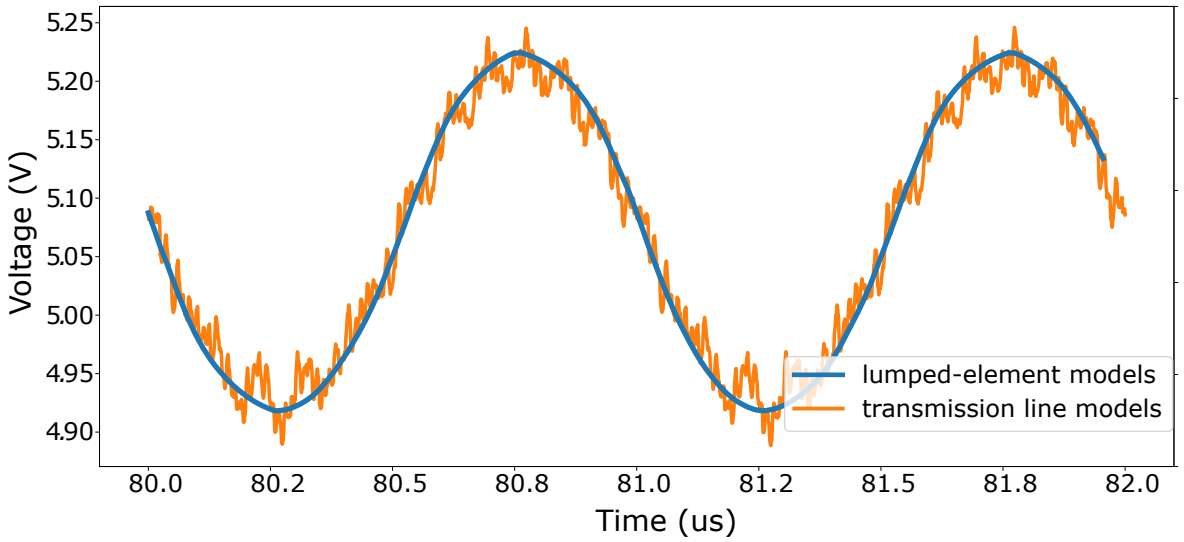

Figure 1.4: Simulation output of a distributed component DC-DC buck converter compared to a lumped-element converter. It is shown that on top of the typical switching ripple, additional high-speed effects exist on the output voltage waveform arising from the transmission line components.

Thereafter, the high-frequency effects shown by the transmission line buck converter is analysed further in simulation by altering the transmission line delay parameter (or length) of the inductor transmission line and investigating the effect that it has on the output. It is shown when comparing data across many alterations that small changes in delay relationship between the transmission line components can have a significant impact on the output waveform of the buck converter. A finding emerges where it appears that when the delay of the transmission lines are approximately integer multiples of one another, the magnitudes of the high-speed effects on the output waveform is most pronounced and less so for fractional (non-integer) multiples. These effects are verified experimentally.

1.1 Dissertation outline

Chapter 2 focusses on providing background information around the usage of distributed components in power electronics, as well as emphasising where this research fits in with existing knowledge.

Chapter 3 details the design, simulation and experimentation of transmission line modelling for capacitors and inductors. This chapter serves to confirm the validity of these components and their suitability in simulation to predict practical behaviour. This chapter will emphasise the necessity for distributed modelling and serves as a strong foundation for the usage of these components in subsequent chapters.

In Chapter 4 the derivation of a standard DC-DC buck converter is provided using common techniques. Thereafter, a buck converter is designed and simulated for confirmation where the theory is shown to match expectations using standard reactive components. Following this is where transmission line components are designed in line with Chapter 3 and substituted for the main capacitor and inductor in the buck converter circuit. This is known as the distributed buck converter (or transmission line buck converter). The circuit is simulated, where it is shown that the overall operation of the buck converter is in good agreement with prior models, except for the additional high-frequencies observed on the time-domain output waveform of the converter. It is these high-frequency effects which are attributed to transmission line components. The chapter concludes with experimental verification of the distributed effects observed in simulation, which reinforces confidence in these components and bridges the theoretical expectations presented by literature with reality.

Chapter 5 uses the circuit and results from Chapter 4 to investigate the effects of transmission line components on the output. We focussed on changing a delay parameter of one of the transmission lines over a range of values and comparing the results across each value. What came out of the results is that there is a significant relationship between the delay values of the components and the magnitude of the distributed effects observed on the output. Specifically it is shown that the effects are most pronounced when the delay values are around integer multiples of each other. This chapter provides good evidence that the effects we see while using transmission line components are indeed a result of them, and that small changes in their parameters can have a significant impact on the output.

Chapter 6 summarizes the work presented by this dissertation as well as offers suggestions for future work within the field.

Chapter 2

Background

This work relies heavily on the theory and application of distributed models for reactive components. As such it is useful to contextualize the work by briefly revising common uses for distributed modelling, when it becomes useful and how this work will use distributed models in the context of power electronics.

Distributed modelling is a technique used to model the behaviour of a component by assuming that the voltages and currents are not spatially constant throughout the component, but rather vary with position inside the component itself. This is a more accurate electrical representation of the physical size of a component, and is useful when the component is large enough (electrical size) that the effects to voltages and currents arising from the size of the component become noticeable (usually at very high-frequencies). These models are extensively used in the RF domain, where frequencies within the VHF and UHF range is common; the wavelength of the signal is often comparable to the electrical size of the component. Typically, a rule of thumb is that if the electrical size of a component is greater than 1/10th of the wavelength of the signal, then distributed modelling should be used [7], [8].

Moreover, distributed models and the transmission line theory that accompanies them are extensively used when designing capacitors and inductors for high-frequency filters and components in RF applications, where intricate planar configurations, microstrip structures and topologies are used to achieve the desired response. Originally pioneered in the 1940s by P. Richards and later built upon by K. Kuroda (among others) who established lumped-element to distributed model transformations (Richards Transformations) and identities (Kuroda Identities) [8] to aid in microwave filter design. These techniques are still widely used today under the blanket term 'Commensurate line theory', and is a testament to the value of distributed modelling in Electrical Engineering.

2.1 Distributed models for reactive components applied to power electronics

Distributed modelling in context to power electronics is commonly used, most prevalently when applied toward modelling wires/traces between components (i.e., differential pairs), planes, via

interconnects and various other structures. Less commonly however is applying distributed models to the reactive components themselves (i.e., capacitors and inductors). This is because the physical size of these components is typically small enough that the effects of the physical construction of the component is negligible. However, as switching frequencies increase, the electrical size of these components becomes more comparable to the rise- and fall times of the signal, and distributed modelling becomes more useful.

To this end, foundational work conducted by J.D. Van Wyk and L. Zhao titled *'Frequency-Domain Modeling of Integrated Electromagnetic Power Passives by a Generalized Two-Conductor Transmission Structure'* [9] established generalized transmission line structures for integrated passives (combining of energy storage components into a single structure). Distributed modelling proved to be most appropriate for this application, and showed that there is merit to using transmission line theory to construct reactive components in power converters. This study, among others [9]–[11] provided good groundwork for distributed modelling for use in power electronics.

Distributed models, when applied to extending the lumped-element models for existing constructions has been shown to better describe the high-frequency behaviour of capacitors [3], [4], [12], [13]. Figure 2.1 (reproduced from Figure 1.2 for convenience) is extracted from [3], [4], [12], [13] where it is shown that a distributed model for an MLC capacitor exists when examining how current travels through the internal construction of the capacitor when not neglecting current transit time.

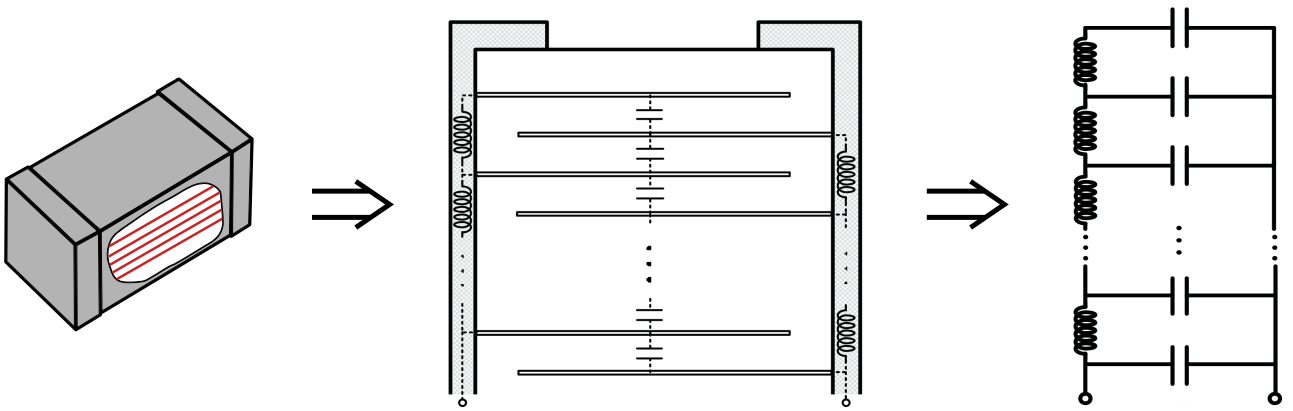

Figure 2.1: Distributed MLC Capacitor Model, extracted from [3], [5]

Building on Figure 2.1, Figure 2.2 is an excerpt of a paper from C.R. Sullivan showing the frequency response of an MLC capacitor for varying models against a measured response. What is evident is that for an MLC capacitor, the distributed model most accurately describes the high-frequency response of the component, whereas the lumped-element model falls short for higher frequencies. In fact, Sullivan argues that if designing for good time-domain performance

is the objective and the electrical size of the component becomes comparable to the rise- and fall times of its currents, then distributed models are the most appropriate design technique [3], [12]. In subsequent studies, Sullivan's models were extended using additional transmission line theory for coupled multi-conductor lines to produce even more accurate distributed models for higher harmonics [13].

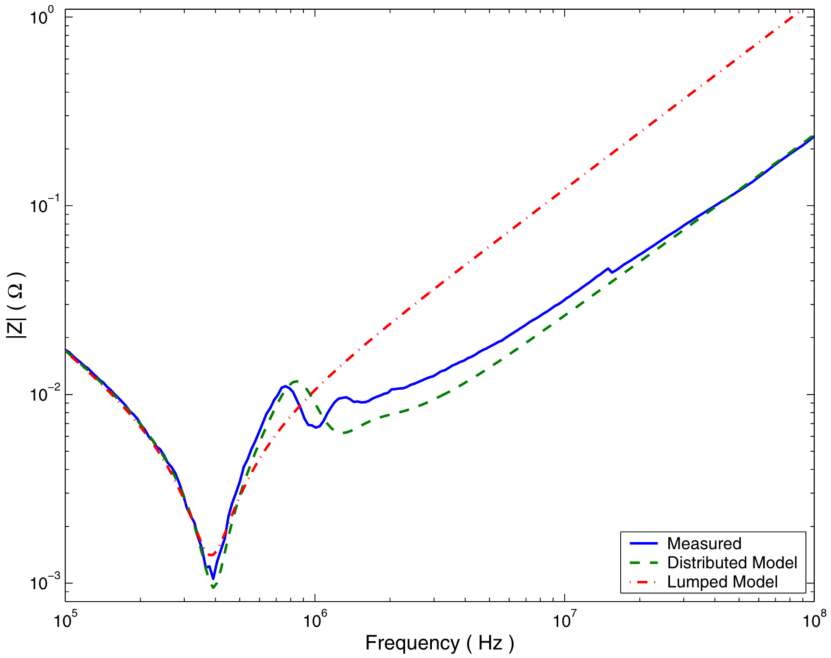

Figure 2.2: Extract of the concluding results from C.R. Sullivan's paper 'Improved distributed model for capacitors in high-performance packages'

While these findings show us the value of distributed models, they typically involve constructing a distributed network of lumped LC components — which is a very common technique for approximating transmission lines; It is however just an approximation and comes with many caveats, such as being band-limited and careful consideration needs to be applied to the amount of LC sections chosen for modelling and simulation [14]. Moreover, when simulating an n-section lumped-LC transmission line, numerous numerical effects come into play (i.e., oscillation) which is inconvenient at best [14]. Taking this into consideration, this dissertation will focus on using the ideal lossless transmission line model, specifically for simulations, as it better accounts for the time delay and instantaneous impedance properties of transmission lines and removes a lot of complexities from an implementation perspective.

It is worth mentioning work conducted by M. Mofu, where the complex interactions of reflections between two distributed components were deeply analysed [15]. Adjacent to the work covered in this dissertation, Mofu established a numerical hierarchy for the severity of wave fragmentation

arising from reflections between two transmission lines at their interface. Mofu's work indicated the complexities which arise from distributed components, and is a motivating factor for using two transmission line components for each reactive component in this work as opposed to approximating them as one transmission line, which has been looked at before [16].

2.2 Distributed modelling for DC-DC power converters

Distributed modelling in power electronics is not a new concept, and has been explored in the past. However, the focus has primarily been on the interconnects (i.e., differential pairs, matched impedance traces, via effects) and planes within the converter, and not the reactive components themselves. This section will briefly review some work conducted in the area of distributed modelling for power converters, specifically for the reactive components themselves.

Work done by S. Sander [17] looked at using transmission line models for the power inductor in a DC-DC converter, and how the use of these models can open up opportunity for further research in power electronics. Much of the work was primarily concerned with topology realization. Moreover, the 'transmission line' component used there was actually a construction of an n-section LC lumped-element transmission line network. This is merely a construction of an approximation, as using the LC components to model a transmission line physically is not really proof of the use of transmission lines for use in power converters. The work presented by this dissertation in fundamentally different, it uses actual transmission lines for power conversion with using ideal delay-based transmission lines for simulation and modelling.

Research more aligned with this dissertation was conducted by C. Huang, K. Robenack and F. Woittenek where the steady-state analysis of a distributed model buck converter was investigated [16]. While this was done in steady-state, and a set of equations was derived based on the LC lumped-element approximation for a transmission line it is a strong case for furthering exploration into these distributed model circuits. Unfortunately, the primary energy storage components (filter capacitor and inductor) of the converter was combined and modelled as one transmission line (as they were in [9]), which does limit analysis and flexibility and is less indicative of what replacing the L and C components within a converter more practically looks like. Moreover, little was done to actually investigate the time-domain output of the distributed converter (i.e., effects that small alterations in delay or other transmission line parameters have on the output), which is likely a limitation due to the singular line approximation they used. Finally, there was no experimental evidence in this paper, which is a major part of what the work in this dissertation is concerned with.

Recent research into the area of distributed modelling in power converters has suggested that using distributed models could provide a new avenue of exploration when describing noise in these circuits [6]. The work identifies interesting time-domain effects which emerge when replacing capacitors and inductors with distributed models. When capacitors and inductors

were substituted for transmission line models in simulation, it was shown that the relationship between delays of these transmission lines, switching frequency and duty-cycle of a switching circuit affects the high frequency output of a test circuit (DC-DC converter). This study is heavily aligned with this work — an effective continuation of it, where the effects of varying delay parameters is more heavily investigated along with providing experimental evidence for the distributed buck converter and the effects associated with that.

Chapter 3

Transmission line models for reactive components

The following chapter is used to introduce the transmission line models for capacitors and inductors that will be used throughout this research. The following work will show the reader that for a given construction of a reactive component, the transmission line model can be derived when required. The value of using transmission line models is shown as it exposes the distributed effects of the component, which is not possible with traditional lumped-element models. The distributed effects of the component are shown to be important when the component is electrically large, and the traditional lumped-element model is shown to be sufficient when the component is electrically small.

Following the modelling, simulations for capacitors and inductors will be shown, and the results will be compared to the traditional models. Thereafter, the results will be validated experimentally.

3.1 Electrically large and electrically small reactive components

The concept of electrically large and electrically small components in this work will govern when the transmission line models are used. When the component is electrically large, the transmission line model will be used, and when the component is electrically small, the traditional lumped-element model will be used. This is not to say that electrically small components cannot be modelled using transmission line models, but rather that it is not necessary to do so as any distributed effects will be negligible.

The definition of electrically large and electrically small differs slightly depending on the application of transmission line models. Typically, in the RF field, a component is considered electrically large when the transit time of voltages and currents within a component is around 0.1 wavelengths of the signal. This is due to the fact that their application is entirely concerning sinusoidal signals, where wavelength is a relevant parameter. This research is centred in power electronics where step-like signals are primarily interacting with components and as a result

the definitions of when distributed modelling is required is different to the RF field. Conventionally, a component is deemed in need of distributed models when the rise- and fall-times of the component are roughly 1.5 - 2 times smaller than the propagation time of the signal within the component itself [2]. Depending on how the component is connected to the signal and the rest of the circuit, this could apply to either the round-trip time or the one-way trip time of the component.

In the context of this work the definition of electrically large and electrically small will be defined as follows:

- **Electrically large**: A component is considered electrically large when the rise- and fall-time of a signal is much smaller than the time taken for a signal to travel through the component. Figure 3.1 illustrates this concept.

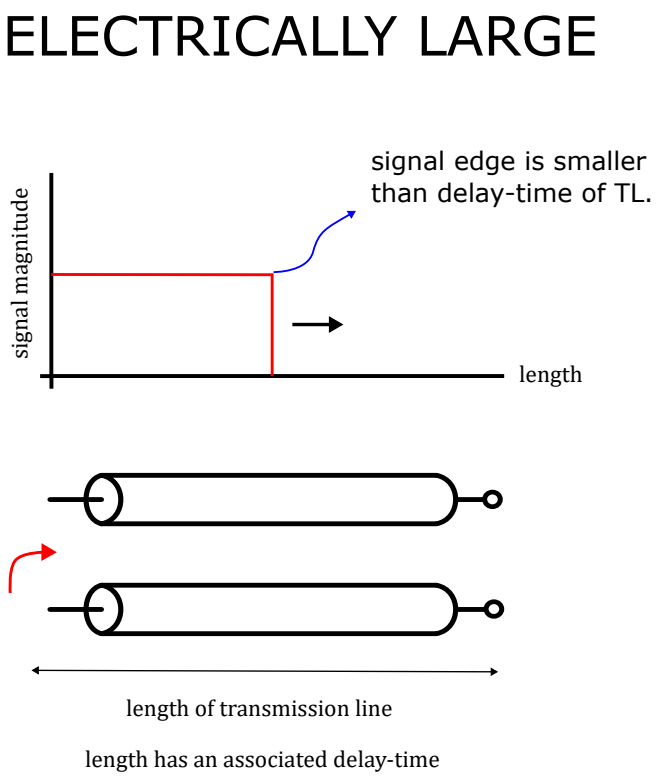

Figure 3.1: Electrically large

- **Electrically small**: A component is considered electrically small when the rise- and fall-time of a signal is larger than the time taken for a signal to travel through the component. Figure 3.2 illustrates this concept.

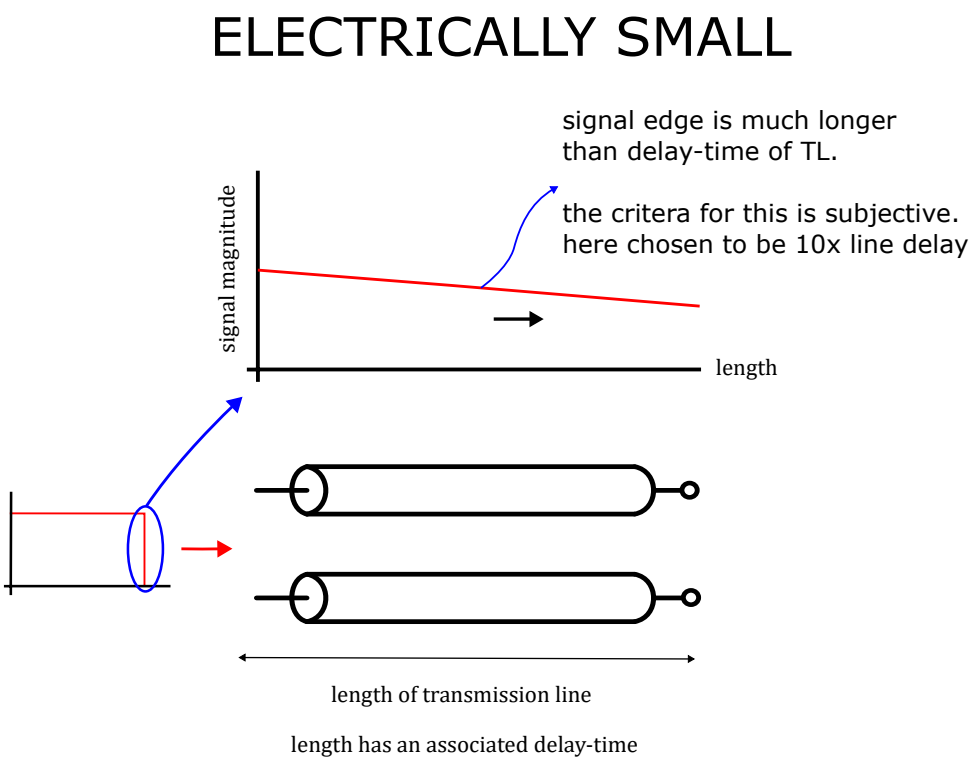

Figure 3.2: Electrically small

When the concept electrically large and electrically small components is referenced in subsequent chapters, the above definitions will be used.

3.2 Transmission line model for a capacitor

This section is going to focus on looking at a parallel plate capacitor from two different perspectives. The first perspective is the traditional circuit theory approach, or the ideal 'lumped-element model', and the second perspective is the transmission line approach. While each model is describing the same physical component, they each have their own advantages and disadvantages. Specifically in regard to the work in this study, the lumped-element model will be shown to lack the ability to account for the transit time of signals within the capacitor, whereas the transmission line model does. Ordinarily this would not be a problem, however, when the signals are of fast enough rise- and fall-times (as discussed in previously), the lumped-element model will not be able to accurately predict the behaviour of the capacitor for high-frequency time-domain effects caused by its electrical size.

The equations describing both the lumped-element and transmission line models will be provided, and the two models will be compared to each other (both in simulation and in a physical

measurement) in terms of their ability to predict the behaviour of the capacitor for electrically small and electrically large constructions.

3.2.1 Lumped-element model

The lumped-element model for a capacitor is what is most commonly used in circuit theory. It consists of two parallel plates separated by a dielectric material. See Figure 3.3. In this idealised model, the charge distribution across the plates is assumed to be uniform and instantaneous, and therefore can be excited at any point along the plates; This in turn allows for any magnetic and/or spatial factors to be negligible within the capacitor, simplifying the model to one metric (the capacitance).

The capacitance of this capacitor is given by Equation 3.1.

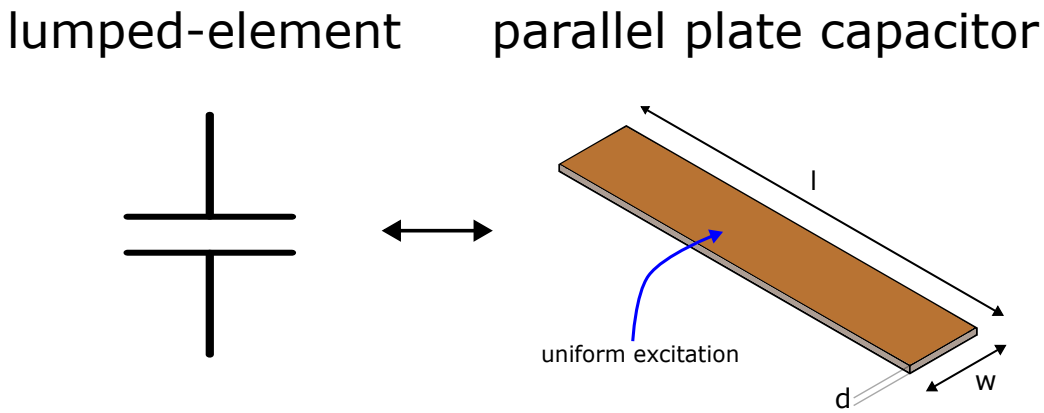

Figure 3.3: Parallel plate capacitor with dielectric material

$$C = \frac{\varepsilon_0 \varepsilon_r w l}{d} \tag{3.1}$$

where:

d = distance between plates
w = plate width
l = plate length
ε_0 = permittivity of free space
ε_r = dielectric relative permittivity

3.2.2 Transmission line model

When the need for accounting for the transit time of signals arises, then the transmission line model is best suited to solve this problem. For clarity, the parallel plate construction is repeated in Figure 3.4. Transmission line theory allows for the modelling of the capacitor as a distributed element, where the voltages and currents take time to travel through the component. While there are numerous transmission line models, for this study the ideal delay-based transmission line model will be used, which can characterize a transmission line entirely through its delay and characteristic impedance. For a capacitor, an open-circuited transmission line is used.

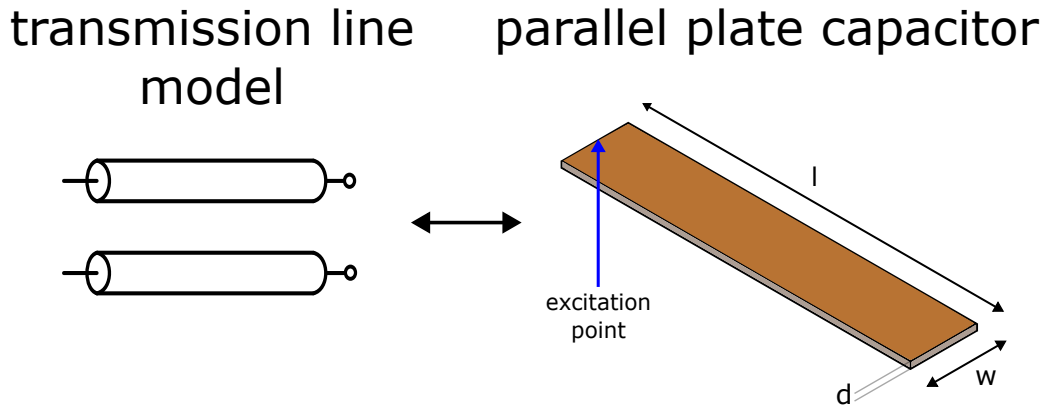

Figure 3.4: Parallel Plate Capacitor Transmission Line

Calculating the delay and characteristic impedance first requires one to determine the per-unit length values for inductance L' and capacitance C' of the transmission line; Equations 3.2 and 3.3 [18] as they relate to Figure 3.4 is used to calculate these quantities. It's crucial to acknowledge that these values, when multiplied by the length of the transmission line, provide the total inductance and capacitance of the parallel plate transmission line (or capacitor). More specifically, applying the length factor to Equation 3.3 retrieves the capacitance value from the lumped element model shown in Equation 3.1. This serves as a bridge between the lumped-element model and the transmission line model, with the former often disregarding inductance as a minor factor, while the latter necessitates accounting of these elements.

$$L' = \frac{\mu_0 \mu_r d}{w} \tag{3.2}$$

$$C' = \frac{\varepsilon_0 \varepsilon_r w}{d} \tag{3.3}$$

where:

d = distance between plates
w = width of plates
μ_0 = permeability of free space
μ_r = relative permeability
ε_0 = permittivity of free space
ε_r = dielectric relative permittivity

Thereafter, the characteristic impedance (Z_0) and delay (τ) of the transmission line are related to the inductance and capacitance of the transmission line as shown in Equations 3.4 and 3.5.

$$Z_0 = \sqrt{\frac{L'}{C'}} \tag{3.4}$$

$$\tau = l\frac{1}{\sqrt{L'C'}} \tag{3.5}$$

where:

l = length of transmission line
L' = inductance per unit length of transmission line
C' = capacitance per unit length of transmission line

3.3 Validation of the transmission line model for a capacitor by comparing simulation and measured results

While the application of lumped-element models from simulation through to physical implementation is well understood, distributed models and their relation to reactive component substitutions in a power electronics simulation is less common. For this reason, it is important to validate the simulation environment's ability to model the behaviour of the capacitor using both the lumped-element and transmission line models. This is done by comparing the simulation results to the measured results for both an electrically small and electrically large capacitor of the same value in a given circuit. If simulation results match the measured results, then not only is the simulation environment validated, but the case for the necessity of the transmission line model is also made when applied to electrically large components in power electronics.

3.3.1 Test circuit used to test reactive components

The circuit used to compare the various models and components will be a simple 5V step input connected to the capacitor through a 75Ω coaxial cable (modelled as a 75Ω transmission line with a delay of 1ns). The choice of a 75Ω coaxial cable is arbitrary, however, a method of connecting the capacitor to the circuit is required, and a coaxial cable is a simple and very well

known quantity to do so (as opposed to uncharacterised wires) and is readily available. The circuit for both models is shown in Figure 3.5.

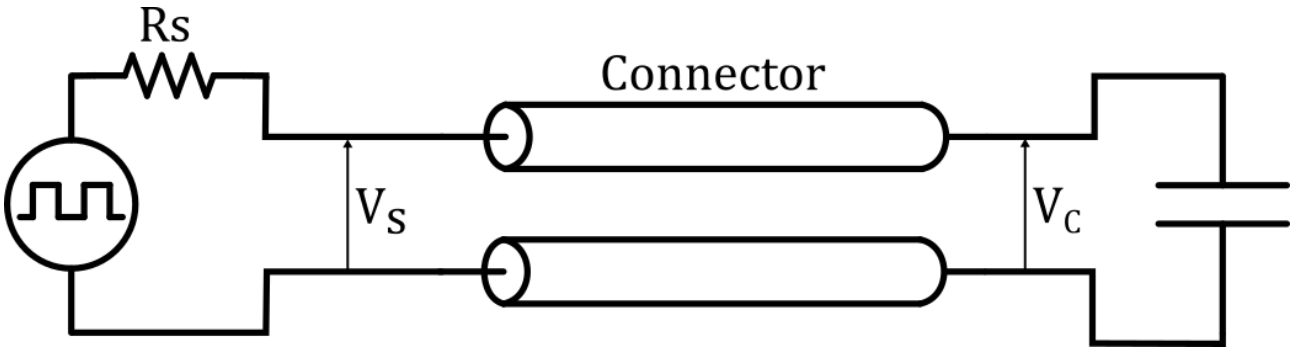

(a) Normal capacitor model

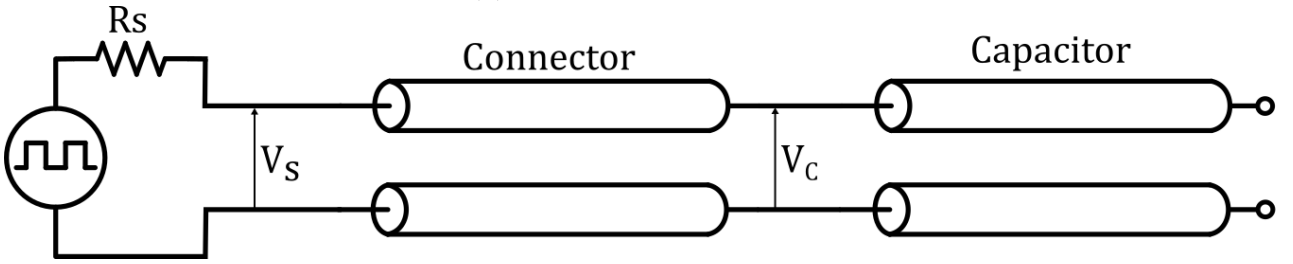

(b) Transmission line capacitor model

Figure 3.5: Transmission line capacitor verification circuit

In simulation, the switching circuit is built using two built-in MOSFET switches controlled by a pulse signal. A rise- and fall-time of 25ns is achieved by tuning the MOSFET and pulse parameters appropriately. A series resistance of 1Ohm and series parasitic inductance of 50nH is provided to make the simulation switch circuit more realistic. Figure 3.6 shows the simulation switch circuit functional diagram.

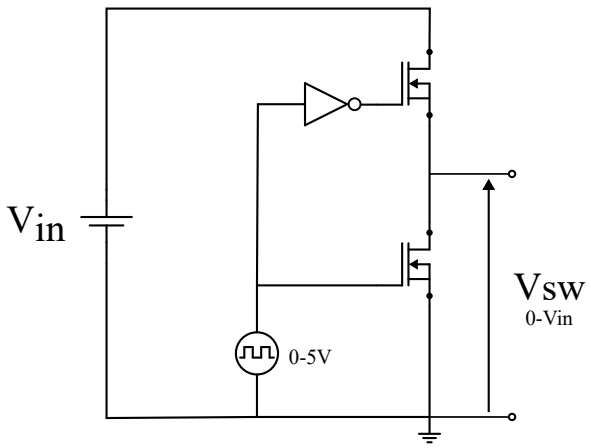

Figure 3.6: Functional diagram of simulation switch circuit

For the physical switching circuit, 6 TC426 CMOS-based MOSFET drivers are placed in parallel to produce a simple yet fast switch. These IC's will provide the fast rise- and fall-times required for the experiments provided the output current is kept low, which is not an issue here. Figure 3.7 shows the internal circuit of one output inside the TC426 IC, it is a simple inverted-output CMOS-based MOSFET driver. Which achieves a fast, yet controlled square wave output. The output was validated against the simulation results and was found to be in good agreement.

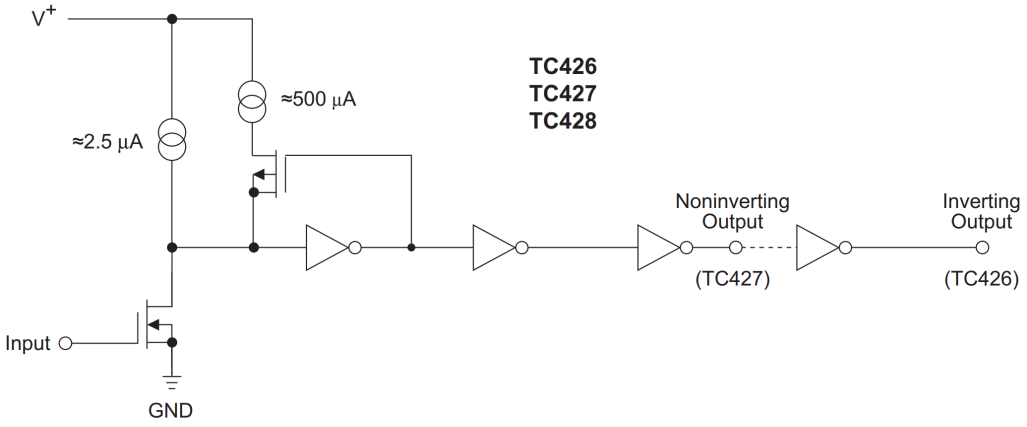

Figure 3.7: Functional diagram of physical switch circuit. Extracted from the TC426 datasheet [19]

The physical measurement setup is shown in Figure 3.8. Care was taken to ensure that connections between components were as clean and short as possible. Moreover, the measurement

probes' loop area was kept to a minimum to reduce the effects of parasitic inductance from the measurement probes.

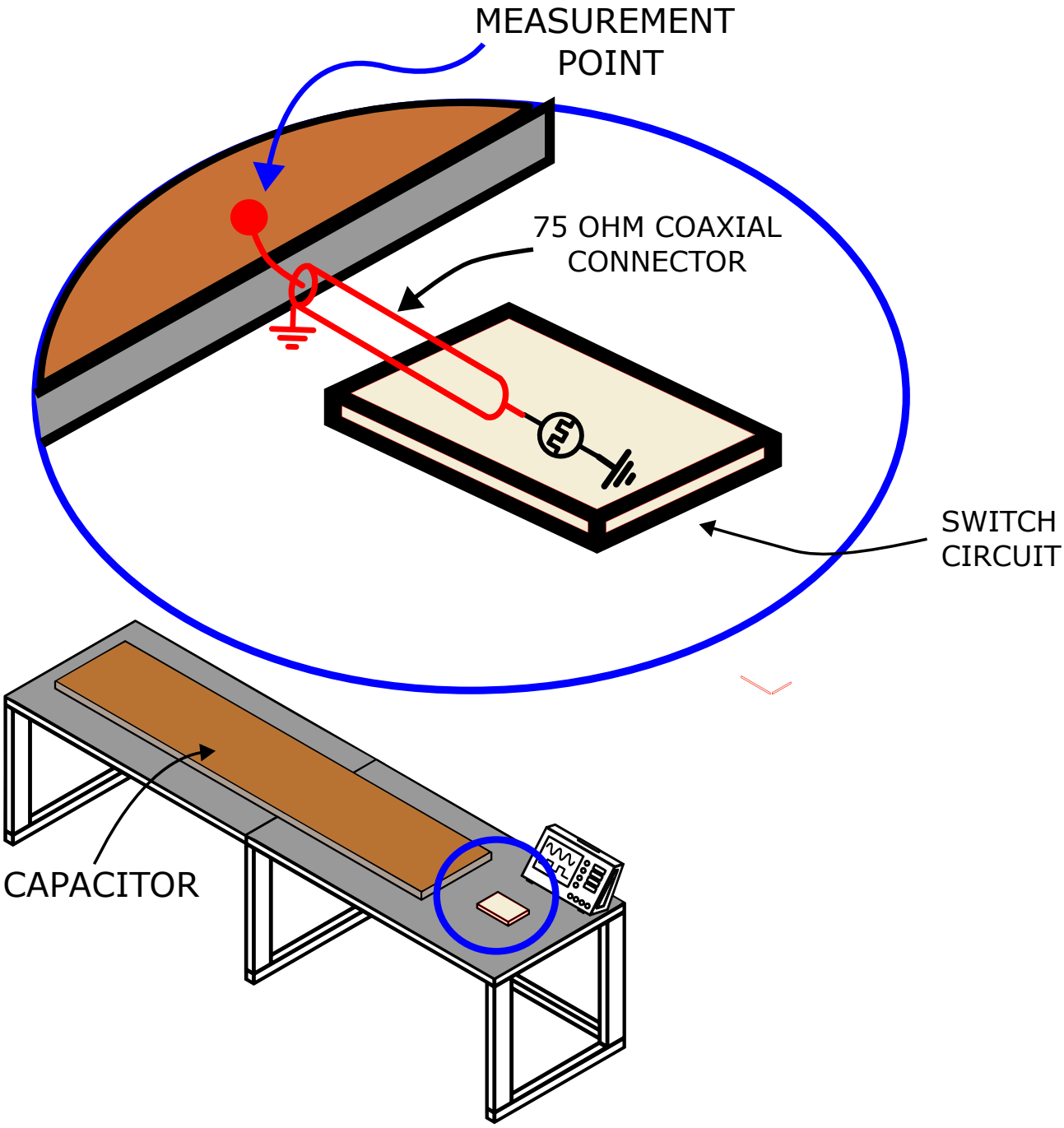

Figure 3.8: Capacitor measurement setup, where the expanded view indicates a coaxial connection between the capacitor and the switch circuit. The coaxial cable is modelled as a 75Ω transmission line in simulation.

3.3.2 Capacitor selection

A capacitor of arbitrary value is chosen (29nF). From this choice, the ideal lumped-element model can be simulated directly in the simulation tool, however, the transmission line model requires the calculation of the per-unit length values for inductance and capacitance such that the delay and characteristic impedance values can be provided to the ideal delay-based transmission line model. This is done using Equations 3.2 and 3.3 shown previously; dimensions were calculated based on an FR4-PCB parallel plate available at the time to the researcher — the width existed as 200 mm with a plate separation of 1.5 mm and the length parameter was tuned to achieve the desired capacitance. The calculated values are shown in Table 3.1.

Parameter	Value	Units
C	29.00	nF
L'	9.42	nH/m
C'	5.23	nF/m
ε_0	8.85	-
ε_r	4.40	-
μ_0	1.25	-
μ_r	1.00	-
d	1.50	mm
w	200.00	mm
l	5.55	m
Z_0	1.34	Ω
τ	38.00	ns

Table 3.1: Transmission line capacitor parameters

Importantly, the required delay of this specific parallel plate capacitor (transmission line) is 38ns, which is longer than the rise- and fall-time of the step input signal (25ns). Recall that this is the key requirement for the transmission line model to be needed for modelling.

3.4 Validation

The following section will compare the simulation results to the measured results for both the lumped-element and transmission line models. The results will be compared in terms of the voltage across the capacitor. The results will be compared for both an electrically small and electrically large capacitor.

3.4.1 Electrically small capacitor

The first capacitor to be tested is an electrically small capacitor. The capacitor is placed in the test circuit described in Section 3.3.1 and the voltage across the capacitor is measured. For the electrically small capacitor, a simple ceramic capacitor was used for the physical measurement. The results are shown in Figure 3.9.

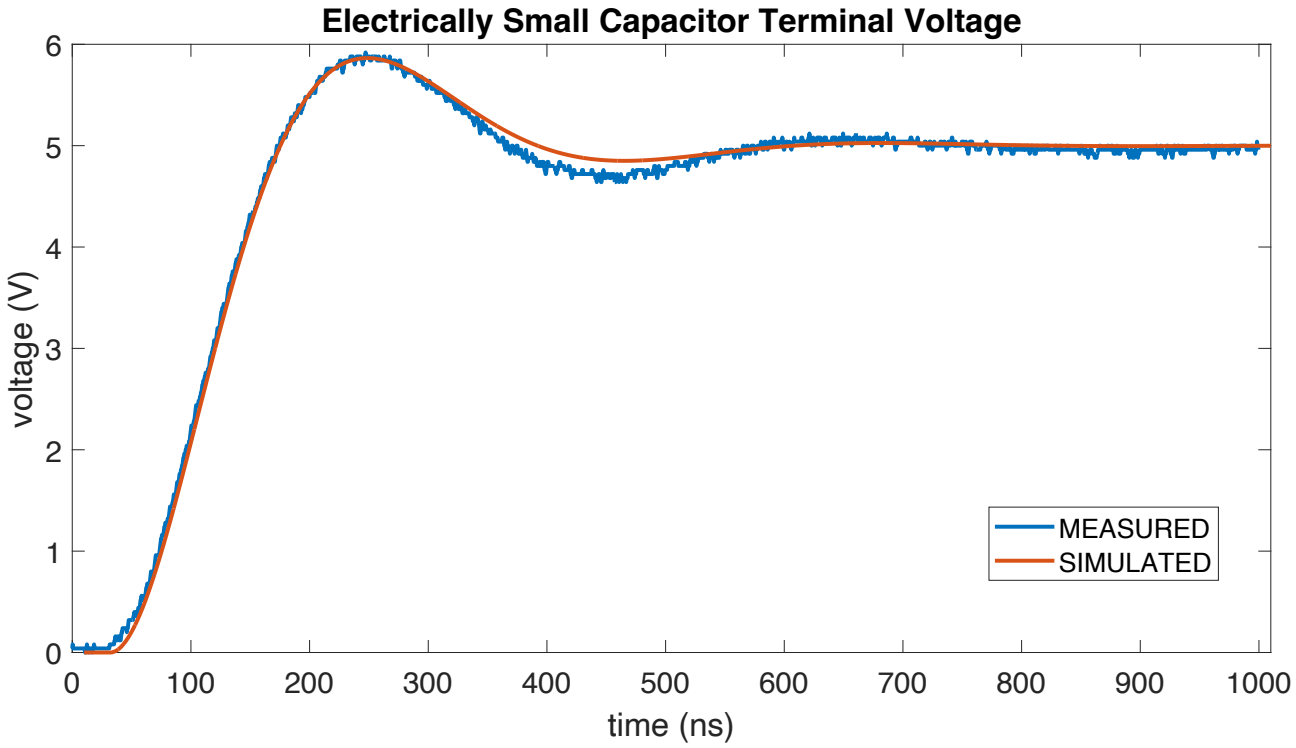

Figure 3.9: Electrically small capacitor verification

What is evident is that for an electrically small capacitor, the simulation matches the measured results almost exactly. This is to be expected as the lumped-element model is sufficient for modelling the behaviour of the electrically small capacitor. While charging, it is seen that there is an oscillation on the voltage across the capacitor. This is due to the inductance of the coaxial cable in conjunction with the source resistance and inductance creating an LC oscillation. This effect is expected, as predicted by the simulation tool.

3.4.2 Electrically large capacitor

The second capacitor to be tested is an electrically large capacitor. The capacitor is placed in the circuit and the voltage across the capacitor is measured. The electrically large capacitor

dimensions were detailed in Table 3.1, and the capacitor is modelled in simulation as an ideal delay-based transmission line. The results are shown in Figure 3.10.

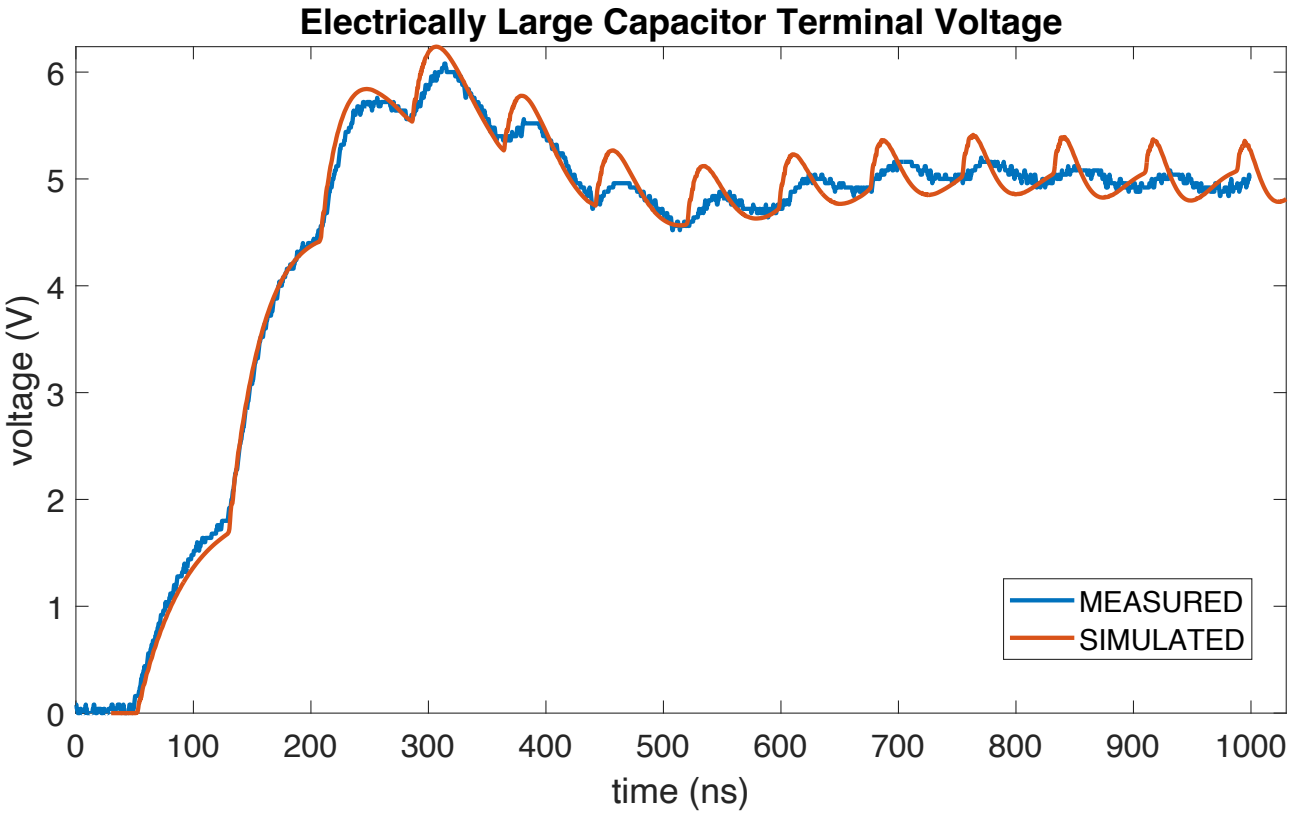

Figure 3.10: Electrically large capacitor verification

Immediately there is a departure from the electrically small results shown previously. Due to the size of the capacitor compared to the rise- and fall-times, we see that here are effects or 'bumps' on the voltage waveform. These are distributed effects, and are caused by the reflections of the voltage and current waveforms operating within the capacitor (or transmission line).

3.4.3 Comparison of electrically small and large capacitor results

For completeness, a comparison of the electrically small and large capacitor results is shown in Figure 3.11.

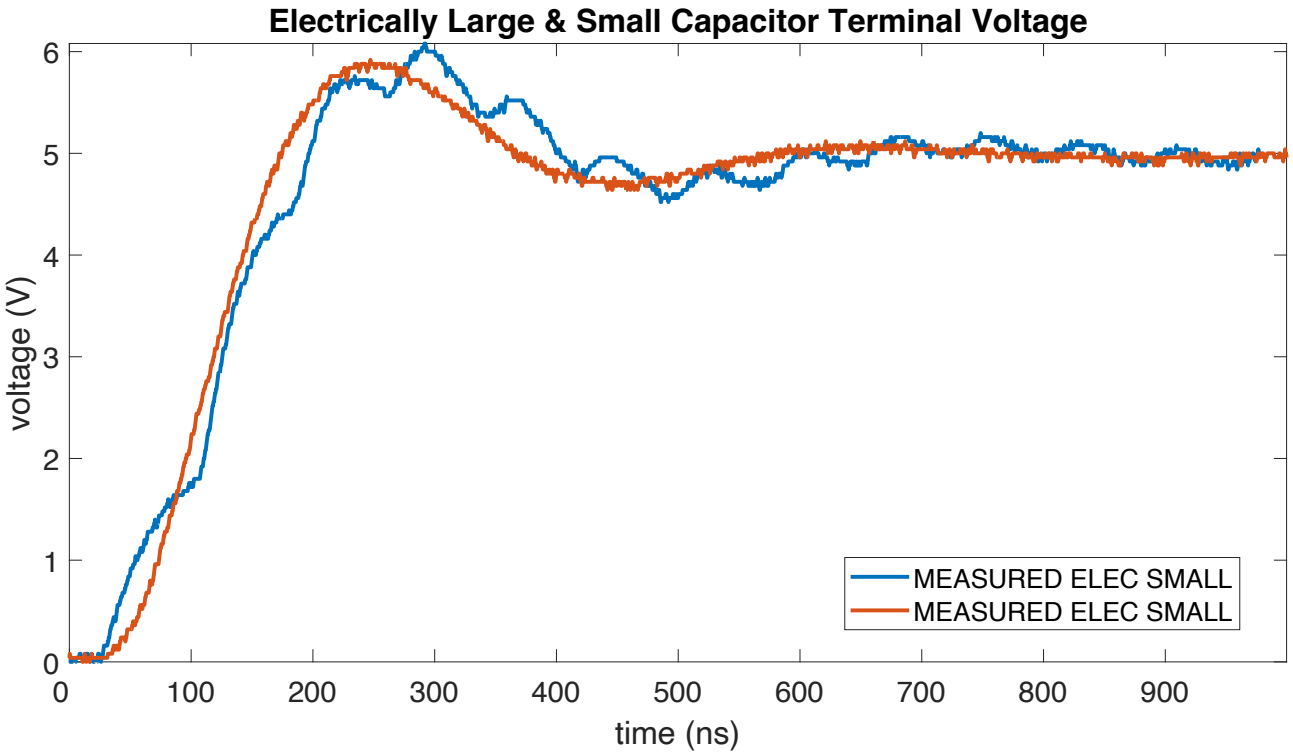

Figure 3.11: Electrically small vs large capacitor verification

3.4.4 Discussion

The results shown in Figure 3.9 and Figure 3.10 show that the simulation results are in good agreement with the measured results for both the electrically small and electrically large capacitors. This is important as it validates the simulation environment's ability to model the behaviour of the capacitor using both the lumped-element and transmission line models in simulation and experimentally. There is therefore confidence for the simulation environment to be used to model more complex configurations of transmission line models in subsequent chapters.

3.5 Transmission line model for an inductor

Similarly to the previous section on capacitors; This section is going to focus on examining a simple loop inductor from two distinct viewpoints. The first viewpoint takes on the conventional circuit theory method, or what's termed the 'lumped-element model'. The second viewpoint adopts the transmission line method. Like before, the lumped-element model will be demonstrated to lack the ability to consider the signal transit time within the inductor. Whereas, the transmission line model successfully accounts for this with the trade-off of being more complex to model.

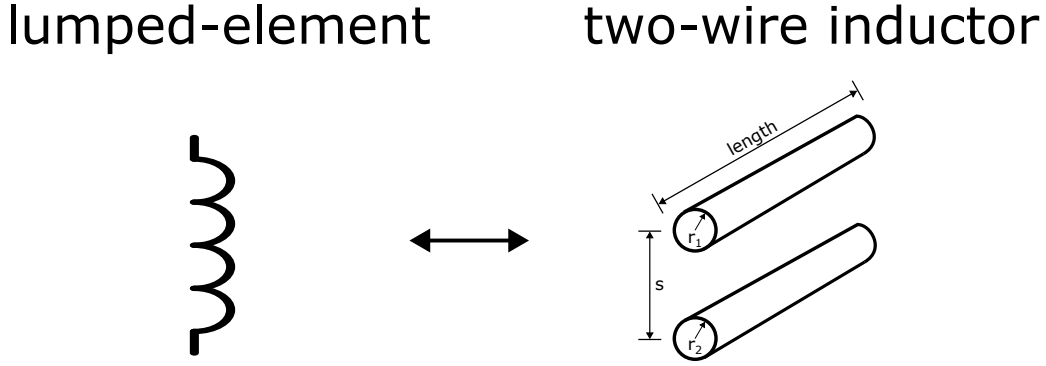

Figure 3.12: Lumped element model of a basic parallel wire inductor

3.5.1 Lumped-element model

The simplest lumped-element model for an inductor views the inductor as having two parallel wires, much like the parallel plates in a capacitor, separated by a material that affects its inductive properties. Between any two wires excited by a source, there exists an inductance. This inductance is a function of the wire's geometry and the medium between the wires. This is commonly referred to as the self-inductance of the wire. For a given set of parallel wires with a length l, radius a, and a distance d between the wires' centres, the self-inductance of the wire can be calculated using Equation 3.6 [20]. In the lumped-element model, similar to the previous section, we assume that the current flow along the wires is even and immediate, and therefore any effects due to the time it takes current to travel through the component is ignored.

$$L = \frac{l\mu_0\mu_r}{2\pi} \cosh^{-1}\left(\frac{s^2 - {r_1}^2 - {r_2}^2}{2r_1r_2}\right) \tag{3.6}$$

3.5.2 Transmission line model for an inductor

As before, when it becomes essential to consider the transit time of signals, the transmission line model becomes the go-to. For a simple parallel two-write transmission line shown in Figure 3.13, the ideal transmission line model is used to model the inductor.

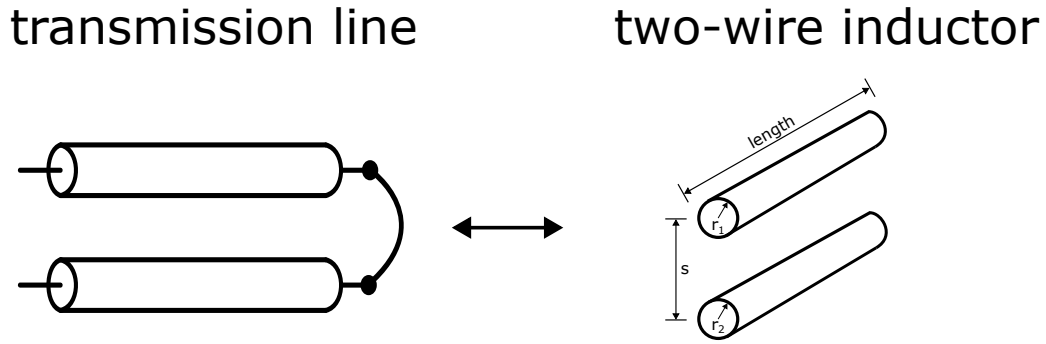

Figure 3.13: Parallel wire transmission line model for an inductor

The transmission line parameters L' and C' are related to the physical construction of the transmission line given by:

$$L' = \frac{\pi \varepsilon_0 \varepsilon_r}{\arccos s/r} \qquad (3.7) \qquad C' = \frac{\mu_0 \mu_r}{\pi} \arccos \frac{s}{r} \qquad (3.8)$$

where:

s = distance between wires' centre
r = wire radius. Both radii are equal
μ_0 = permeability of free space
μ_r = relative permeability
ε_0 = permittivity of free space
ε_r = dielectric relative permittivity

As in the previous section, values for the total inductance (i.e., Equation 3.6) and capacitance of the component can be calculated by multiplying the per-unit length values by the length of the transmission line. Thereafter, the characteristic impedance (Z_0) and delay (τ) of the transmission line are related to the inductance and capacitance of the transmission line as shown in Equations 3.4 and 3.5.

$$Z_0 = \pi \frac{\mu_0 \mu_r}{\varepsilon_0 \varepsilon_r} \arccos \frac{s}{r} \qquad (3.9) \qquad \tau = l\sqrt{L' \cdot C'} \qquad (3.10)$$

where:

l = length of transmission line
L' = inductance per unit length of transmission line
C' = capacitance per unit length of transmission line
s = distance between wires' centre
r = wire radius. Both radii are equal
μ_0 = permeability of free space
μ_r = relative permeability
ε_0 = permittivity of free space
ε_r = dielectric relative permittivity

3.6 Validation of the transmission line model for an inductor by comparing simulation and measured results

Section 3.2 has already established the simulations' efficacy regarding lumped-element simulations, and as such the following section will compare the simulation results to the measured results only for electrically large inductors. Moreover, the same switching circuit and measurement setup will be used as in Section 3.2, with the sole departure being that due to the nature of the parallel lines, there is no need for a connector transmission line as the inductor can be directly connected across the test circuit.

3.6.1 Inductor selection

An inductor of arbitrary value is chosen (36nH). From this choice, the ideal lumped-element model can be simulated directly in the simulation tool, however, the transmission line model requires the calculation of the per-unit length values for inductance and resistance such that the delay and characteristic impedance values can be provided to the ideal delay-based transmission line model. This is done using appropriate formulas (referred here as needed); dimensions were calculated based on available geometries to the researcher at the time. The calculated values are shown in Table 3.2.

Parameter	Value	Units
L	36.00	nH
C	69.61	pF/m
L'	2.40	μH/m
C'	4.64	pF/m
Z_0	718	Ω
τ	50	ns
ε_0	8.85	-
ε_r	1	-
μ_0	1.25	-
μ_r	1.00	-
length	15.00	m
distance (s)	300.00	mm
radius (r)	0.75	mm

Table 3.2: Transmission line inductor parameters

In order to test the component, inductor models will be charged and discharged using a square-wave source of known impedance connected to a load resistor. Figure 3.14

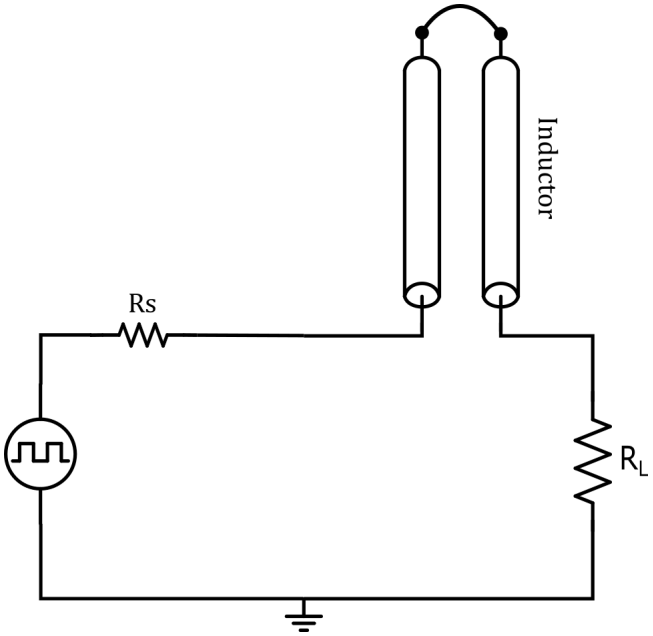

Figure 3.14: Transmission line inductor test circuit

Furthermore, Figure 3.15 shows the physical measurement setup for the inductor. The physical

inductor is constructed using a 1.5mm diameter copper wire separated by wooden spacers at a desired distance to keep the wires parallel. The inductance is then controlled by manipulating the length and distance between the wires as per Section 3.5.2. The inductor is then connected to the test circuit as shown in Figure 3.15.

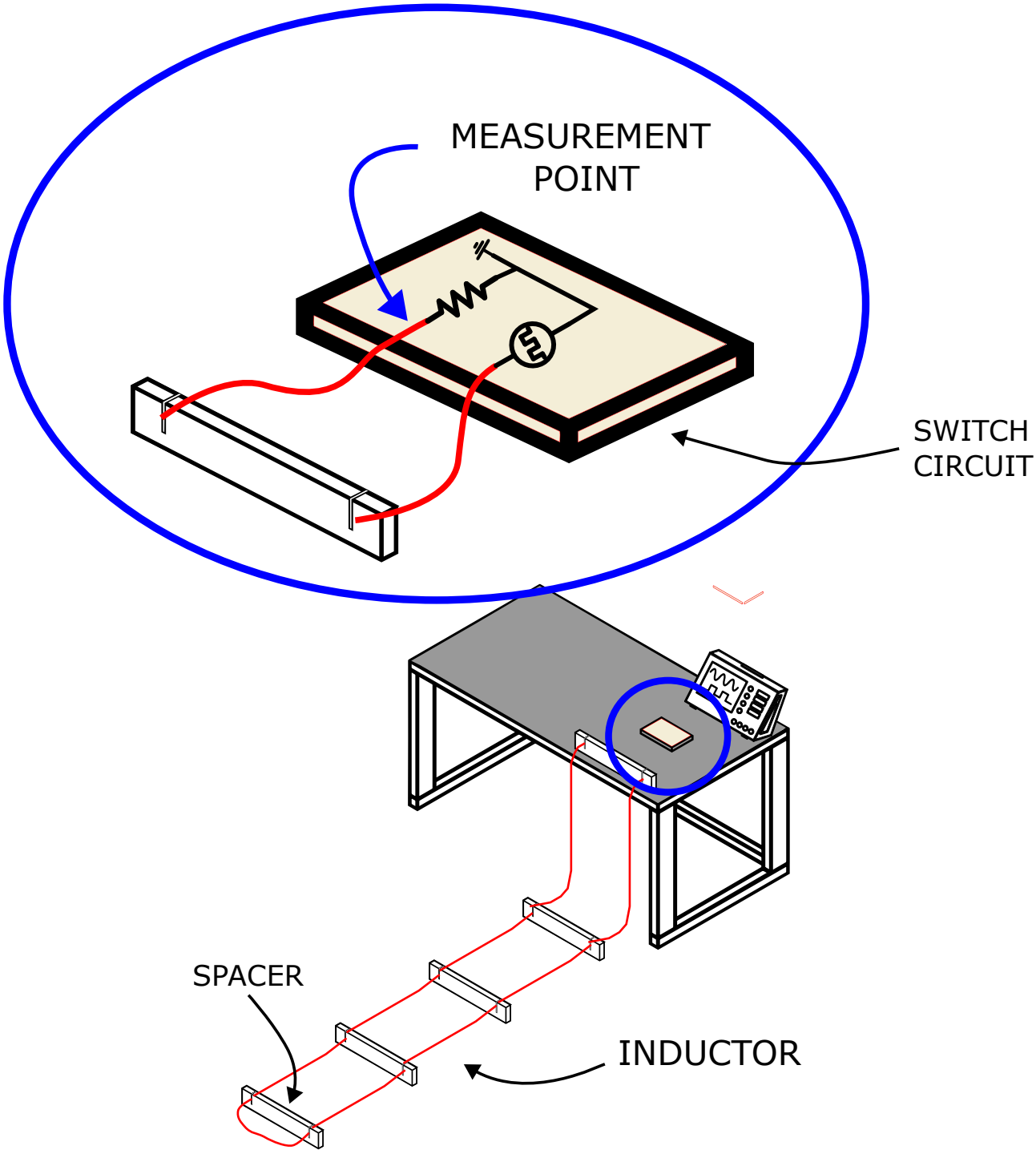

Figure 3.15: Inductor measurement setup

3.7 Electrically large inductor validation

The electrically large inductor dimensions were detailed in Table 3.2, and the inductor is modelled in simulation as an ideal delay-based transmission line. The experimental results were then compared with simulation findings and the results are shown in Figure 3.16. While not perfectly aligned, the results are in good agreement with each other for the purposes of this study.

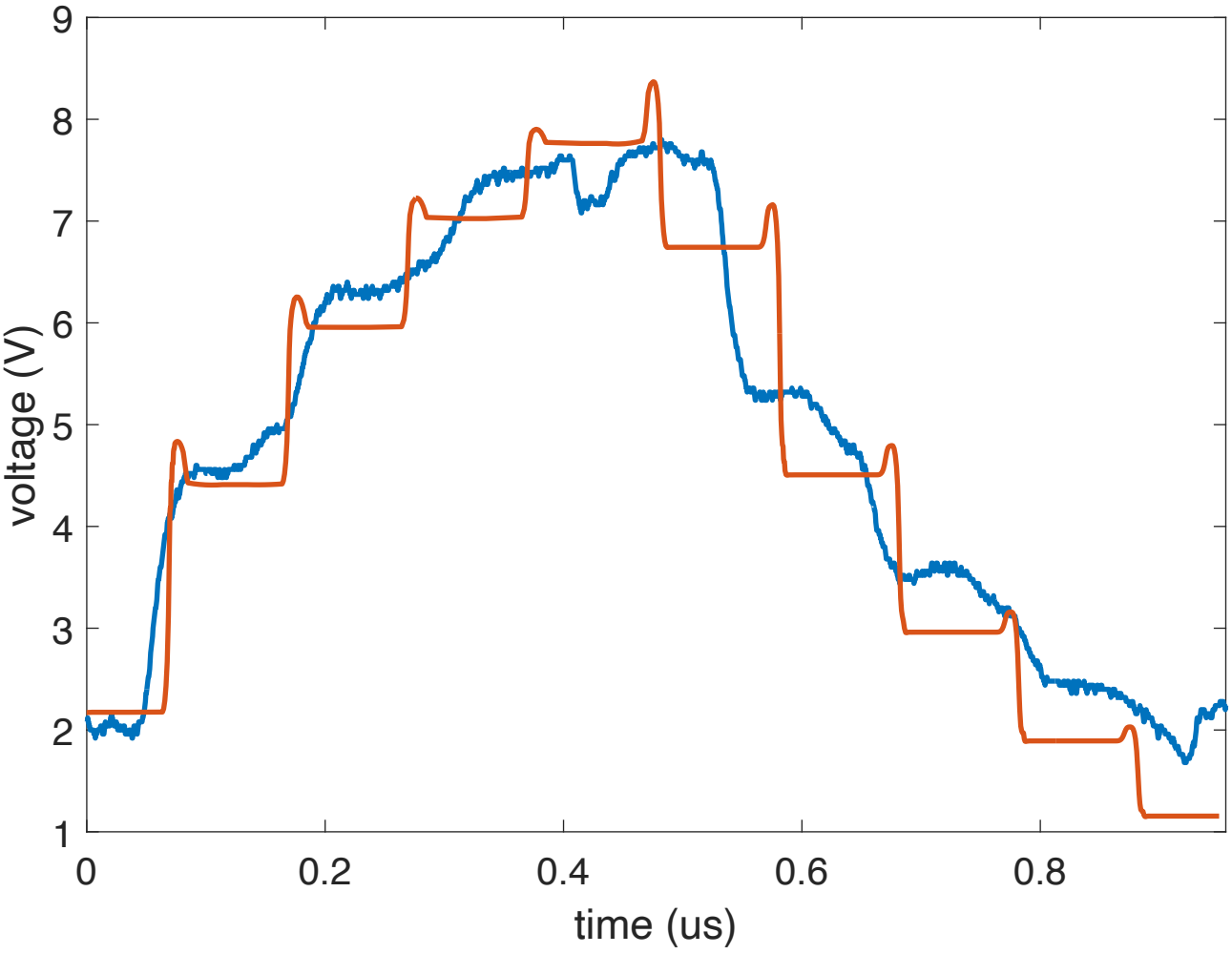

Figure 3.16: Electrically large inductor verification

3.7.1 Discussion

The results shown in Figure 3.16 show that the simulation results are in good agreement with the measured results for electrically large inductors. This validates the simulation environment's

ability to model the behaviour of the inductor transmission line models in simulation and experimentally. There is therefore confidence for the simulation environment to be used to model more complex configurations of transmission line models in subsequent chapters, in conjunction with the work done previously on capacitors.

Chapter 4

Buck Converter

A central part of this research is using the theory established in Sections 3.2 and 3.5 and applying them to a power-electronic circuit in aims to gain understanding of the effects of transmission line components in such circuits. A buck converter is chosen; its design, component substitution, simulation and experimental results will be presented in the following chapter. It is worth noting that any switching circuit would do fine, however in this study a buck converter was chosen.

A basic, idealized buck converter is presented in Figure 4.1. This circuit will be used and transformed in other portions of the research and are all based on the circuit and design principals outlined within this section.

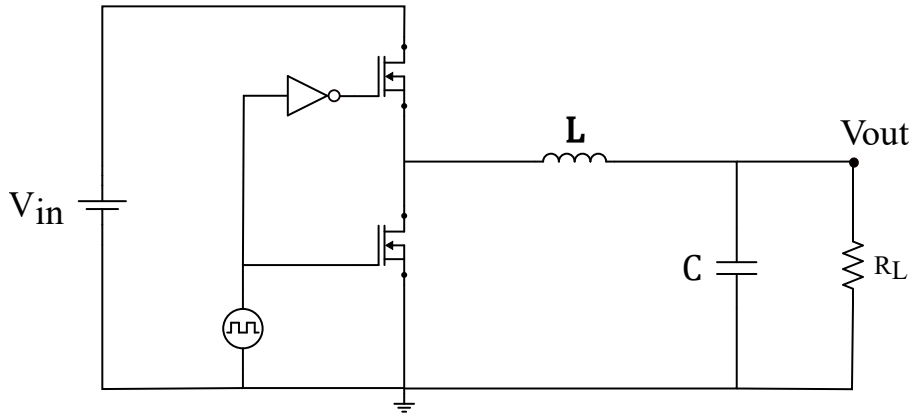

Figure 4.1: Synchronous Buck converter

4.1 Buck Converter Design

The parameter selection of the buck converter will be based on the volt-second principal within the inductor and the charge balance of the capacitor for designing the DC-DC switching circuit [21].

With reference Figure 4.1, the operation of the buck converter is split into two sub-intervals 1 and 2 shown in Figure 4.2. Interval 1 when the switch is closed on position 1 (high-side MOSFET is 'on'), and 2 when it closed on position 2 (low-side MOSFET is 'on').

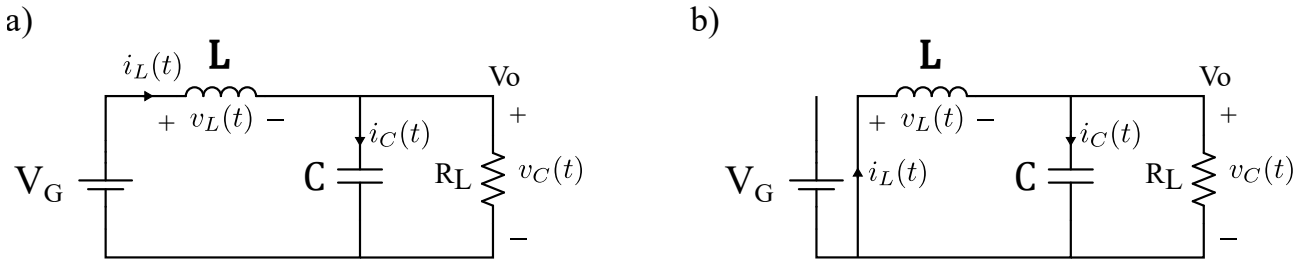

Figure 4.2: Buck converter circuit: (a) while the switch is in position 1, (b) while the switch is in position 2

During each sub-interval in order to specify components according to the desired ripple magnitudes, we make the assumption that the ripple amplitude on both the voltage and current waveforms is small enough to where we can assume that the converter output voltage $v(t)$ and output current $i(t)$ can be approximated by their DC component. This is known as the *small-ripple approximation* and has been long deemed a good method of designing converters as it removes many complexities [21].

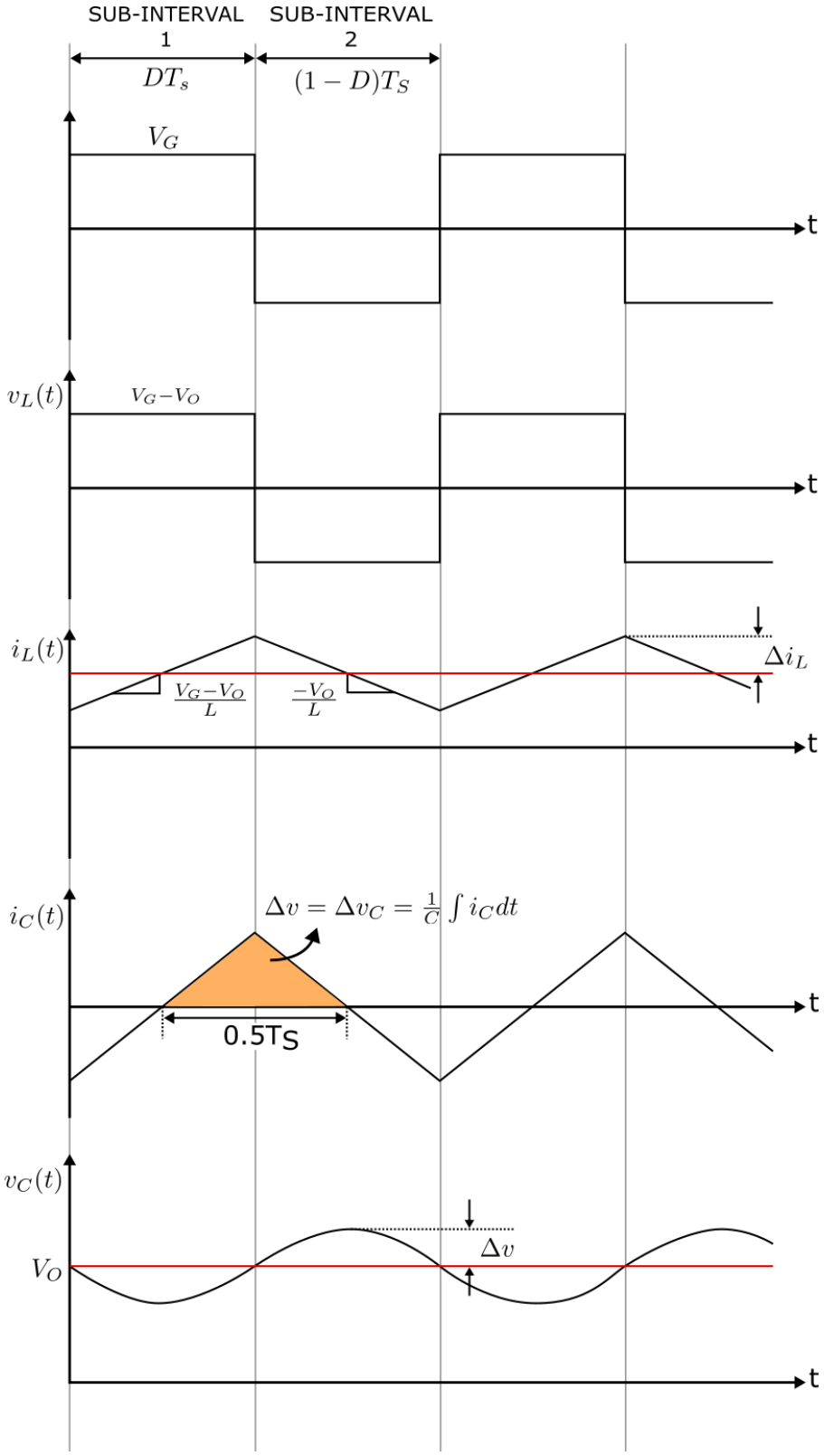

Figure 4.3: Buck converter timing waveforms

Figure 4.3 contains all major steady-state waveforms occurring across the buck converter over the switching cycle T_S. During the first sub-interval (DT_S), the voltage across the inductor is $V_G - V_O$ with its current $i_L(t)$ increasing with a gradient of $\frac{V_G - V_O}{L}$. As per Figure 4.3 the ripple across the inductor can be calculated graphically.

$$\Delta i_L(t) = \frac{V_G - V_O}{2L} \cdot DT_S \tag{4.1}$$

Equation 4.1 can then be rearranged to yield the inductor value:

$$L = \frac{V_G - V_O}{2\Delta i_L(t)} \cdot DT_S \tag{4.2}$$

Applying the principal of *capacitor charge balance* [21] - where the average current through the capacitor is zero over T_S, it can be seen that the capacitor voltage ripple $\Delta v_c(t)$ magnitude is the integral of the capacitor current $i_c(t)$ over either it's positive or negative half cycle yielding equation 4.4.

$$\Delta v_C = \frac{1}{C} \int i_C(t) dt \tag{4.3}$$

Equation 4.3 can be evaluated graphically as shown in Figure 4.3. Using the knowledge that the capacitor current is simply the inductor current less it's DC component, the capacitor ripple magnitude Δv_C is calculated to be:

$$\Delta v_C = \frac{\Delta i_L}{4C} \cdot T_S = \frac{\Delta i_L}{4fC} \tag{4.4}$$

Equation 4.4 can then be rearranged to yield the capacitor value:

$$C = \frac{\Delta i_L}{8f\Delta v_C} \tag{4.5}$$

4.1.1 Simulation of a buck converter

A buck converter is presented, operating under continuous conduction mode (CCM) at 1MHz with a duty cycle of 50%. Table 4.1 summarizes the converter operational parameters.

Parameter	Value	Unit
V_G	10	V
V_o	5	V
I_o	1	A
f_{sw}	1000	kHz
duty	0,5	1
Δv_C	150	mV
Δi_L	30	mA

Table 4.1: Buck converter variables

Based on Table 4.1, the equations 4.2 and 4.5 can be solved to yield the following values for the inductor and capacitor:

$$L = \frac{5}{2 \cdot 0.030 \cdot 1 \times 10^6} = 36\mu H \qquad C = \frac{0.030}{8 \cdot 1 \times 10^6 \cdot 0.15} = 29nF$$

Verification of the design equations is done through simulation. Figure 4.4 shows the output of an LTSpice simulation of the buck converter designed above. The output voltage is correctly around the desired 5V value and is within the desired ripple values of 150mV and 30mA.

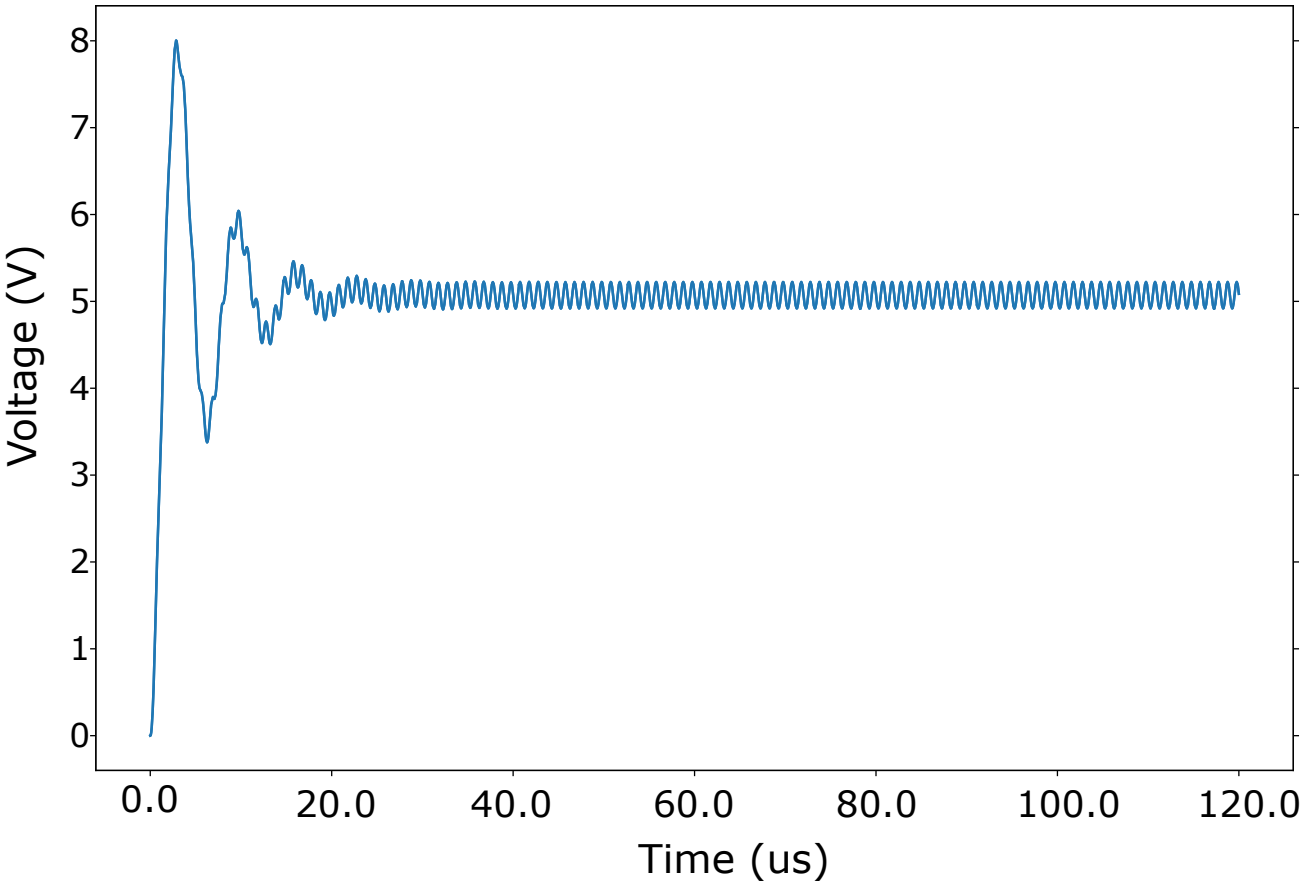

Figure 4.4: Standard buck converter output simulation

4.2 Transmission line based buck converter

For this study, the transmission line based buck converter is simply the standard buck converter from Figure 4.1 where the capacitor and inductor is replaced with equivalent transmission line components. Specific derivations were previously outlined in Sections 3.2 and 3.5.

(a) Inductor TLM substitution

(b) Capacitor TLM substitution

Figure 4.5: Reactive components replaced with transmission lines

$$Z_0 = \sqrt{\frac{L'}{C'}} = \sqrt{\frac{L}{C}} \qquad \tau = l\sqrt{L'C'} = \sqrt{LC}$$

Where Figure 4.1 shows the standard buck converter, Figure 4.6 shows the TLM buck converter.

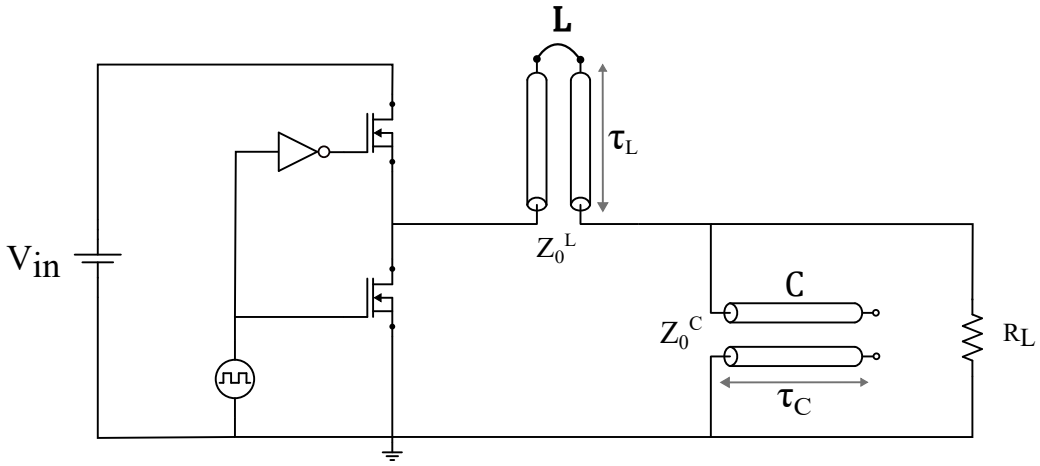

Figure 4.6: Transmission line based buck converter

4.2.1 Simulation of a transmission line based buck converter

A 5V transmission line based buck converter is designed according to the methodology outlined in Section 4.1. For comparison, the same values are used from Table 4.1, with the transmission line variables calculated. The component values are tabulated in Table 4.2.

Parameter	Value	Unit
V_{in}	10	V
V_{out}	5	V
I_{out}	1	A
f_{sw}	1000	kHz
duty	0,5	1
Δv_C	150	mV
Δi_L	30	mA
L	36	μH
C	29	nF
Z_0^C	1.35	Ω
Z_0^L	719	Ω
τ_C	39	ns
τ_L	50	ns

Table 4.2: TLM based buck converter variables

The buck converter shown in Figure 4.6 is simulated in LTSpice using the parameters chosen in Table 4.2. The simulation results are shown in Figure 4.7 for the full output waveform, with Figure 4.8 showing an expanded portion between $80\mu s$ and $90\mu s$.

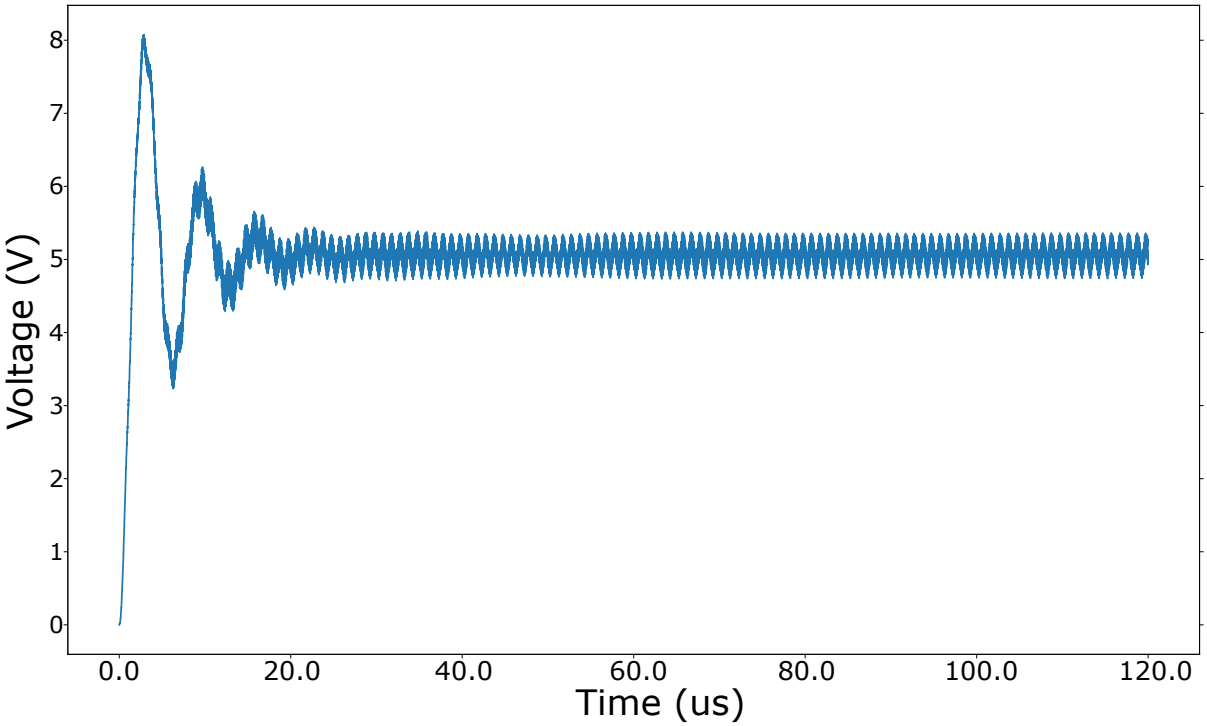

Figure 4.7: Transmission line buck converter simulation

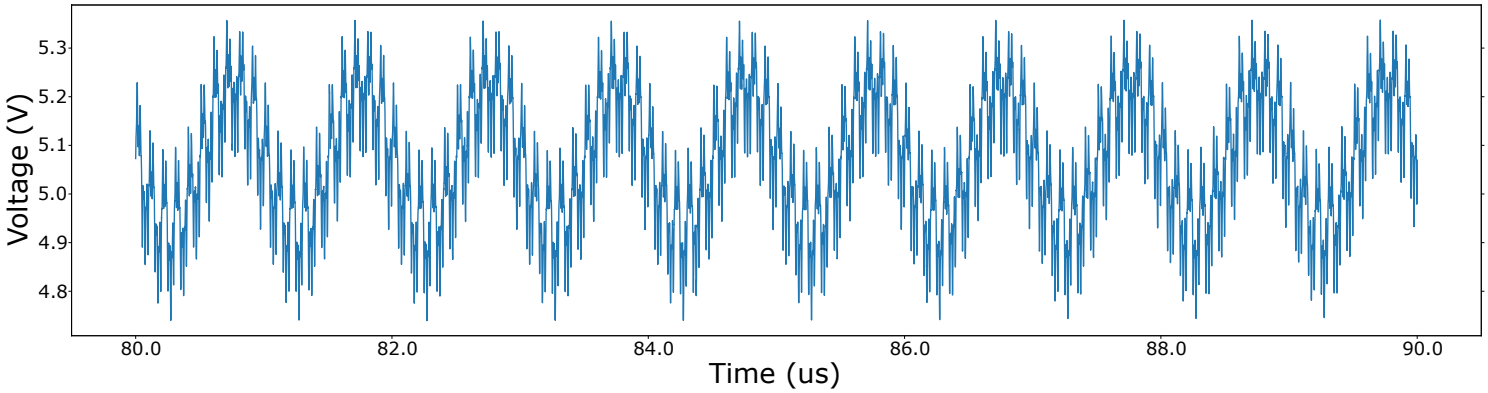

Figure 4.8: Transmission line buck converter simulation zoomed

The simulation results from the transmission line buck converter and the standard buck converter are compared in Figure 4.9. What is immediately apparent is that the overall operation

of the transmission line buck converter is in good agreement with the standard buck converter, with the mean and ripple values within acceptable limits.

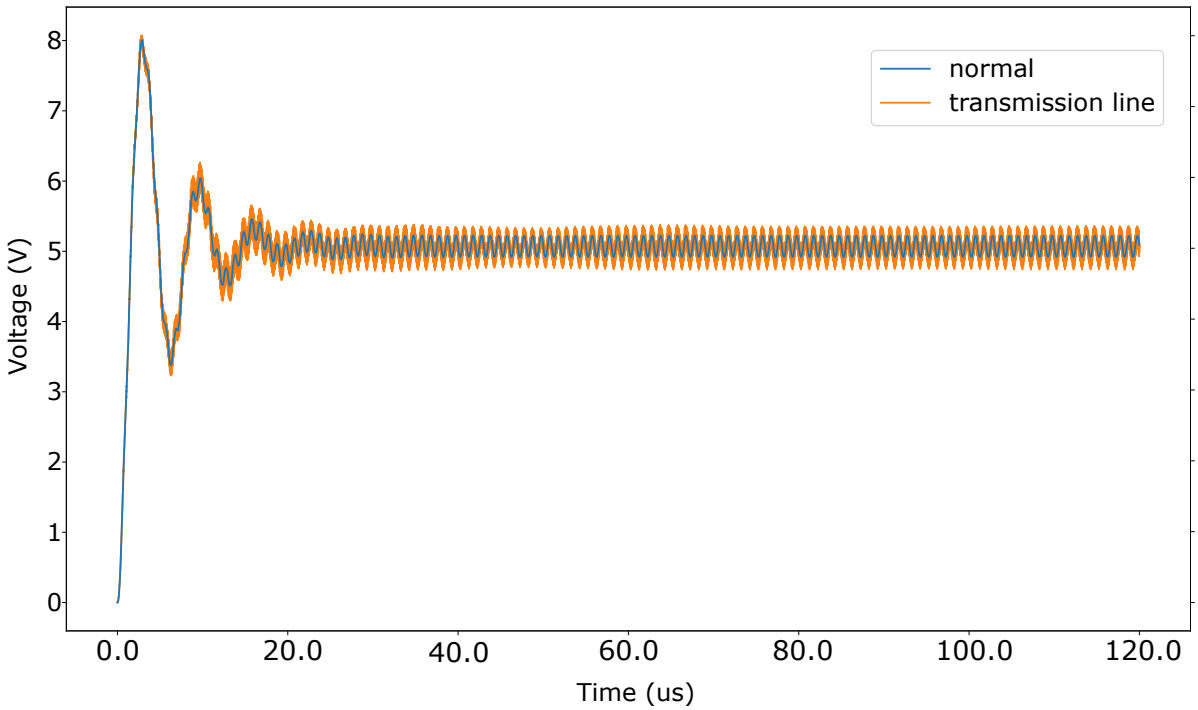

Figure 4.9: Transmission line buck converter simulation vs standard buck converter simulation

Figure 4.10 shows an expanded in view of the transmission line buck converter and the standard buck converter between $80\mu s$ and $90\mu s$. It is shown that the transmission line converter does contain additional high frequency effects superimposed onto the typical output ripple. These high frequency effects are believed to be the result of the transmission line components, and will be the focus of this study.

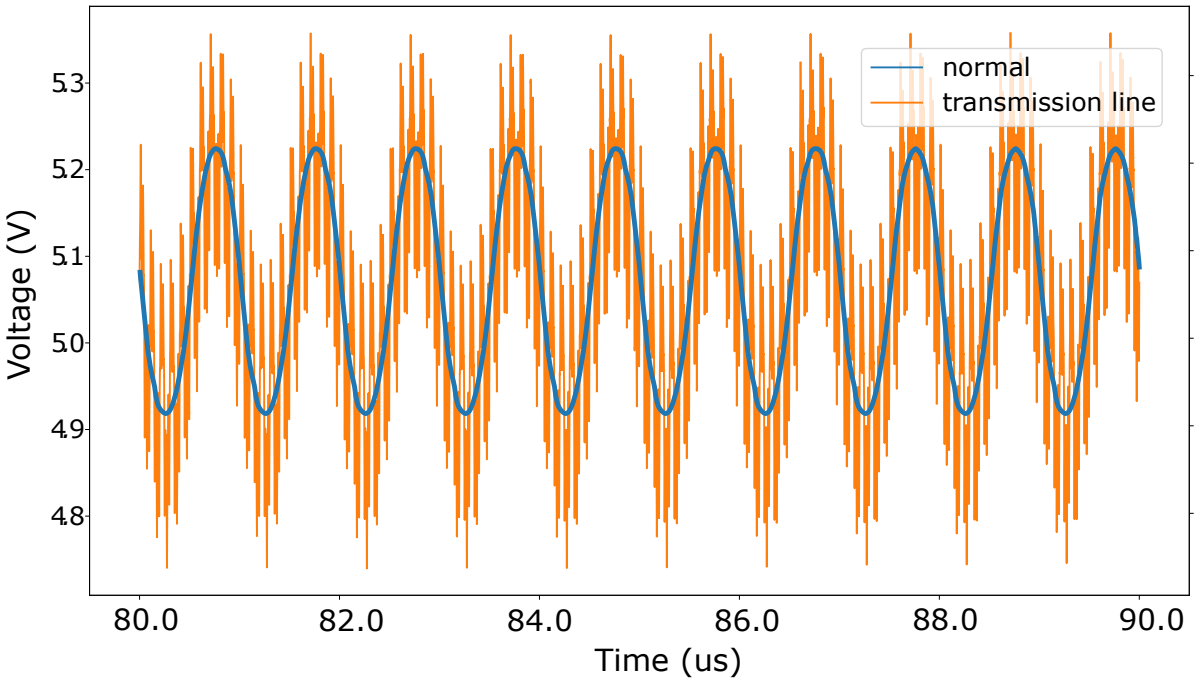

Figure 4.10: Transmission line buck converter simulation vs standard buck converter simulation zoomed

4.2.2 Experimental results of a transmission line based buck converter

A substantial goal of this research is prove that a transmission line based buck converter is a valid concept. To this end, a physical transmission line buck converter was built and tested where component values were chosen according to Table 4.2. With regards to the physical construction of the capacitor and inductor transmission lines, the same construction techniques and material choices were used as outlined in Section 3.2 and Section 3.5.

Physical construction of inductor and capacitor transmission lines

For the $36\mu H$ inductor, the resultant equivalent two-wire transmission line stub is a pair of 0.75mm diameter parallel wires separated by 30cm for 15m in length. This achieves a 50ns delay time at 719Ω characteristic impedance, satisfying the requirements of Table 4.2. The two wires are kept at a consistent separation distance using a wooden spacer with two slots carved 30cm apart to hold the wires in place. Specific care was taken to isolate the parallel wires from any external metal planes, objects and other wires to ensure that the transmission line had a best possible chance to avoid external interference. Of course avoiding all external interference

is not possible - such as antenna affects, but the goal was to minimize it as much as possible. Figure 4.11 shows the physical construction of the inductor transmission line.

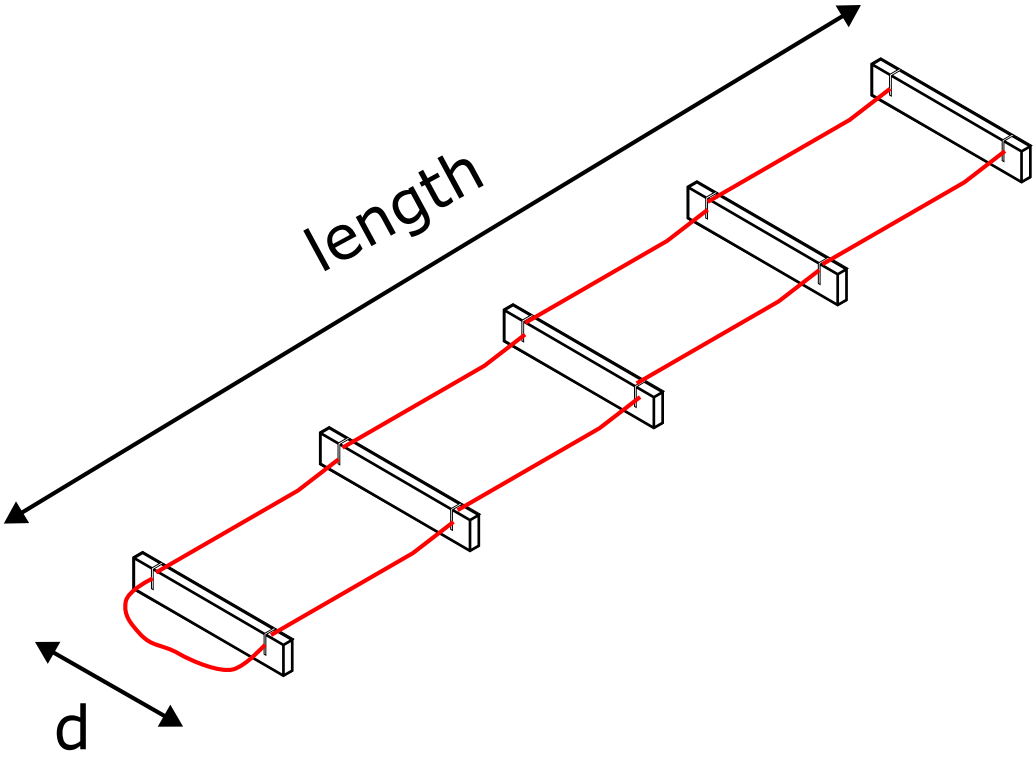

Figure 4.11: Physical construction of the inductor transmission line

In a similar manner, a 29nF parallel plate capacitor transmission line is constructed by using a 1.5mm thick two-sided copper clad PCB of width 200mm and length 5.55m. This achieves a 39ns delay time at 1.35Ω characteristic impedance, satisfying the requirements of Table 4.2. It is uncommon to acquire a PCB sheet with such dimensions, and as such a larger sheet of $2m \times 2m$ was cut appropriately and sheets were soldered together where necessary to achieve the desired length. Care was taken to ensure that the solder joints were as small as possible to minimize any additional effects. Figure 4.12 shows a diagram of the physical construction of the capacitor transmission line.

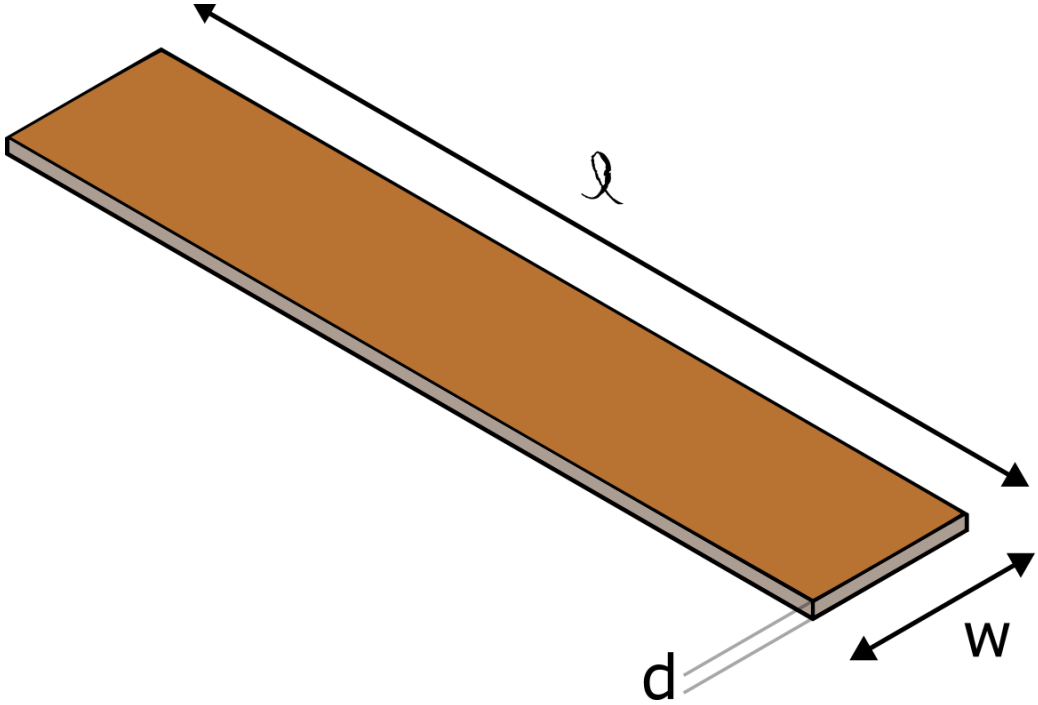

Figure 4.12: Physical construction of the capacitor transmission line

Construction of buck converter switch circuit

The desired buck converter operates at a frequency of 1MHz with very low output current requirements. Along with that, we naturally want the switch to be as simple and as close to an ideal square-wave as possible whilst still begin able to drive the circuit and isolate the PWM controller from the rest of the components. To this end, an off-the-shelf MOSFET driver circuit was determined to be the best choice for this study, in this case the TC426 driver was chosen. The TC426 is a dual MOSFET driver with suitably fast rise and fall times of 25ns. To minimize the output resistance of the switch, six TC426 drivers were driven in parallel with their inputs and outputs tied together. This effectively reduces the output resistance of the switch by a factor of six — which was measured to be 1Ω. The TC426 drivers were driven by a PWM signal from a microcontroller, where the microcontroller was programmed to generate a 1MHz PWM signal with a 50% duty cycle. The TC426 drivers were powered by a 10V supply, with the PWM signal being generated by the microcontroller being powered by a 5V supply with the same ground reference. Throughout this process, emphasis was placed on minimising any unnecessary loop inductances and placing capacitors in optimal positions with relation to the drivers to ensure smooth switching. Figure 4.13 shows the functional diagram of the switch circuit used to create a square-wave source.

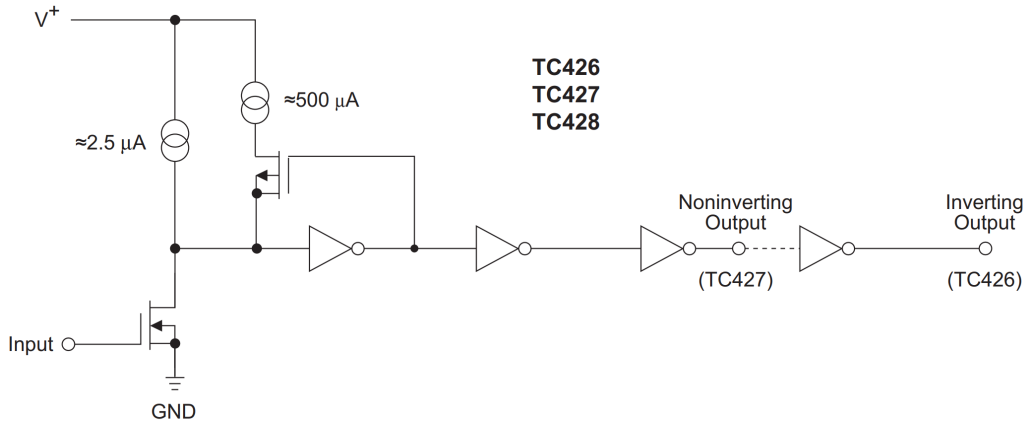

Figure 4.13: Functional diagram of physical switch circuit. Extracted from the TC426 datasheet [19]

Construction of transmission line buck converter

The switch circuit from Figure 4.13 is connected to the transmission line components as per Figure 4.6. Care was taken where possible to minimize unwanted effects. The inductor transmission line is connected directly to the switch and capacitor, with the 100Ω load resistor connected directly across the capacitor transmission line. Ground connections from the capacitor and load with the switch were as short as possible.

A diagram of the macro view of the physical measurement setup and buck converter structure is shown in Figure 4.14.

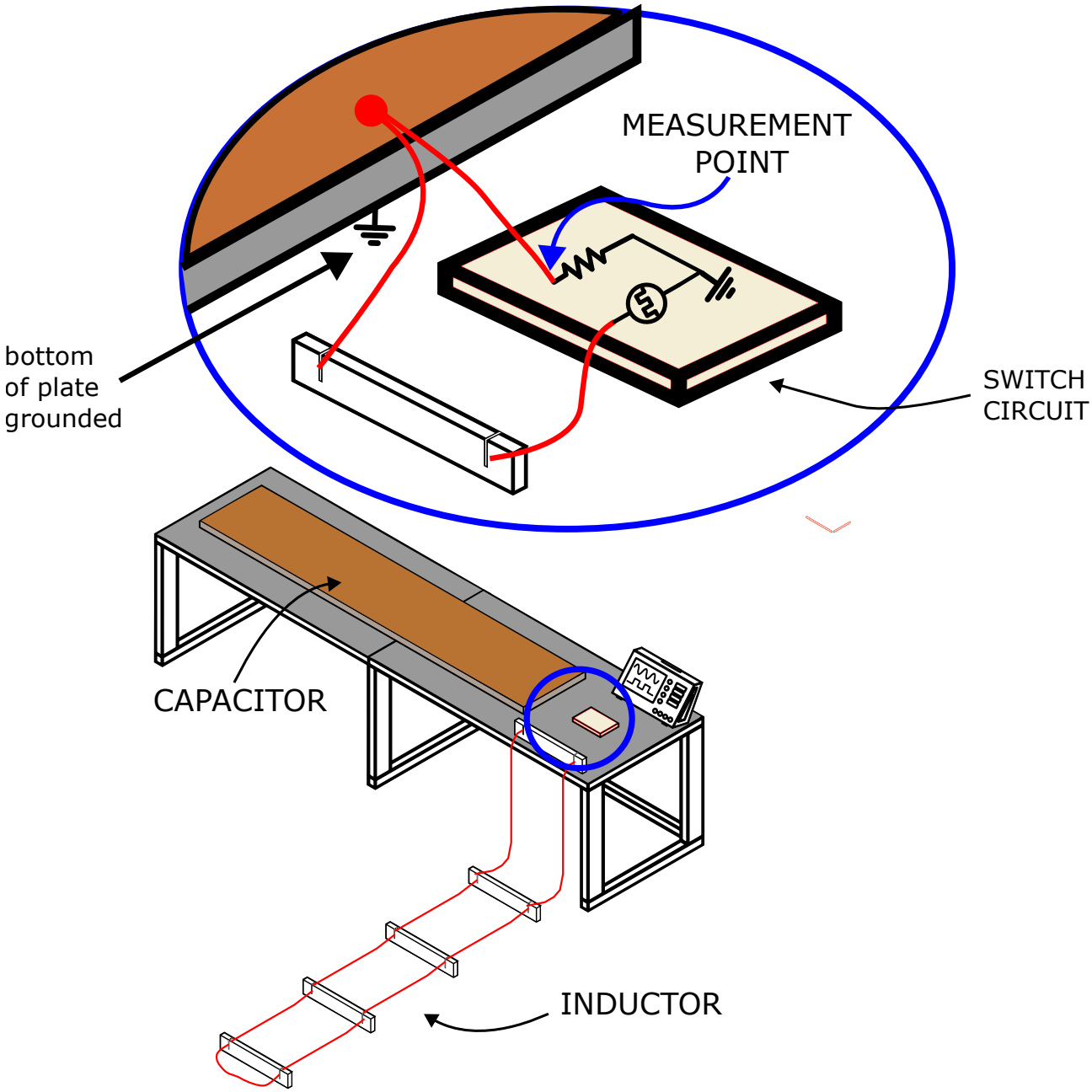

Figure 4.14: Physical TLM buck converter measurement setup

For clarity, a picture of the physical transmission line buck converter components layed out in a laboratory is shown in Figure 4.15. In this photo, the inductor transmission line is visible on the right, and the capacitor transmission line is visible on the left. This photo was taken before the inductor transmission line spacers were added.

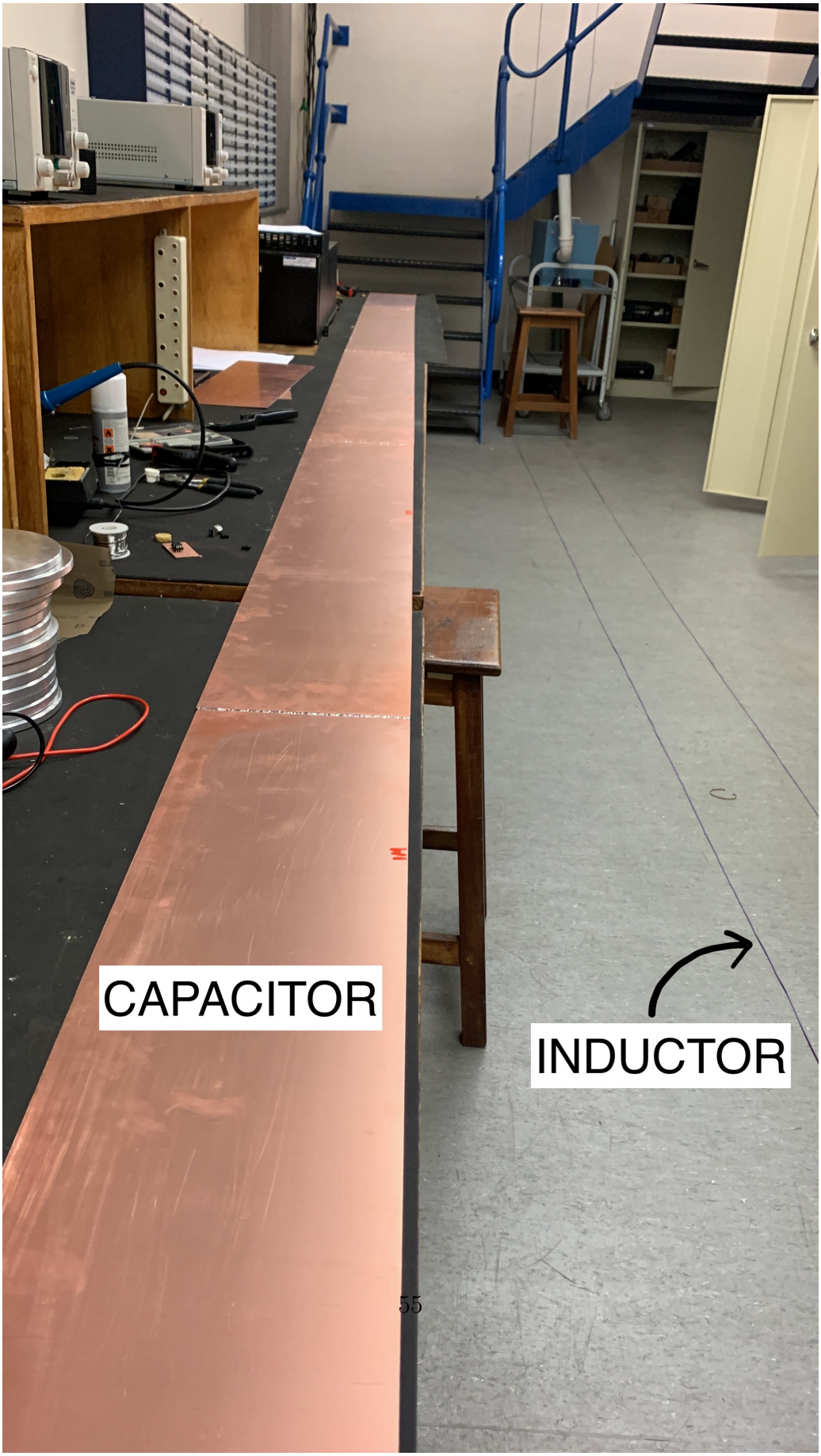

Figure 4.15: Physical TLM buck converter photo

Measured results

The transmission line buck converter was then powered on and results captured. The steady-state voltage output of the TLM buck converter is shown in Figure 4.16.

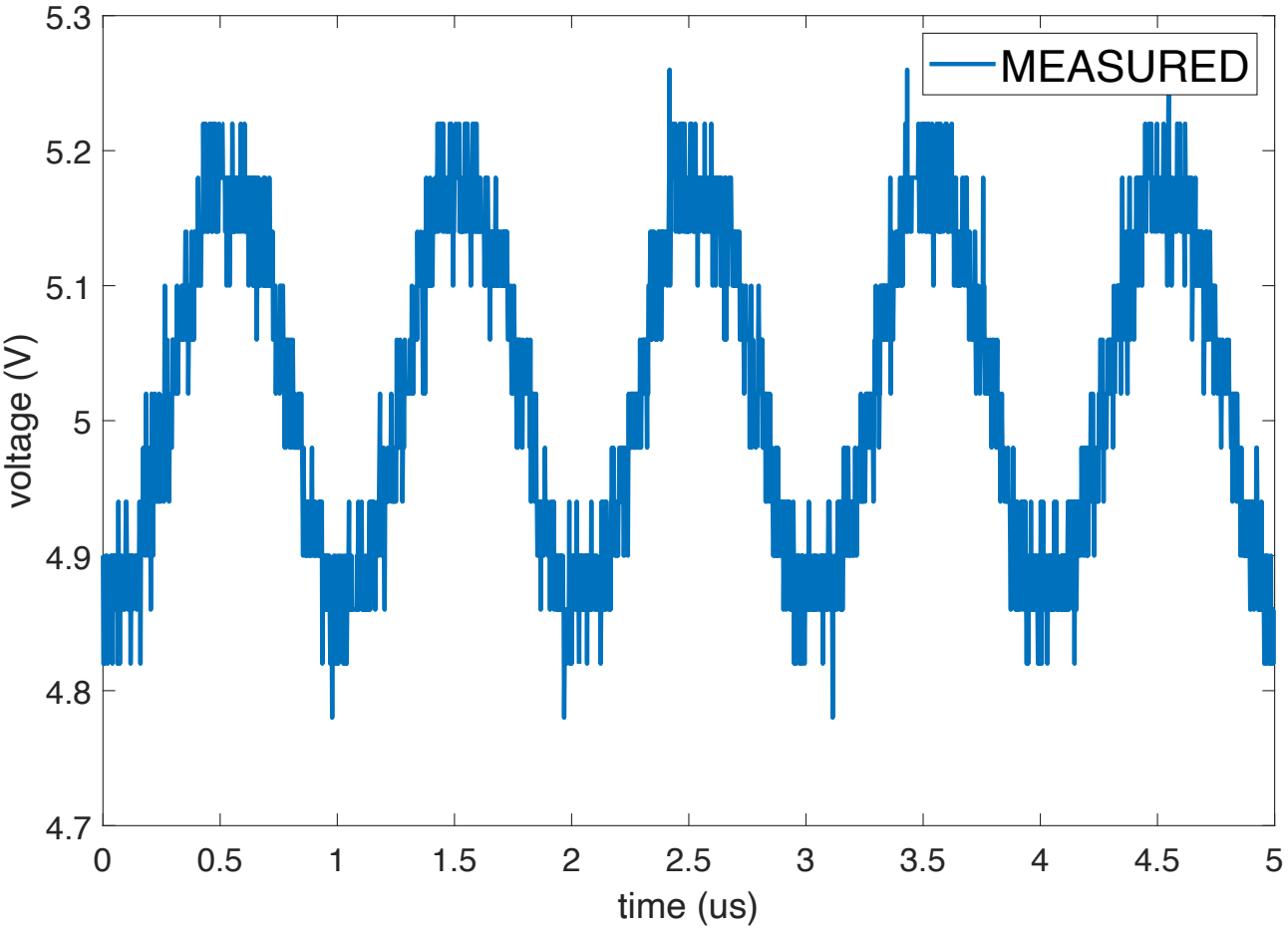

Figure 4.16: Measured transmission line buck converter output

The output is familiar to that seen previously in our simulations of the transmission line buck converter (see sec. 4.2.1).

A comparison between the simulations of the transmission line buck converter and the experimental transmission line converter is shown in Figure 4.17. This figure is interesting, as it shows that the simulation results do indicate the real-world behaviour of the transmission line converter, however we can see from Figures 4.16, 4.17 and 4.18 that the real-world circuit contains significant damping and less erratic behaviour than the simulation. This is likely due to the parasitic effects of the real-world circuit, which are not accounted for in the simulation.

Perfect matching is not expected, but this does show that we can indeed use simulation to predict the behaviour of the transmission line buck converter, and the high-frequency effects are shown to visible in the physical domain too.

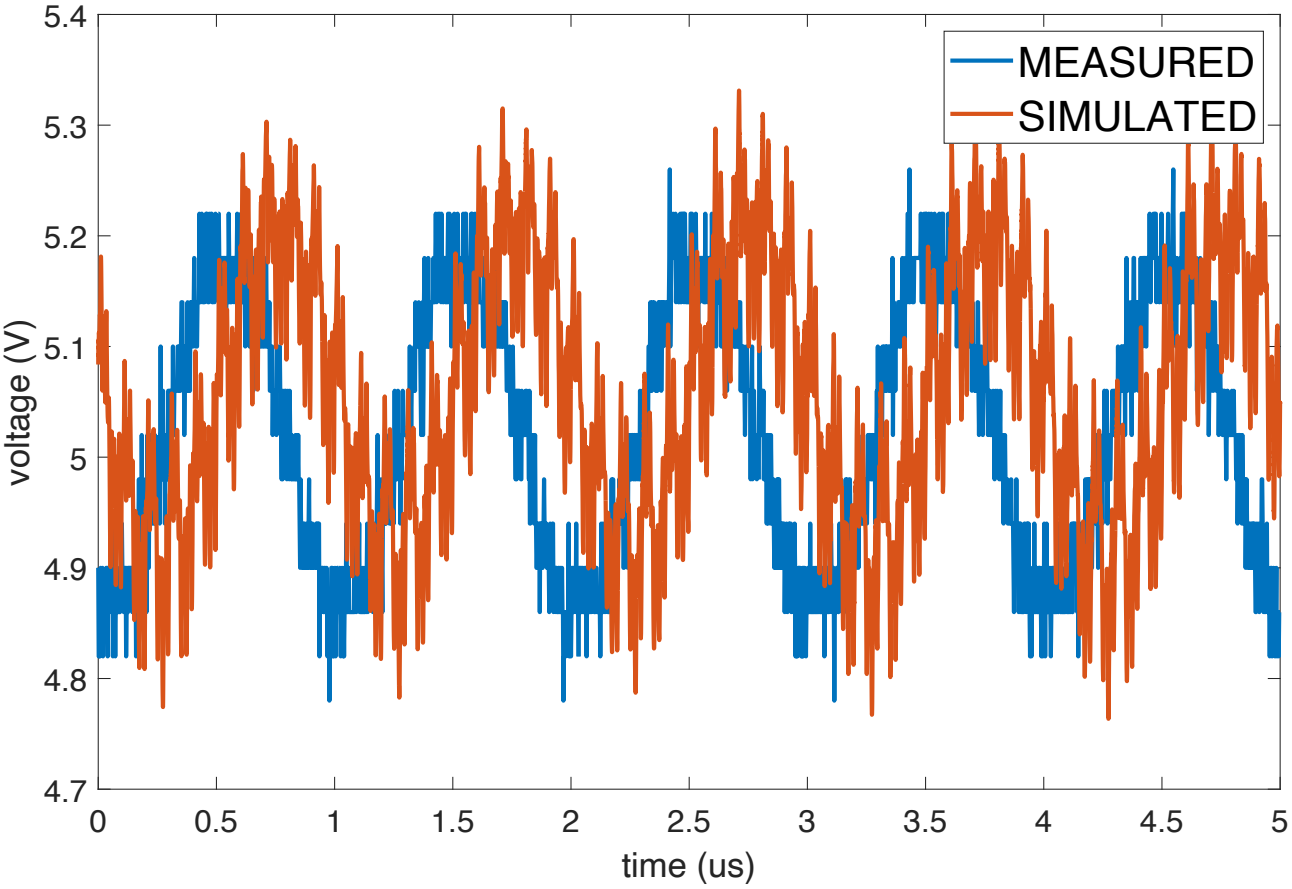

Figure 4.17: Measured transmission line buck converter output vs simulated transmission line buck converter output

Figure 4.18 shows an expanded view of the transmission line buck converter output as Figure 4.17 is difficult to see the high-frequency effects. It is clear that the transmission line buck converter does indeed contain high-frequency effects, and that the simulation results do indeed predict this behaviour to a degree. It is these effects that will be investigated further in the following sections.

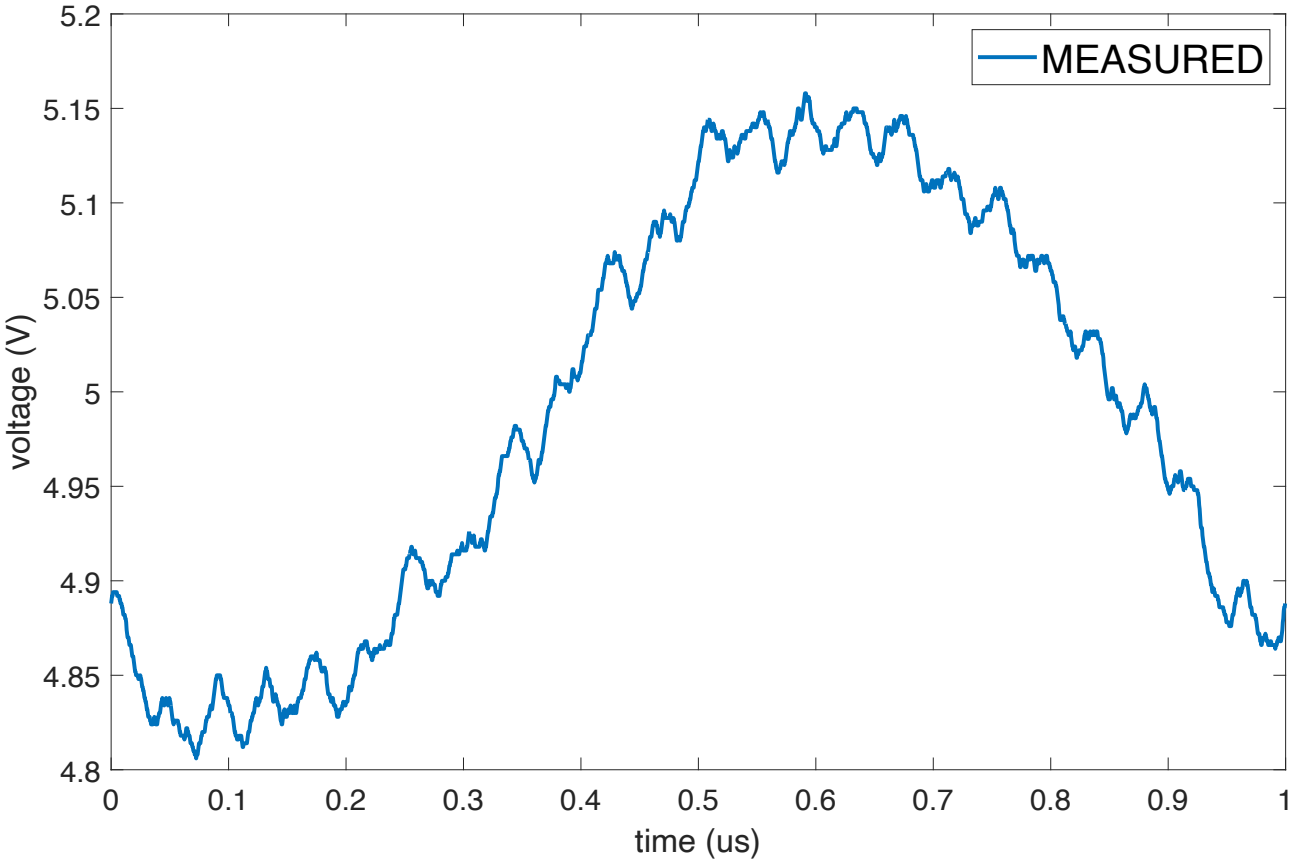

Figure 4.18: Measured transmission line buck converter output zoomed

4.2.3 Discussion

The main points are discussed in this chapter are summarized below:

- A buck converter using normal lumped-element components was designed and simulated. The results of simulation were shown to be within good agreement of the calculated values.
- The lumped-element components were replaced with transmission line based components, and the concept of a transmission line based buck converter was introduced. The transmission line components were designed using the methodology outlined in Chapter 3.
- The transmission line based buck converter was simulated and the results compared with the standard buck converter. The results were shown to be in good agreement with the standard buck converter with regards to overall operation (low-frequency)
- The simulation of the transmission line buck converter exposed additional high frequency effects superimposed onto the typical output ripple. These high frequency effects are

believed to be the result of the transmission line components, and requires further investigation.

- The transmission line buck converter was built and tested experimentally in the physical domain. The results were collated and compared with the simulation results. While the results contained a lot of damping, overall the results were in good agreement with the simulation results and importantly indicated similar high frequency effects as those seen in simulation.

The results of this chapter are important as it shows that the transmission line based buck converter is able to operate in a similar manner to a standard buck converter, albeit with some additional effects arising from the transmission lines. The simulation results compared with experimental findings indicated that simulated results do indicate the real-world behaviour of the transmission line converter, even though simulation data does not perfectly match experimental data.

The high frequency effects arising from the transmission line components are of extreme interest, and require further investigation. Following chapters will focus on investigating these effects.

Chapter 5

High-frequency effects of transmission line components in a buck converter

In this chapter, the high-frequency time-domain effects which arise from the use of transmission line (or electrically large) components in a buck converter are further investigated, with a focus on the experimental results as they compare to simulation predictions. We first saw these effects in Chapter 4 where the output of a buck converter with transmission line components was compared to that of a conventional buck converter. In this section, the output of the TL-based buck converter contained noticeable 'bumps' superimposed on top of the voltage we expect from a buck converter. It is worth emphasising that these bumps were not present in simulations of the buck converter using standard lumped element (or electrically small) component models. These effects naturally stem from the distributed effects outlined in the individual transmission line models in Chapter 3, and as the buck converter uses both inductors and capacitors, we expect to see these effects in both the inductor and capacitor for electrically large components. This section aims to shed some light on the nature of these effects, how they manifest in the output of the buck converter in relation to their respective transmission line components, and how we can quantify them.

The delay parameter of a transmission line component is varied across a number of values and the resulting output waveforms are compared, primarily through visual inspection. It is shown that the delay parameter has a direct impact on the output waveform, specifically in regard to the high-frequency 'bumps' mentioned previously.

5.1 Distributed buck converter for effect investigation

Figure 5.1 shows the annotated circuit diagram of the buck converter chosen to investigate the effects of transmission line components. The derivation for the converter and component substitutions was outlined in prior chapters. This converter with its current values will serve as the baseline converter for the investigation. In later sections, we will be altering values of the transmission line components to investigate the effects of these components, however all

variations will be made relative to the baseline converter shown in Figure 5.1.

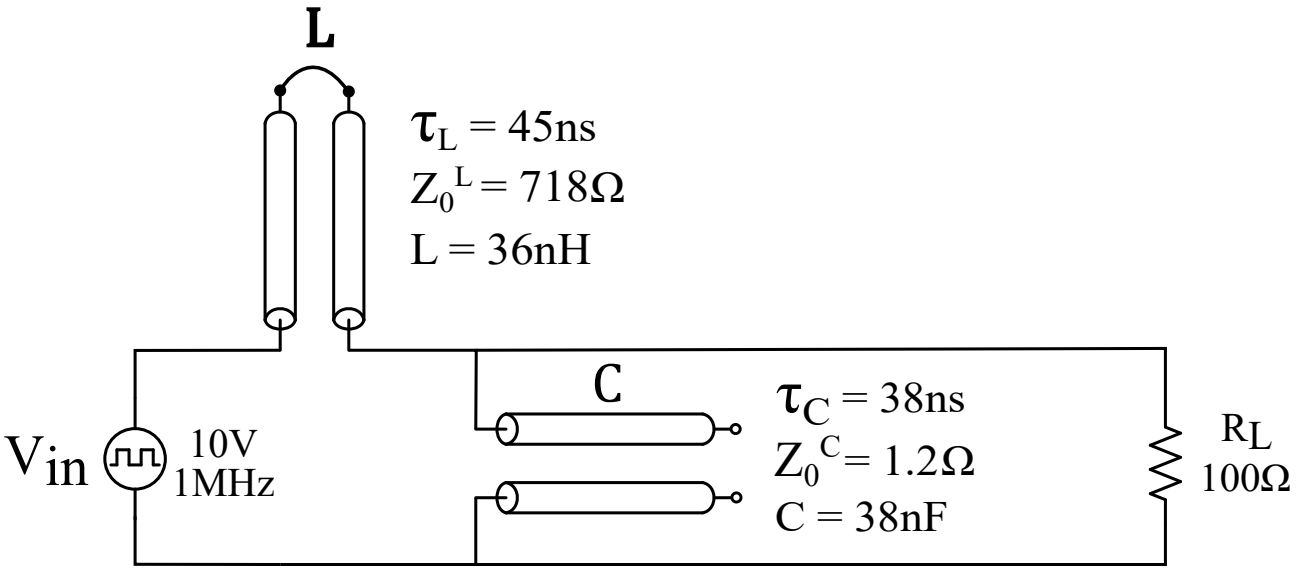

Figure 5.1: Transmission line based buck converter

To clarify exactly what we mean by transmission line 'effects', 'bumps' or 'spikes', it is helpful to look at Figure 5.2, where the area of interest in a simulated output of Figure 5.1 is emphasised.

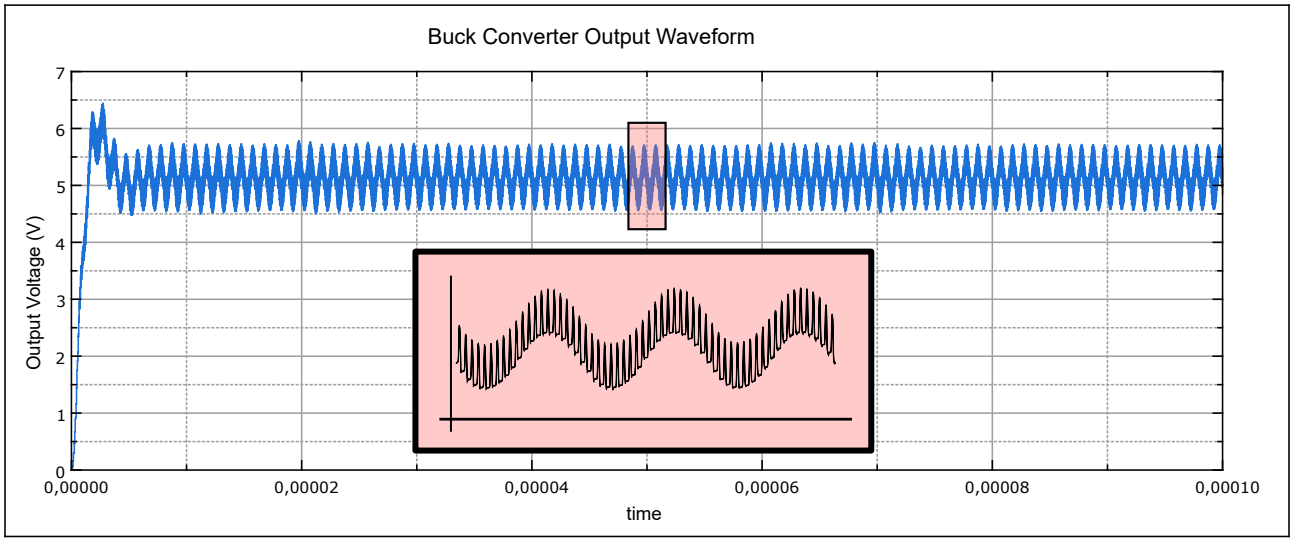

Figure 5.2: Simulated output of TL buck converter showing area of interest

The sine-like oscillation is what we expect from a buck converter in CCM with a frequency of 1MHz (switch frequency). The deviations from that sine-wave are what in this work we refer to

as 'bumps' or 'spikes'; **They are high-frequency time-domain effects which arise from the use of transmission line components in a buck converter. These effects occur at higher frequencies than the fundamental switching frequency of the converter.**

5.2 Choosing a transmission line parameter to vary

In order to investigate the effects of the transmission line components, we need to choose a parameter to vary of these components. Recall that we are using the ideal transmission line model in simulation (Section 3), which describes a line completely by its delay and characteristic impedance. Which means that we can vary either of these parameters to investigate the effects of the transmission line components.

For this study, we are going to choose the **delay parameter** as the primary parameter to vary (as opposed to the characteristic impedance). There are two main reasons for this choice:

1. The delay parameter is entirely determined by the length of the transmission line for a given propagation speed. This is in contrast to the characteristic impedance, which is determined more by the cross-sectional dimensions of the lines, as detailed in Section 3. This essentially means that an alteration to the impedance would necessitate awkward changes in the physical construction of the components, which is not always feasible or convenient in a real-world setting. For example, it is easier to change the length of a copper-clad PCB (parallel plate transmission line) than it is the distance of the FR4 substrate. While we are primarily doing the analysis in simulation which frees us from 'awkward' choices, we would like to keep the process as applicable to real-world scenarios as possible, as experimental verification is performed at the end of the chapter.
2. The delay parameter only affects the time taken for signals to travel along the transmission line. It does not affect the magnitude of the signals, which is the case for the characteristic impedance. This means that we can look at how changing the delay parameter affects the time-domain effects of the transmission line components, without having to worry about the magnitude of the reflections travelling through the circuit. We can see how the reflections interact with one another for changes in their transit time.

In the following simulation analysis, results for various delay values of the inductor and capacitor transmission lines will be shown. For illustration purposes, delay values chosen are so deliberately to show the effects of the transmission line components. 3 delay values will for each component are chosen. Two are when the delay values of the capacitor and inductor lines are integer multiples of each other, and the third is when they are not. From experience, these numerical relationships and the comparison thereof are of primary focus for the high-frequency effects we see on the output waveforms. From these results, further simulations and analysis will be performed to further expand our understanding of the effects of transmission line components within a buck converter.

Note on parameter variations

For variations in any parameter of the transmission line components going forward, care was taken to make sure that output characteristics (output voltage, inductor and current ripples) of the buck converter (from 5.1) for the given load does not vary significantly; A maximum of 10% off the baseline operation of the converter waveforms is chosen as acceptable. Because we are focussing on the high-frequency effects amongst the output waveform, the low-frequency characteristics of the converter are not of primary concern, however we still want to make sure that the converter is operating more or less as it should. This meaning that the output voltage is still regulated around its desired mean value, and the inductor and capacitor currents are still continuous. This is to ensure that any changes in the output waveform are due to the transmission line effects, and not due to the converter operating in a different mode or state.

5.2.1 Effect of adjusting the delay parameter of the inductor transmission line

The inductor delay is varied by adjusting the length of the transmission line. Specifically, we can either increase the delay parameter by appending an additional length of transmission line to the existing inductor transmission line, or decrease it by reducing the length.

Figure 5.3 shows the output of the buck converter if we simulate a range of inductor delay values. The capacitor delay is kept constant at 38ns, while the inductor delay is varied from 36ns to 45ns and finally to 76ns. The output is shown for each delay value, with the corresponding delay information shown in the legend.

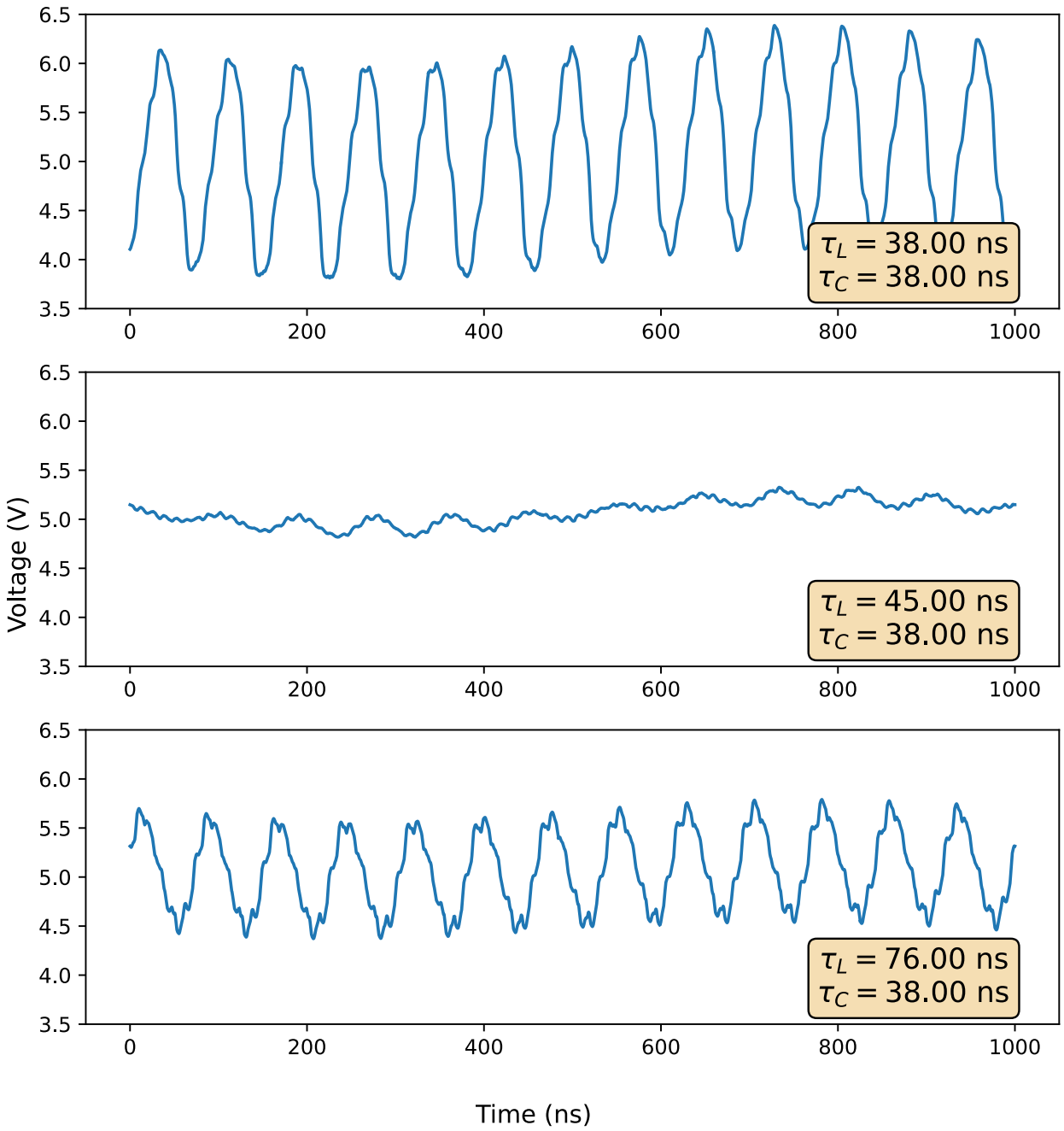

Figure 5.3: Output of TL-based buck converter for a range of inductor delay values

What is quite clear already from this limited set of results is that the change in delay has a significant impact on the output. The output waveform is noticeably different for each delay

value, with the high-frequency effects becoming more or less pronounced as the delay changes. This is a clear indication that the delay parameter of the inductor transmission line has a direct impact on the output waveform.

5.2.2 Effects of adjusting the delay parameter of the capacitor transmission line

Similarly to the inductor transmission line, we can adjust the delay parameter of the capacitor transmission line by changing its length. Figure 5.4 shows the output of the buck converter if we simulate 3 capacitor delay values. The inductor delay is kept constant at 76ns, while the capacitor delay is varied from 36ns to 45ns and finally to 76ns. The output is shown for each delay value, with the corresponding delay information shown in the legend.

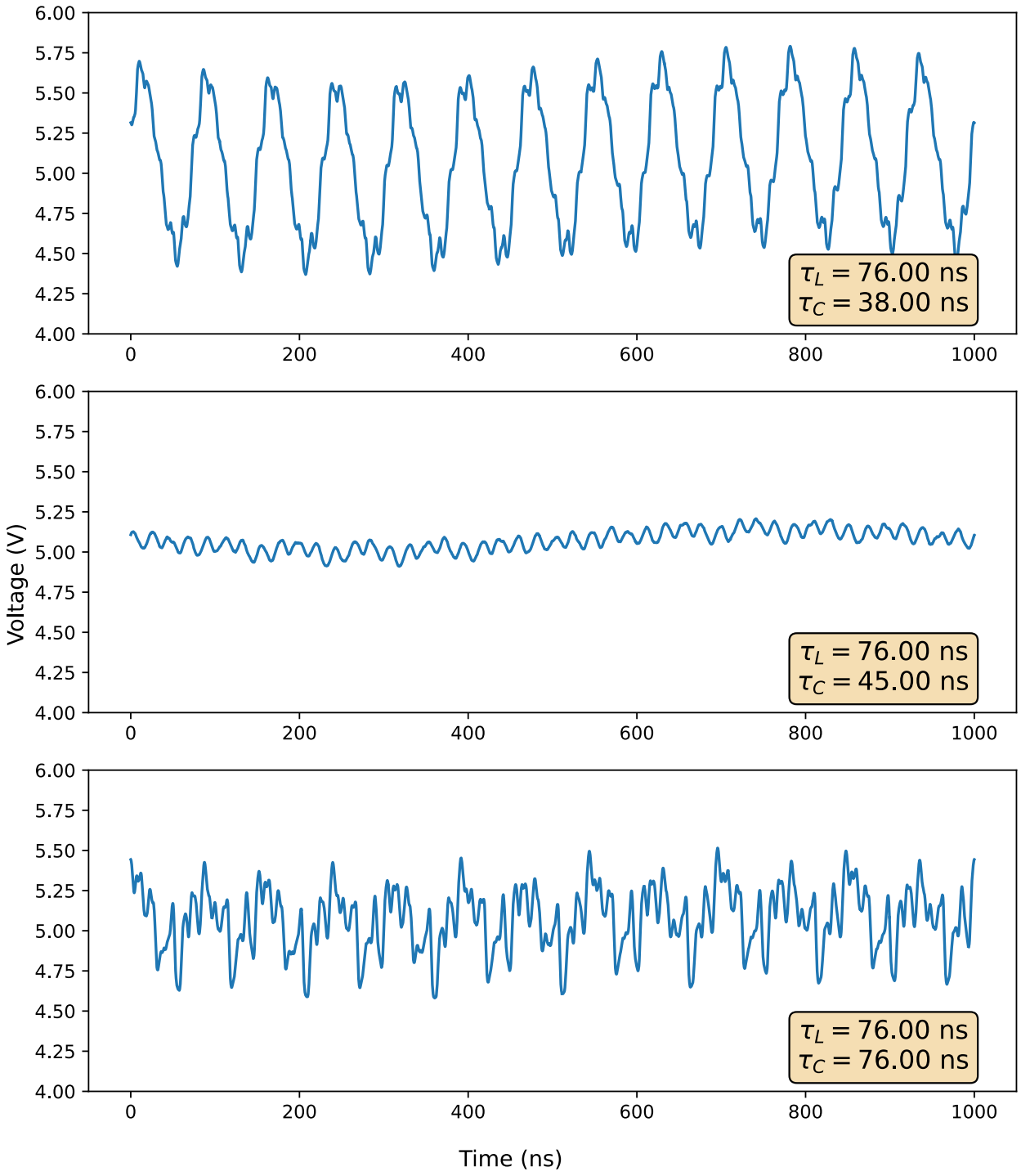

Figure 5.4: Output of TL-based buck converter for a range of capacitor delay values

A similar result is obtained as before, where we see that small changes in a transmission line parameter can have a significant impact on the output waveform. Moreover, we see that the capacitor delay has a similar effect on the output waveform as the inductor delay without disturbing the low-frequency characteristics of the converter.

5.2.3 Discussion of the simulation results

The results from the previous two sections show that the delay parameter of the transmission line components has a direct impact on the output waveform of the buck converter. Moreover, what we notice is that depending on the delay values of the inductor and capacitor transmission lines, the 'bumps' can become more or less pronounced. Either delay parameter can be varied to achieve this effect, and initially it appears that the effect is more pronounced when the delay values are integer multiples of each other. This is a very interesting result, and it is worth investigating further.

An important thing to keep in mind when looking at the simulation data is to note that due to the numerical nature of the simulation, the output waveforms are not expected to match the real-world results exactly. However, we do expect that the general trends in the simulation results should be reflected in the experimental results. i.e., if we see large oscillations or 'noisy' simulation results, we expect to see some analogous behaviour in the experimental results — relative to the other results of course. A good example of this is shown in Figure 5.4 for the case where the capacitor and inductor delays are both 76ns. The output waveform is very 'noisy' and has a lot of high-frequency oscillations, spikes etc. In the real-world measurements however, it is not expected to see such a level of erratic effects in this level of detail, as the physical measurement will likely have damping, measurement noise, sampling rate limitations etc. That being said, relative to the other experimental results (say for mismatched delays) we expect to see a similar level of 'noisiness' in the output waveform.

5.3 Quantifying high-frequency effects

Figure 5.3 clearly indicates that as a result of the transmission line components, there is a lot of complex behaviour occurring in the output waveform. The question is, how do we quantify this behaviour? How do we extract meaningful information from the waveforms? This section will cover some methods used to extract information from the waveforms, and the difficulties associated with doing so. The goal is to somehow link the time-domain variations in the waveforms to the properties of the transmission lines, or a combination of the transmission lines, trying to formulate an understanding of

Focussing on the inductor variations, Figure 5.3 is re-shown below in Figure 5.5 for clarity of discussion.

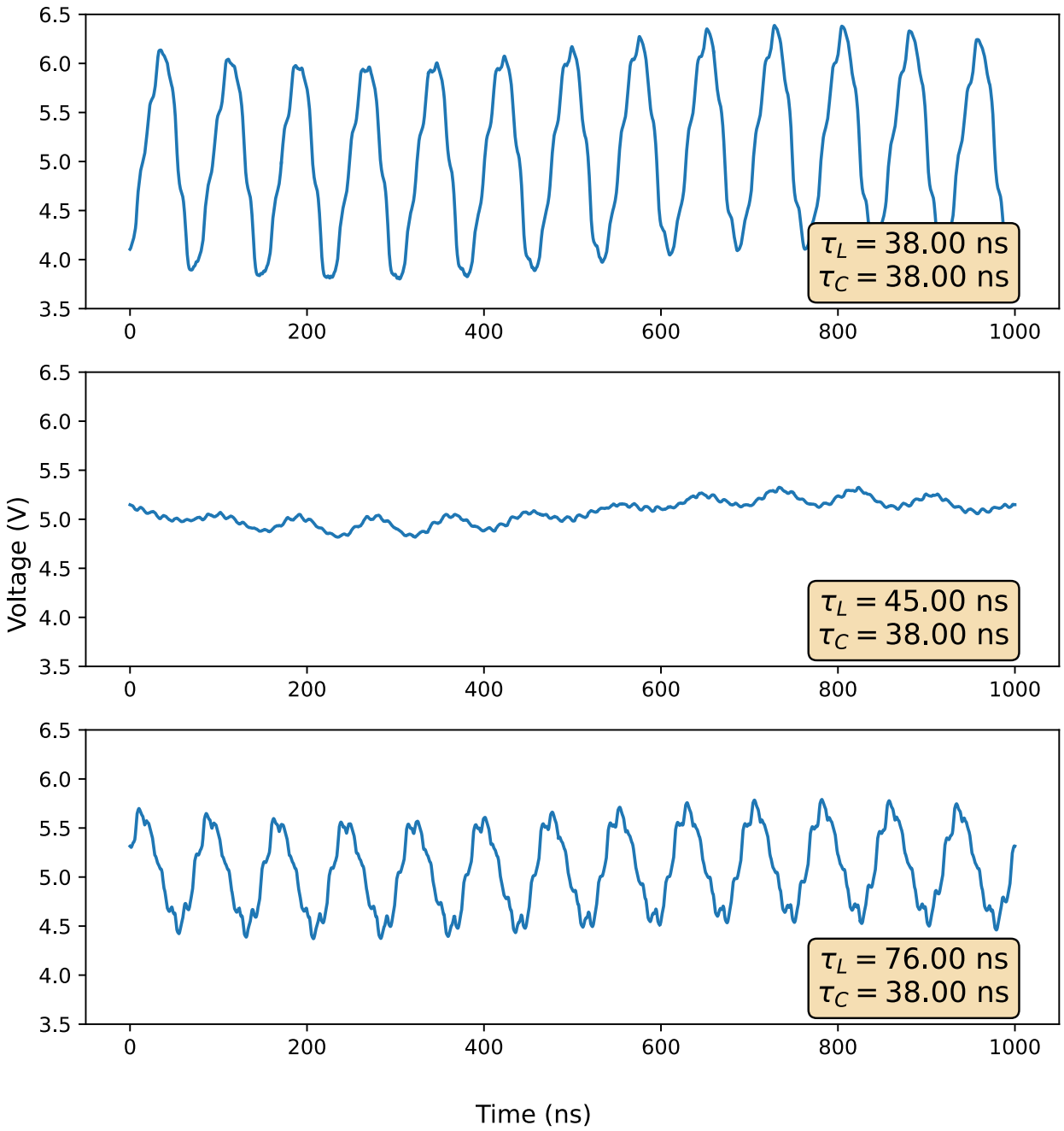

Figure 5.5: Zoomed in view of the output waveforms for the inductor delay sweep

Looking at Figure 5.5, visually the bumps appear somewhat periodic. Although between result sets it varies drastically. Unfortunately, extracting any periodic waveforms from the bumps

graphically is difficult, and this is exposed from Figure 5.5. With the large variations and differing shapes across result sets, simply placing a cursor and measuring the periods is not feasible, and further attempts at extracting periodicity out of the result sets proved unsuccessful. The third plot illustrates this well; it is not as simple as just measuring peak-to-peak or trough-to-trough — it is clearly a very complex output.

5.3.1 Quantification through mean and sum of squares analysis

Accepting that periodic analysis of the output waveforms is not currently possible, the next step is to find a good way quantify the effects of the transmission line on the output waveform in a meaningful way. We can clearly see that there are large variability of the magnitudes of the high-frequency effects for small changes in delay; If we focus on comparing changes in magnitudes across result sets for changes in delay values then we can analyse how transmission line components affect the output of the buck converter circuit.

For this study, we will quantify the magnitude changes through comparing the mean and total sum of squares (SST) of the output waveforms across result sets.

For the following data-processing, the inductor delay is swept from 30ns to 120ns in 1ns increments. This provides 90 simulations to analyse and should be a sufficient number of data points to investigate the effects of the transmission line parameter variations on the output waveform.

Calculate the Mean:

First, find the mean $\bar{y}$ of the dataset y. This is done by summing all the n data points in y and then dividing by n.

$$\bar{y} = \frac{1}{n} \sum_{i=1}^{n} y_i$$

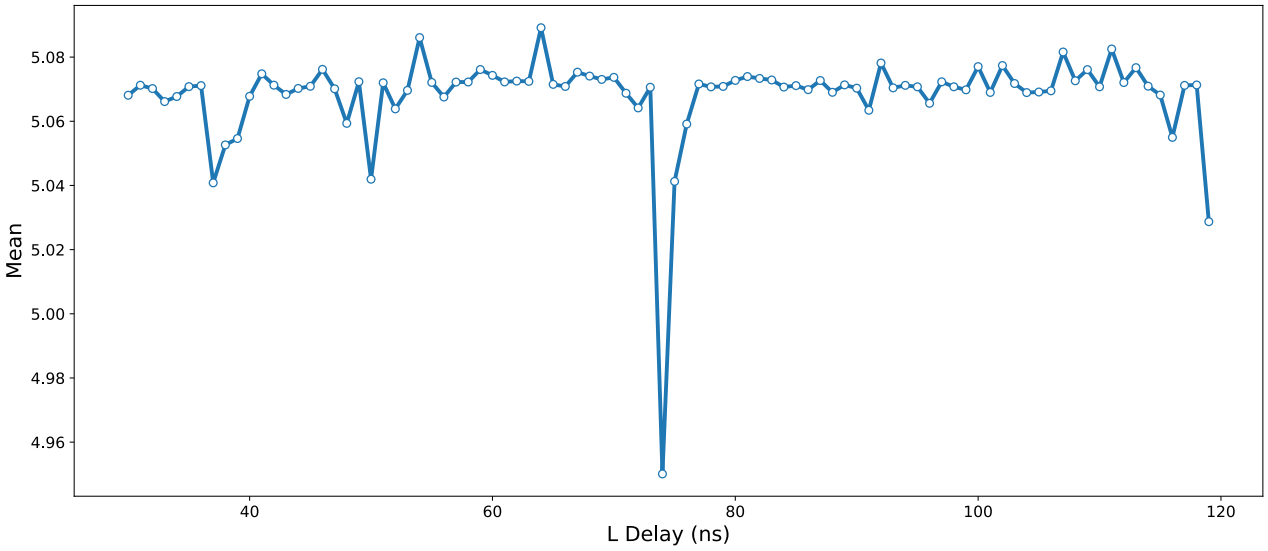

Figure 5.6: Mean of the swept data

The mean data shows us that across the variations for the inductor delay, the mean of the output waveform is relatively constant. This is expected as the mean of the output waveform is the DC component of the waveform, and seeing as the circuit is a buck converter the mean should lie around the desired DC voltage (5V). Even at the most significant departure from the mean at 76ns, the value is 4.9V, which is a 0.1V difference from the mean of 5V. This is a 2% difference. This means that the changes in the inductor delay has not changed the DC (or low frequency) operation of the buck converter; Previous figures indicated this fact too.

Departures from the mean do occur at interesting points in the waveform, and it is these departures that we are interested in. Unfortunately the mean does not provide us with much insight into what is happening at these points. The mean is a good way to quantify the DC component of the waveform, but it does not provide us with much information about the high-frequency components of the waveform. For this, we need to look at the total sum of squares (SST), where the high-frequency effects essentially add variance to a waveform. The larger the magnitude of effects, the more variance from the mean a waveform will have.

Total Sum of Squares (SST)

The SST indicates the total variance in the dataset. For each data point in y, subtract the mean of y and square the result. Sum up all these squared values.

$$SST = \sum_{i=1}^{n} (y_i - \bar{y})^2$$

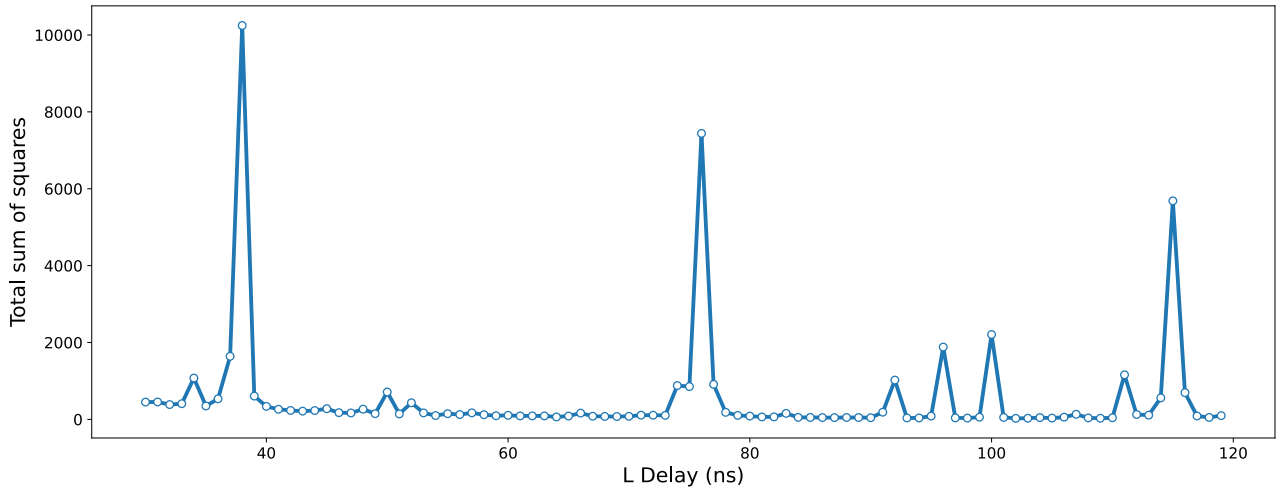

Figure 5.7: Total sum of squares of the swept data

The SST emphasises the deviations from the mean that was seen in Figure 5.6, and makes it easier to isolate true departures from the overall mean.

Discussing the spikes in the mean and SST

To make it easier to process we can split the SST into two regions of interest. **Region 1** is concerning the large spikes at 38ns, 76ns, 100ns and 114ns. **Region 2** is concerning the flatter regions of the plot, where SST values are low in comparison.

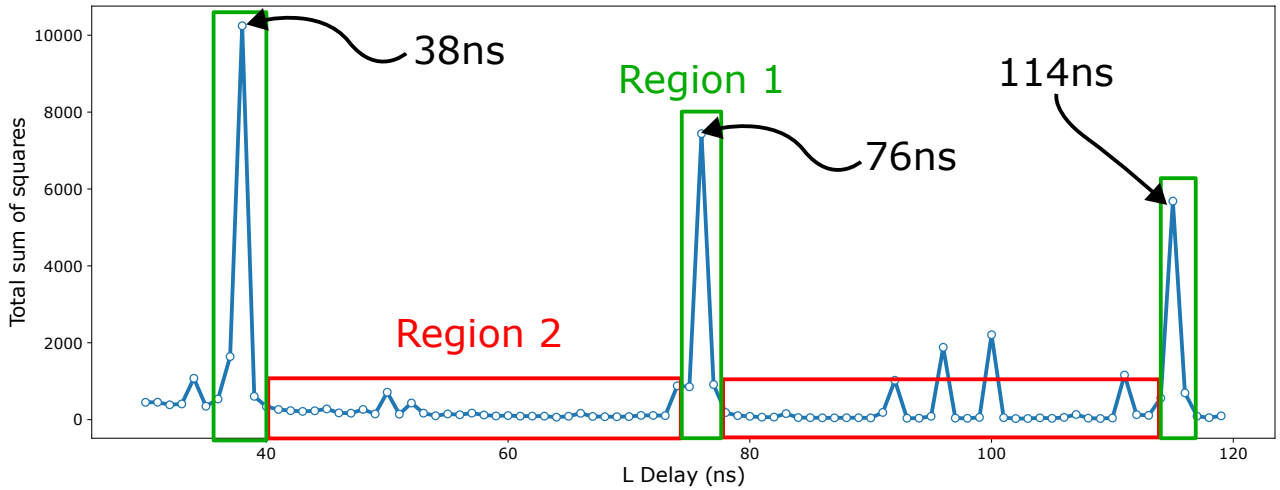

Figure 5.8: Residual sum of squares of the swept data split into regions

For **Region 1**, the spikes occur when the inductor delay values (38ns, 76ns and 114ns) are around integer multiples of the capacitor delay (38ns).

In **Region 2**, the delay relation becomes more fractional (non-integer), the magnitude of the spikes decrease.

Figure 5.9 illustrates a few of the expanded sections of the output waveforms for each region.

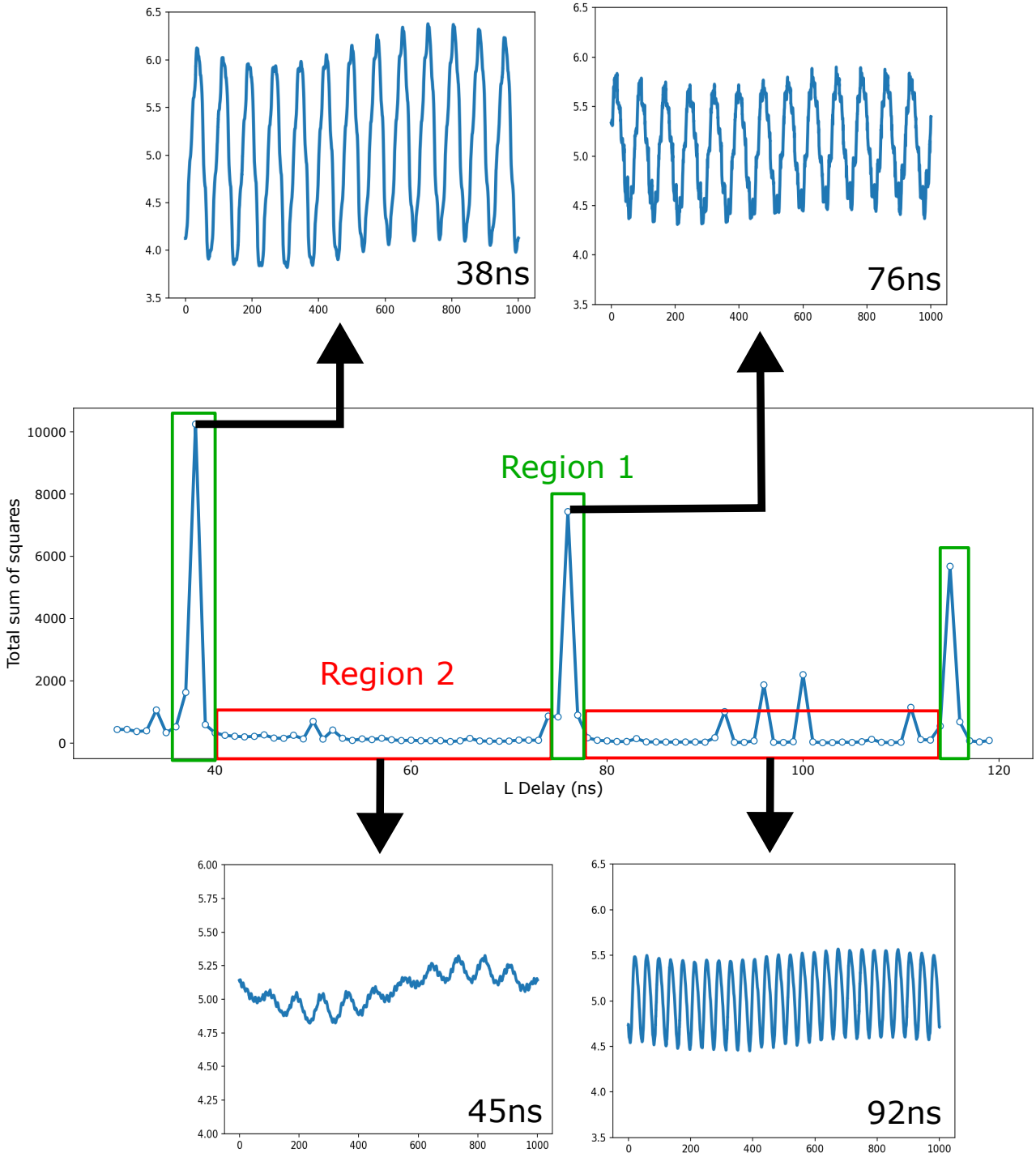

Figure 5.9: Expanded output waveforms for each region

Figure 5.9 shows that Region 1 graphs are where the spikes are most prevalent. Region 2 graphs are where the spikes are less prevalent and hence less bumpy and less erratic. An interesting point to consider when comparing the time-domain outputs of the two regions is that the while region 1 has a higher magnitude of spikes, the frequency of the spikes is lower. Region 2 has a lower magnitude of spikes, but the frequency of the spikes is higher.

Result outlier: 100ns

The only point of interest from the SST (from Figure 5.7) which does not conform to the general trends in Regions 1 and 2 is the spike around 100ns. The 100ns spike is a bit larger than we can really ignore. Currently, it is unclear if it is a simulation numerical artefact or a real effect. There is however a possible explanation for the spike at 100ns.

Further investigation through simulation indicated that the delay of 100ns is an integer multiple of the switching frequency of the buck converter (1MHz). When changing the switching frequency such that the delay is no longer an integer multiple, the spike at 100ns disappears.

If the 100ns deviation is a real effect, then it is a very interesting result. If true, it would imply that not only should we consider the effects of the capacitor delay and the inductor delay, but also the effects of the switching frequency and how these three variables interact with one another. This would be a very interesting result, and would be worth investigating in further research.

What we think is happening

The author believes that the reasons for the spike magnitudes being largest at integer multiples of the capacitor delay is due to the reflections of the transmission lines interacting at the interface of one another. As reflections travel through each transmission line, they each take a certain amount of time to travel through the line. Thereafter, the reflections are superimposed on top of one another at the interface between the two transmission lines across the load. While this seems obvious, in the context to the graphs produced, we believe that if the reflections are in phase with one another (arrive at the interface at similar times), then the magnitude of the resultant reflection at the interface is increased. Conversely, if the reflections are out of phase (arrive at the interface at different times) then the resultant magnitude is smaller than that of the in phase case.

It is believed that the reflections are in phase with one another at integer (or close-to-integer) multiples, and out of phase with one another at fractional (non-integer) multiples for the delay relationship between transmission lines.

5.4 Experimental validation of high-frequency effects

While Section 4 validated that the transmission line buck converter works as expected in the real world, it is also useful to validate the simulation results that were obtained in Section 5.2.1 where it was shown that small changes in transmission line parameters for electrically large components can have a significant effect on the high-frequency time-domain output of the converter.

5.4.1 Experimental setup

The experimental setup is identical to that established in Section 4.2, and the derivations for the distributed components were outlined in Section 3. For convenience, a visual diagram of the experimental setup is reproduced in Figure 5.10.

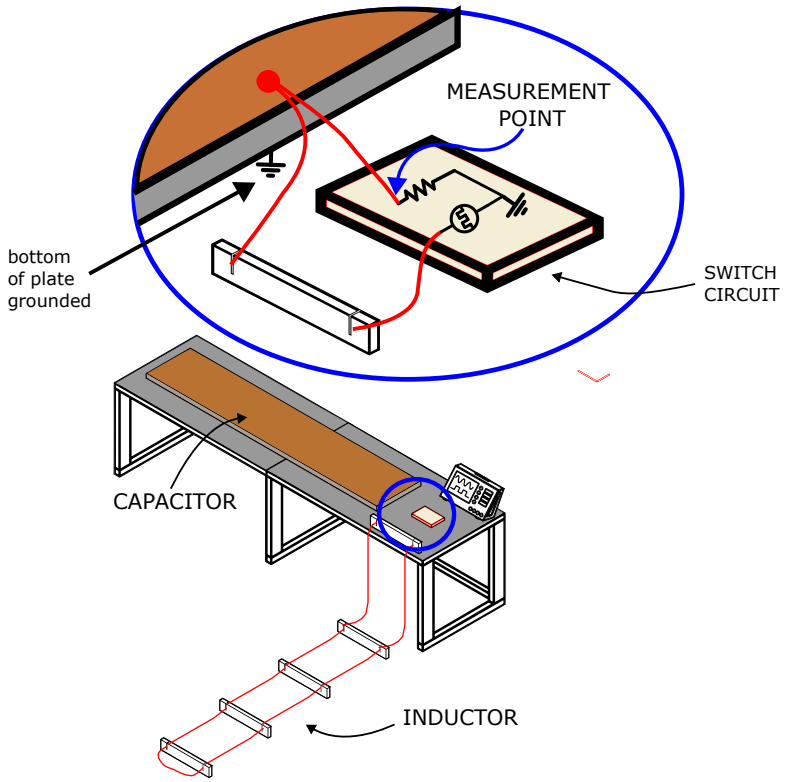

Figure 5.10: Experimental setup for validating high-frequency effects

The process for varying the delay of the inductor transmission line physically is to add or remove 30 cm sections of the transmission line (which corresponds to a delay of 1ns) while keeping the cross-sectional characteristics of the component the same. Care was taken when

splicing sections of the line together to keep splice-points as clean as possible, and to keep the length of the transmission line as close to the desired length as possible. The capacitor delay is not varied experimentally, as the parallel plate capacitor is not spliced in the same way as the inductor transmission line is making it physically impractical, moreover it is not practical to change the distance between the plates either — resulting in the inductor being of primary focus.

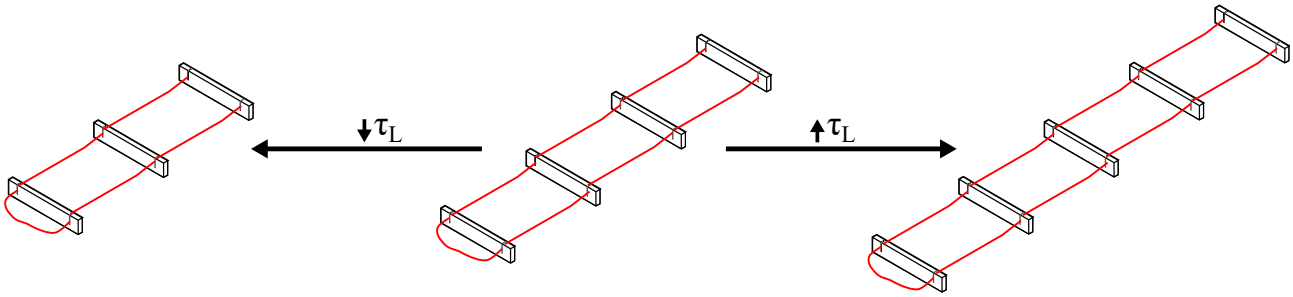

Figure 5.11: Adjusting the delay parameter of the inductor transmission line

5.4.2 Experimental results

As in Section 5.2.1, the inductor delay is varied from 33ns to 80ns by changing the length of the transmission line by 30 cm sections, which corresponds to a delay of 1ns. As a reminder, the capacitor delay is fixed at 38ns across all experiments, and legends across all proceeding figures refers to the inductor transmission line delay value. Recall that previously the simulations predicted that the high-frequency effects would be most pronounced when the inductor delay is close to and around integer multiples of the delay of the capacitor. A sweep of 33ns to 80ns gives us 20 different values of the inductor delay to investigate and compare to the predictions.

For completeness, Appendix A shows the full 20 experimental results for the inductor delay sweep. From there, the reader can see the full extent of the experimental results, and how the output voltage of the converter changes as the inductor delay is varied. For the purposes of this section, we will only be looking at a few select results to compare to the simulation predictions seen in Section 5.2.1

Inductor delay around 38ns

Figure 5.12 shows the experimental output of the buck converter with the inductor delay set to 38ns. This is an integer multiple of the capacitor delay. As in the prior section, the high-frequency effects are still visible — the interesting analysis comes however when we compare results for delay values slightly around this value.

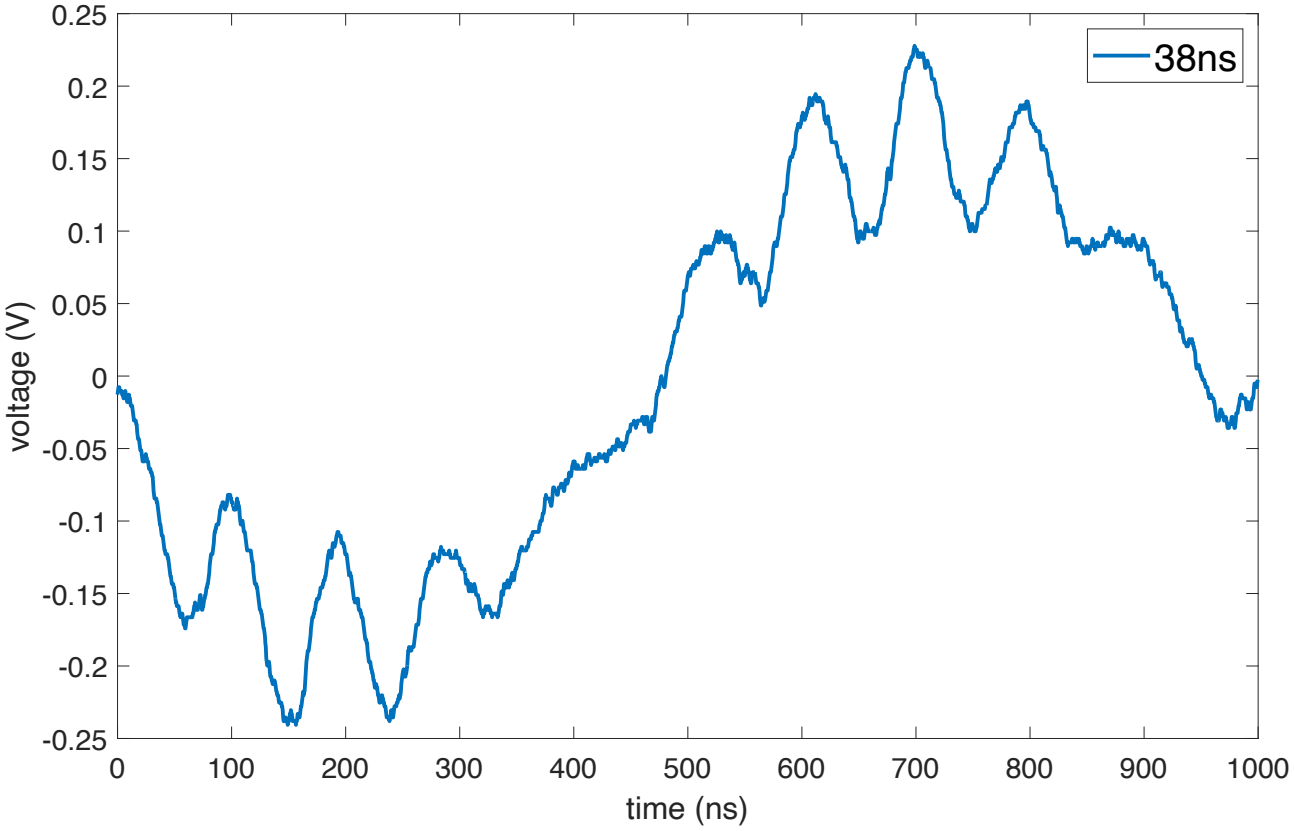

Figure 5.12: Experimental results for validating high-frequency effects

Looking back at the simulation results in Figure 5.7 we expect the relative 'severity' of the high-frequency effects to be highest when the inductor delay is close to integer multiples of the capacitor delay, and to be less severe when the inductor delay is not. This is indeed the case, and is shown in Figures 5.13 and 5.14,where the integer multiple delay of 38ns is compared to values slightly away from it; being 37ns and 36ns (non integer multiples of the capacitor delay).

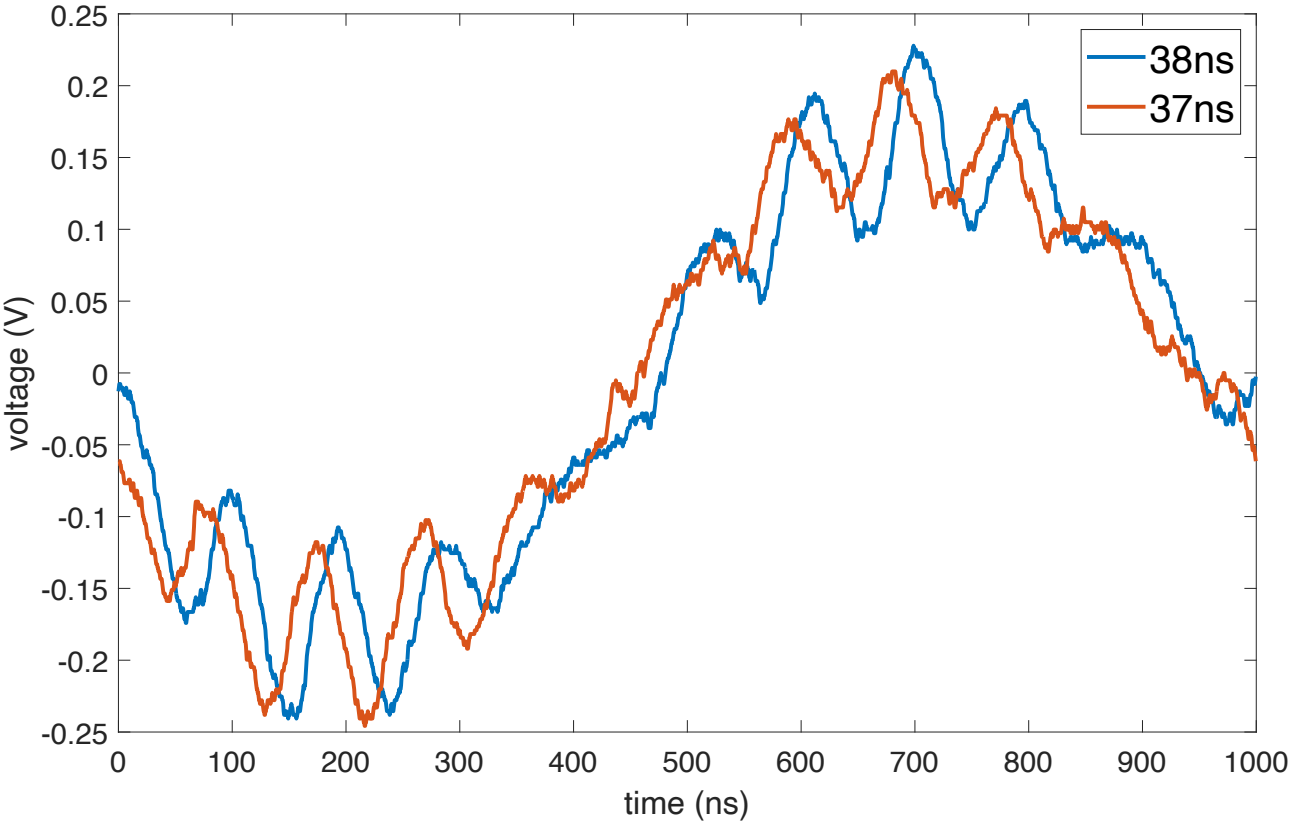

Figure 5.13: Experimental results for validating high-frequency effects

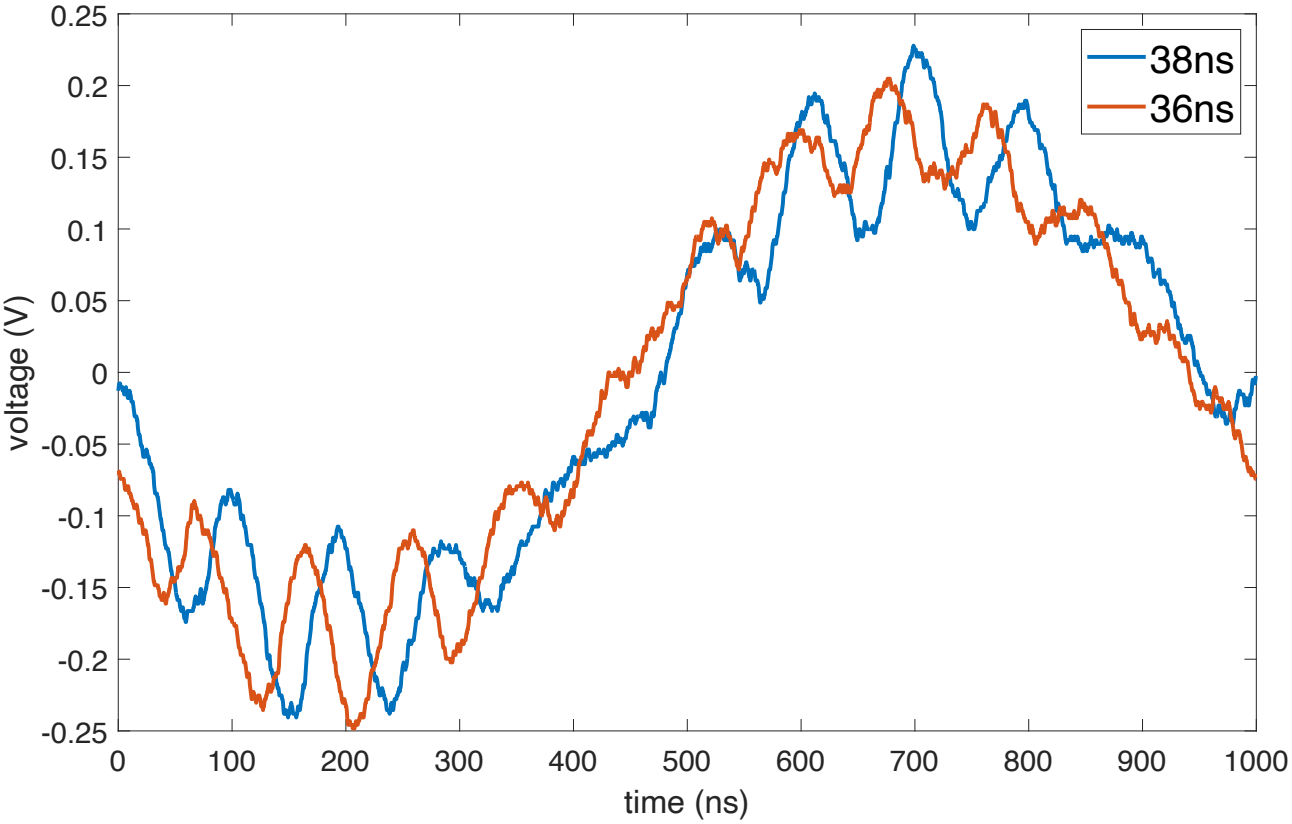

Figure 5.14: Experimental results for validating high-frequency effects

As is shown, the high-frequency effects of 37ns and 36ns are less severe than that of 38ns, and are in fact quite similar to each other. This is actually completely in agreement with the simulation predictions, as recall from the total sum of squares plot in Figure 5.7 that the simulation results for the high frequency effects around 37ns and 36ns were similar to each other when compared to the effects at 38ns. Figure 5.15 shows the experimental results for 38ns, 37ns and 36ns together for comparison, and supports this fact.

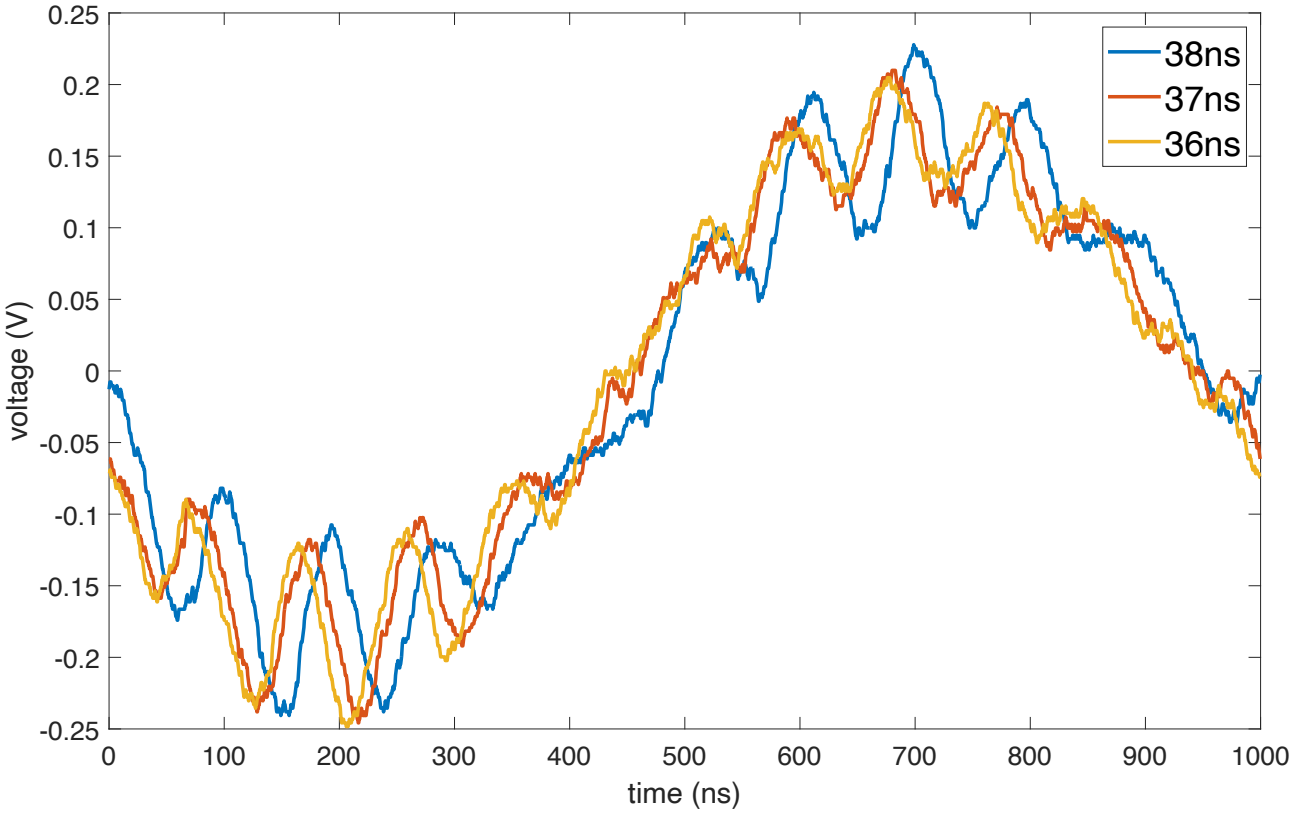

Figure 5.15: Experimental results for validating high-frequency effects

Fractional delay ratios (48ns — 50ns)

Fractional (non-integer) delay ratios in the context of these experiments are referring to values where the inductor delay is not an integer multiple of the capacitor delay. While this technically applies to all values of the inductor delay that are not integer multiples of the capacitor delay, the focus here is on the values of 48ns, 49ns and 50ns. These values are a lot further away from being integer multiples of the capacitor delay than the values of 37ns and 36ns, and so we expect the high-frequency effects to be even less severe than those values as the change for any 'overlap' in the integer relationships is reduced.

Figure 5.16 shows the experimental results for these values.

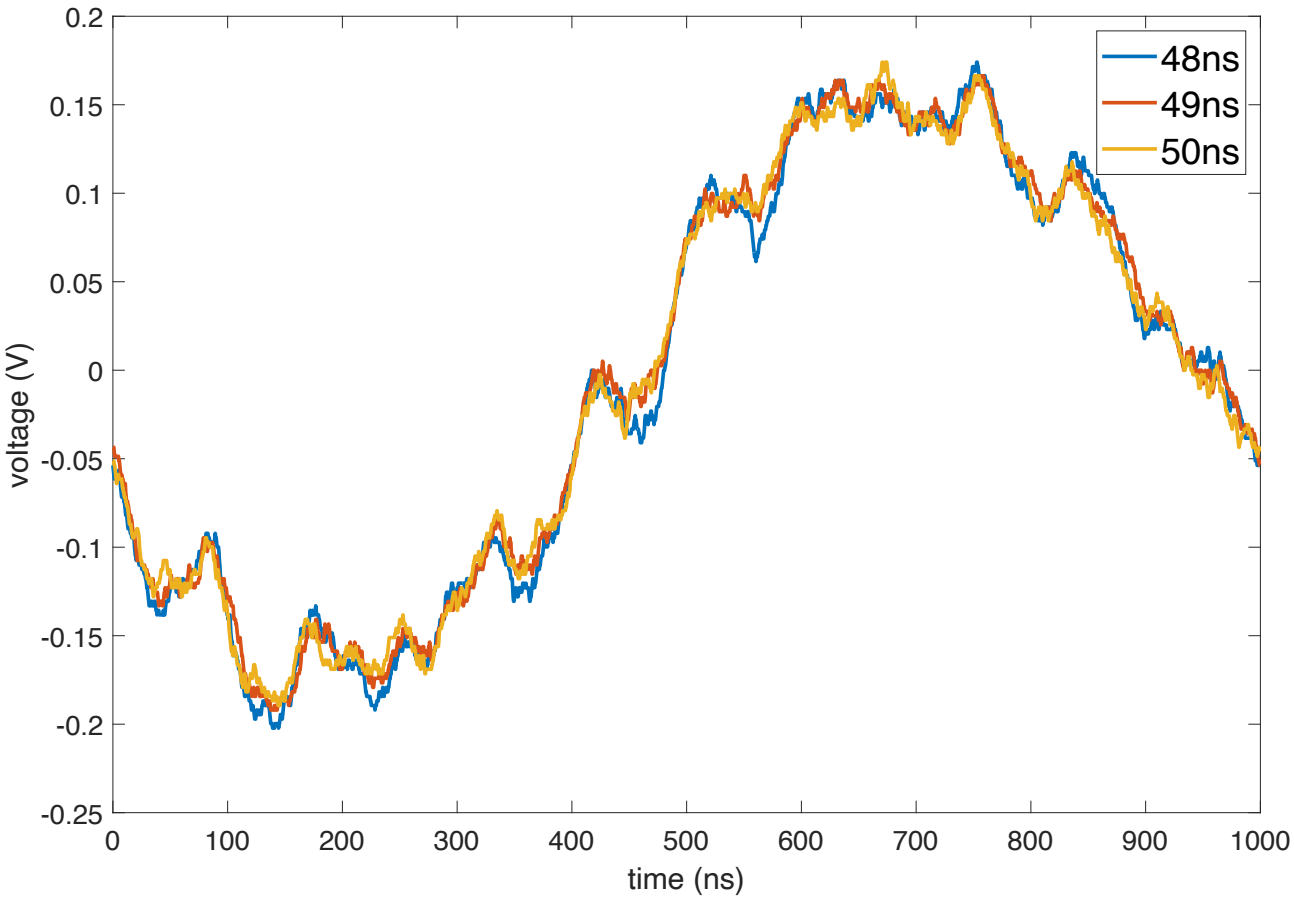

Figure 5.16: Experimental results for validating high-frequency effects

It is quite clear to see that the high-frequency effects are much less severe than the integer multiple cases. This is too what we expect from the prior analysis in Section 5.3. For completeness, Figure 5.17 shows the comparison between the integer multiple case of 38ns and the fractional delay case of 48ns, cementing our finding.

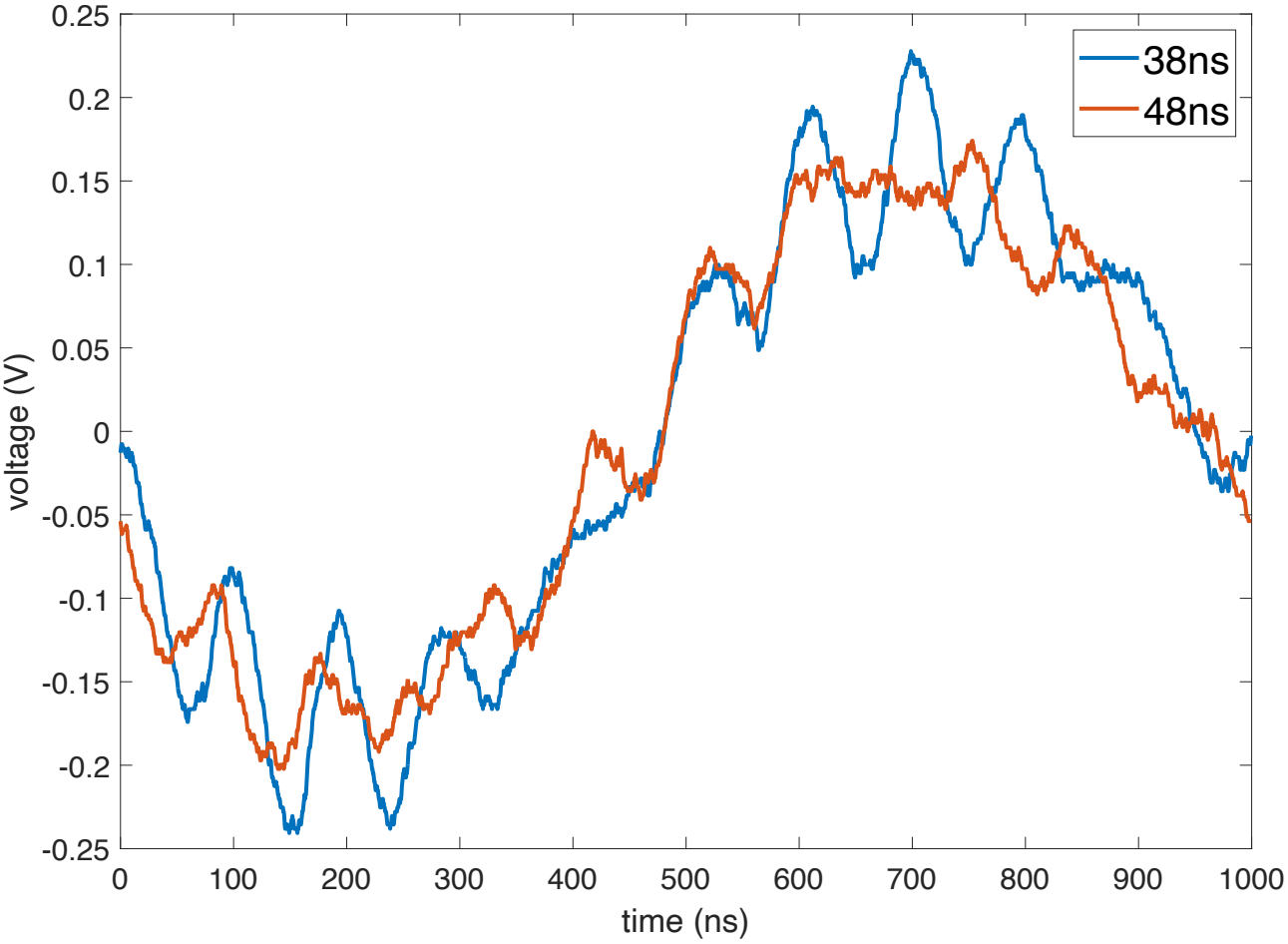

Figure 5.17: Experimental results for validating high-frequency effects

Inductor delay around 76ns

Finally, the next interesting case to look at is when the inductor delay is around 76ns, which is also an integer multiple of the capacitor delay. The expectation based on prior analysis suggests much of the same as the results from Figure 5.15. Figure 5.18 shows the experimental results for this case. The results are quite similar in behaviour to the 38ns case, with the high-frequency effects being most pronounced when the inductor delay (76ns) is an integer multiple of the capacitor delay (38ns).

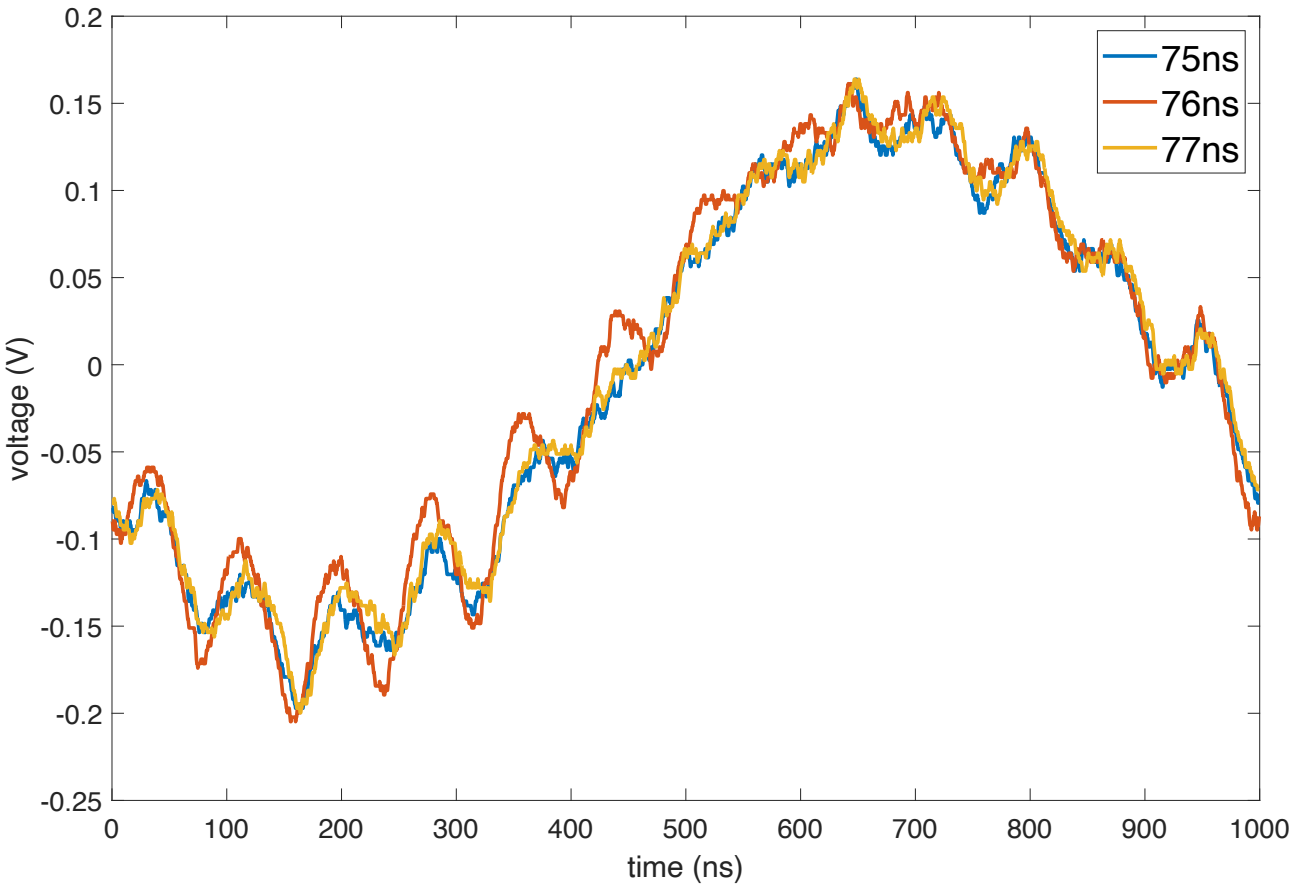

Figure 5.18: Experimental results for validating high-frequency effects

This is a strong confirmation of the simulation results as well as reinforcement of the measured results obtained for the 38ns results. These results all indicate that there are certainly high-frequency effects that are present in the converter as a result of the transmission line components.

Another interesting result to look at is when we compare the results for 76ns to those of the 38ns case, essentially comparing the results of the integer multiples of the capacitor delay. These results are shown in Figure 5.19.

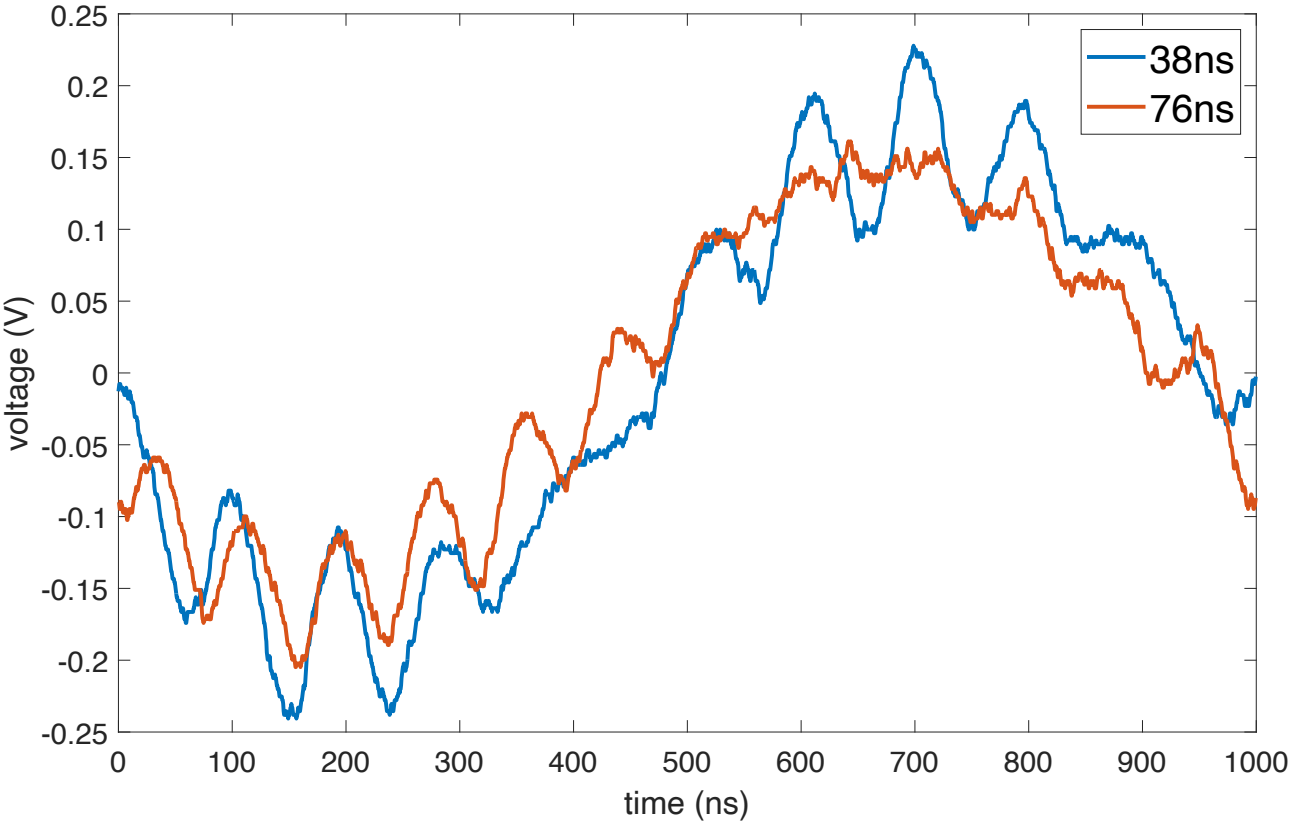

Figure 5.19: Experimental results for validating high-frequency effects

What is interesting to note here is that while of course the converter output sine wave is slightly different (on account of the larger inductance value of the 76ns transmission line), the high-frequency effects are actually quite similar. The number of 'bumps' effectively remains the same in the trough region of the waveform, albeit with different (but not too far removed) amplitudes. Curiously however, along the peaks of the waveform, the 76ns case has a drastically reduced amplitude and discernibility of the high-frequency effects. It is not entirely clear why this is the case, it is not believed to be a measurement artefact and requires further analysis — this is left for future work.

5.5 What quantifying the high-frequency effects does and does not mean

We have so far shown that the high-frequency time-domain effects of transmission line components can be significant, and that their magnitudes can be quantified and related back to transmission line parameters. We have also shown that changes in these effects can be validated

experimentally. The results show that changes in the relation of transmission line delay parameters can have and effect on the magnitude of the high-frequency time-domain 'bumps' that we observe on the output waveform. Ultimately it is clear that we can manipulate the time-domain high-frequency effects of the converter by changing the transmission line components in small ways, and that we can measurably quantify these changes.

While this is significant, this work did not quantify what effect these bumps have on the frequency spectrum of the converter output, nor what this means for the performance of the converter holistically. There is a belief that it does impact this significantly, but this is out of the scope of this dissertation. This is left as future work.

Chapter 6

Conclusion

6.1 Summary

Chapter 3 introduced the concept of transmission line modelling, and how it can be used to model physically large reactive components. The chapter focused on capacitors and inductors, and how their conventional models fall short when dealing with effects arising from their physically larger versions. The chapter also introduced the concept of applying common transmission line theory to model these physically large reactive components. The components were then simulated and built. With simulation values being compared with experimental results. The chapter concluded with a discussion on using distributed models for physically large reactive components, where ultimately it is shown that distributed modelling is required for accurate modelling of physically large components.

Chapter 4 applies the outcomes from Chapter 3 towards a DC/DC buck converter. A standard 5V buck converter design is detailed using common techniques. Thereafter, we introduced the concept of a transmission line based buck converter, where the lumped-element capacitor and inductors are replaced with physically large equivalent components modelled using transmission line theory. The converter is simulated and built, with simulation values being compared with experimental results. It is shown that a transmission line component buck converter is able to operate in a similar manner to a standard buck converter, albeit with some additional effects arising from the transmission lines. The simulation results compared with experimental findings indicated that simulated results do indicate the real-world behaviour of the transmission line converter, even though simulation data does not perfectly match experimental data.

Effects of using transmission line components were investigated in Chapter 5 where the effects of varying transmission line parameters were of focus. Specifically the delay of one transmission line was chosen to be varied over a range of values, and the effects of this variation are shown to have a profound effect on the output of the converter. It was shown that the variations needed to be quantified as a direct relation towards transmission line parameters from inspection of the output waveform is not possible at this time. Statistical analysis in the form of a polynomial curve fit and in combination with mean and residual comparisons were used to quantify those effects. A trend emerged within the data where the magnitude of the bumps on the output

waveform were dependent on the delay ratio between the transmission lines. This was shown to be true for both simulation and experimental results. More specifically, the closer the delay ratio between the lines are to integer multiples of each other, the larger the magnitude of the bumps. For fractional delay ratios — even as close as $1 - 2ns$ from being an integer multiple — the magnitude of the bumps decrease significantly. This is an important finding, as it shows that the magnitude of the bumps can be influenced by varying the delay ratio between the lines, and that very small changes in this relationship have a measurable impact on the output we observe without meanfully degrading the converters low-frequency output. This finding is also inline with literature [6].

It stands to reason then, that if the magnitude in those bumps cause an increase or decrease in converter performance (i.e., EMI) in some meaningful way, then the delay ratio between the lines can be used to influence the converter performance. This work does not serve as a definitive answer to that question, nor does it attempt to assess the performance implications of these components, rather the work presented here is more focussed on providing strong experimental evidence that distributed component effects are indeed valid as literature would suggest. This was achieved.

6.2 Future work

As mentioned above, the work presented here is by no means a complete investigation into the effects of transmission line based reactive components, but rather a starting point for further investigation. In fact the scope for future work is practically unbounded. Nevertheless, there are some natural continuances from the research presented.

Developing a way to track the waveforms and reflections either mathematically or through some software solution would be interesting. This work showed how complex the interactions of the reflections are between the two lines, and how they can superimpose on each other. A lot of insight can be gained from investigating this further, especially should these effects be investigated in more complex switching circuits.

This work focussed on varying only the delay parameter of the transmission line components, however there is more scope to investigate how other circuit parameters affect the noise output of the circuit as they interact with the transmission lines i.e., duty-cycle [6].

Perhaps the most interesting area for study is with regards to how these components influence the EMI of a converter. Developing understanding for how these components influence the EMI of a converter is worth studying. Moreover, if it becomes more reasonable to experimentally measure the disputed effects arising from compact transmission line components [3] (such as MLC capacitors) within switching circuit, then this research would have greater applicability to modern switching circuits and how we package them today.

References

[1] H. W. Ott, *Electromagnetic compatibility engineering*. John Wiley & Sons, 2011.

[2] E. Bogatin, *Signal and Power Integrity - Simplified* (Signal Integrity Library). Pearson Education, 2017, ISBN: 978-0-13-451366-9.

[3] C. Sullivan and A. Kern, "Capacitors with fast current switching require distributed models," in *2001 IEEE 32nd Annual Power Electronics Specialists Conference (IEEE Cat. No.01CH37230)*, ISSN: 0275-9306, vol. 3, Jun. 2001, 1497–1503 vol. 3. DOI: 10.1109/PESC.2001.954331.

[4] C. Sullivan and Y. Sun, "Physically-based distributed models for multi-layer ceramic capacitors," in *Electrical Performance of Electrical Packaging (IEEE Cat. No. 03TH8710)*, Oct. 2003, pp. 185–188. DOI: 10.1109/EPEP.2003.1250028.

[5] M.-G. Kim, B. H. Lee, and T.-Y. Yun, "Equivalent-circuit model for high-capacitance MLCC based on transmission-line theory," *IEEE Transactions on Components, Packaging and Manufacturing Technology*, vol. 2, no. 6, pp. 1012–1020, Jun. 2012, Conference Name: IEEE Transactions on Components, Packaging and Manufacturing Technology, ISSN: 2156-3985. DOI: 10.1109/TCPMT.2011.2170990.

[6] I. Hofsajer, "A new noise mechanism in power converters," in *2022 IEEE 31st International Symposium on Industrial Electronics (ISIE)*, ISSN: 2163-5145, Jun. 2022, pp. 604–607. DOI: 10.1109/ISIE51582.2022.9831642.

[7] K. Kaiser, *Electromagnetic Compatibility Handbook* (Electrical engineering handbook series). Taylor & Francis, 2004, ISBN: 9780849320873. [Online]. Available: https://books.google.co.za/books?id=nZzOAsroBIEC.

[8] D. M. Pozar, *Microwave engineering*, Fourth Edition. Hoboken, NJ: John Wiley & Sons, Inc, 2012, 732 pp., ISBN: 978-0-470-63155-3.

[9] L. Zhao and J. vanWyk, "Frequency-domain modeling of integrated electromagnetic power passives by a generalized two-conductor transmission structure," *IEEE Transactions on Circuits and Systems I: Regular Papers*, vol. 51, no. 11, pp. 2325–2337, Nov. 2004, ISSN: 1057-7122. DOI: 10.1109/TCSI.2004.832797. (visited on 08/07/2023).

[10] J. Ferreira and J. Van Wyk, "Electromagnetic energy propagation in power electronic converters: Toward future electromagnetic integration," *Proceedings of the IEEE*, vol. 89, no. 6, pp. 876–889, Jun. 2001, Conference Name: Proceedings of the IEEE, ISSN: 1558-2256. DOI: 10.1109/5.931481.

[11] J. vanWyk, F. Lee, Z. Liang, R. Chen, S. Wang, and B. Lu, "Integrating active, passive and EMI-filter functions in power electronics systems: A case study of some technologies," *IEEE Transactions on Power Electronics*, vol. 20, no. 3, pp. 523–536, May 2005, ISSN: 0885-8993. DOI: 10.1109/TPEL.2005.846553. (visited on 08/07/2023).

[12] C. Sullivan, Y. Sun, and A. Kern, "Improved distributed model for capacitors in high-performance packages," in *Conference Record of the 2002 IEEE Industry Applications Conference. 37th IAS Annual Meeting (Cat. No.02CH37344)*, ISSN: 0197-2618, vol. 2, Oct. 2002, 969–976 vol.2. DOI: 10.1109/IAS.2002.1042675.

[13] H. Sun, Z.-J. Jin, M.-G. Kim, C.-S. Park, and T.-Y. Yun, "Equivalent-circuit modeling for multilayer capacitors based on coupled transmission-line theory," *IEEE Transactions on Components, Packaging and Manufacturing Technology*, vol. 1, no. 5, pp. 731–741, May 2011, Conference Name: IEEE Transactions on Components, Packaging and Manufacturing Technology, ISSN: 2156-3985. DOI: 10.1109/TCPMT.2011.2115241.

[14] H. Zhou, T. Lu, S. Zhang, and X. Zhang, "Lumped-circuits model of lossless transmission lines and its numerical characteristics," *Frontiers in Energy Research*, vol. 9, p. 809 434, Dec. 22, 2021, ISSN: 2296-598X. DOI: 10.3389/fenrg.2021.809434. (visited on 08/03/2023).

[15] M. Mofu, *Investigation into energy manipulation in reactive components using transmission line modelling*, Ph.D. dissertation, 2019.

[16] C. Huang, F. Woittennek, and K. Röbenack, "Steady-state analysis of a distributed model of the buck converter," in *2013 European Conference on Circuit Theory and Design (ECCTD)*, Sep. 2013, pp. 1–4. DOI: 10.1109/ECCTD.2013.6662332.

[17] S. Sander, "Buck and boost converters with transmission lines," *IEEE Transactions on Power Electronics*, vol. 27, no. 9, pp. 4013–4020, Sep. 2012, Conference Name: IEEE Transactions on Power Electronics, ISSN: 1941-0107. DOI: 10.1109/TPEL.2012.2188044.

[18] N. N. Rao, *Elements of Engineering Electromagnetics*. Pearson Prentice Hall, 2004, 876 pp., Google-Books-ID: 5rseAQAAIAAJ, ISBN: 978-0-13-113961-9.

[19] Microchip, *1.5a dual high-speed power MOSFET drivers*, 2012.

[20] C. R. Paul, *Inductance: loop and partial*. Hoboken, NJ: Wiley, 2010, 379 pp., ISBN: 978-0-470-46188-4.

[21] R. W. Erickson and D. Maksimovic, *Fundamentals of Power Electronics*. Springer Science & Business Media, May 8, 2007, 882 pp., Google-Books-ID: B4XhBwAAQBAJ, ISBN: 978-0-306-48048-5.